The Organization and Regulation of Small Conductance Ca^{2+} Activated K Channel (KCNN2) Multiprotein Complexes

by

Duane M. Allen

A Dissertation

Presented to the Neuroscience Graduate Program

and the Oregon Health and Science University School of Medicine

in partial fulfillment of the requirements

for the degree of

Doctor of Philosophy

29 April, 2008

School of Medicine

Oregon Health and Science University

CERTIFICATE OF APPROVAL

This is to certify that the Ph.D. thesis of

Duane M. Allen

has been approved

[redacted]

Professor in Charge of Thesis

[redacted]

[redacted]er

Committee Member

[redacted]

[redacted]

[redacted]

Committee Member

Table of Contents

Table of Contents	i-ii
List of Figures	iii-v
Abbreviations	vi-vii
Acknowledgements	viii
Abstract	ix-xi
Chapter I. Introduction to the hippocampus, plasticity at the CA3-CA1 synapses, and the known components of the SK2 channel multi-protein complex	1-52
A Brief History of Neurophysiology and Ion Channels	2-5
The Hippocampal Formation	6-9
A brief background on synaptic plasticity and LTP	10-27
Calmodulin	28-30
SK channels	31-36
Protein Kinase CK2	37-41
Protein Phosphatase 2A (PP2A)	42-44
Bildl Paper	45-52
Chapter II. The structural and functional relationship between SK2, CK2 and PP2A	53-147
Introduction and Background	54-55
Methods	56-61
Results	62-130

Discussion 131-147

Chapter III. The *in vivo* function of SK2 channel Ca2+ sensitivity modulation 148-178

Introduction and Background 149-158

Additional Methods 159-165

Results 166-172

Discussion 173-178

Chapter IV. Thesis Discussion 179-188

Chapter V. Summary and Conclusions 189-193

References 194-202

Appendix A., Manuscripts resulting from this thesis work 203-204

List of Figures

		Page
Figure 1.	Basic anatomy and wiring of the hippocampal formation.	9
Figure 2.	CaM and CK2 coassemble at the CaMBD of SK2 Channels	48
Figure 3.	CaM surrogate T80D alters SK2 channel gating kinetics and Ca2+ sensitivity	52
Figure 4.	The current amplitude and τ_{off} of SK2 channels is stable in CHO cells	64
Figure 5.	Activation of CK2 speeds SK2 channel deactivation and reduces the apparent Ca2+ sensitivity.	67
Figure 6.	CaM surrogate T80D significantly decreases SK2 channel deactivation kinetics, but CaM surrogate T80A does not alter SK2 channel deactivation kinetics because it is not expressed.	71
Figure 7.	Preincubation with TBB blocks the MgATP effect.	74
Figure 8.	CK2 is stably associated with the SK2 channel multi-protein complex.	77
Figure 9.	CK2 activity for SK2-associated CaM is state dependent.	80
Figure 10.	A phosphatase inhibitor cocktail containing PP2A inhibitors (PIC1) speeds τ_{off} but a phosphatase inhibitor cocktail lacking PP2A inhibitors (PIC2) does not.	83
Figure 11.	PP2A is stably associated with the SK2 channel multi-protein complex.	86
Figure 12.	SK2 channel associated PP2A activity is slow to reverse changes in the equilibrium caused by MgATP application, is not state-dependent and is not affected by shrimp alkaline phosphatase (SAP).	90
Figure 13.	PP2A is co-assembled with SK2 channels	94
Figure 14.	The truncation of SK2 at amino acid 471 leads to rapid rundown, which is not rescued by Ca/CaM application (10μM)	97
Figure 15.	Interactions between domains of SK2 and CK2.	101
Figure 16.	The binding sites of CK2 and PP2A both map to regions that could accommodate a large protein-binding partner.	104
Figure 17.	CK2 (green underlining) and PP2A (blue underlining) binding site conservation among SK channel family members.	107
Figure 18.	The SK2 N-terminal domain activates CK2.	111

Figure 19.	K121 regulates CK2 co-assembled with SK2 channels.	113
Figure 20.	Model for co-assembled SK2, CaM, CK2, and PP2A.	116
Figure 21.	Summary of τ_{off} obtained from SK2 channel N-terminal mutants before and after 2.5 minute application of 5mM MgATP.	126
Figure 22.	Summary of τ_{off} obtained from SK2 channel C-terminal mutants before and after 2.5 minute application of 5mM MgATP.	128
Figure 23.	Other possible mechanisms of τ_{off} modulation do not appear important for our model of the SK2 channel multi-protein complex.	130
Figure 24.	Our strategy for in vivo mutagenesis in SK2-null mice.	156
Figure 25.	Our strategy for in vivo mutagenesis in SK2-floxed mice.	158
Figure 26.	Minimal apamin-sensitive currents are detected in SK2 floxed mice.	164
Figure 27.	Floxed mice do not express SK2-L and have decreased expression of SK2-S.	169
Figure 28.	Summary of the SK2 channel multiprotein complex in a low Ca^{2+} environment	180
Figure 29.	Summary of the SK2 channel multiprotein complex in a high Ca^{2+} environment	182

Abbreviations

ACh	Acetylcholine
ACSF	Artificial cerebrospinal fluid
AMPA	α-amino-3-hydroxy-5-methylisoxazole-4-propionic acid
AP	Action Potential
CA1	Cornu Ammonis 1
CA2	Cornu Ammonis 2
CA3	Cornu Ammonis 3
CHO	Chinese Hamster Ovary
CK2	Casein Kinase II
EPSP	Excitatory Post-Synaptic Potential
ER	Endoplasmic Reticulum
ER	Endoplasmic Reticulum
fEPSP	field Excitatory Post-Synaptic Potential
HCN	Hyperpolarization-activated cyclic-nucleotide gated
IPSCs	Inhibitory Post-Synaptic Currents
KO	Knock-out
LTD	Long-term Depression
LTP	Long-term Potentiation
nAChR	nicotinic Acetylcholine Receptor
NMDA	N-methyl-D-aspartate
PDZ	postsynaptic density 95, disk large, zona occludens-1

PMCA	Plasma Membrane Ca2+ Pumps
Po	Probability of Opening
PP1	Protein Phosphatase 1
PP2A	Protein Phosphatase 2A
PSD	Post-Synaptic Density
PWB	Protein Wash Buffer
REM	Rapid Eye Movement
rtPCR	Reverse-transcription Polymerase Chain Reaction
SCG	Superior Cervical Ganglia
shRNAs	short-hairpin RNAs
SK	Small conductance K channel
SLM	Stratum Lacunosum-Moleculare
SPW	Sharp Waves
STDP	Spike-Timing Dependent Plasticity
TBB	4,5,6,7-tetrabromo-2-azabenzimidazole
VGCC	Voltage Gated Ca2+ Channels

Acknowledgements

After eight years in graduate school there are probably many people I should acknowledge, but here are the most important. First, I would like to thank John Adelman, for accepting me into his laboratory after having an untraditional start to graduate school, and for providing encouragement and support for six of those years. I would also like to thank Jim Maylie for all his patience and technical assistance with my electrophysiology experiments and my hundreds of related questions. Chris Bond also deserves many thanks for helping me through my cloning and molecular biology difficulties. I would also like to thank lab members Wendy Wu and Mike Lin for their assistance with my slice physiology and Jason Deignan for providing me with a fuzzy footrest for much of my thesis writing. I would also like to thank all the aforementioned people again plus my committee members, John Williams, Peter Larsson and Dave Farrens, and Matthew Frerking for many helpful and thought provoking discussions. My parents Del and Carolee and my sister Lara also deserve a big thank you for all their support and encouragement. And finally, I would like to thank my family Andie and Kenai for making all my efforts worth-wild, and for putting up with this lengthy project.

Abstract

Potassium channels regulate a diverse array of physiological processes, including key aspects of learning and memory. Small-conductance calcium-activated potassium (SK or KCa2) channels are voltage insensitive K channels that are gated solely by intracellular Ca2+. Functional SK channels are formed through heteromeric complexes of α-pore-forming subunits and CaM, with which they are constitutively associated. Ca2+ gating occurs when Ca2+ binds to the N-lobe EF-hands of CaM inducing conformational changes that open the gate and allows K+ to flow through the pore of the channel. Previous work using a proteomics approach demonstrated that SK2 channels bind protein kinase CK2 (CK2) and protein phosphatase 2A (PP2A) to form a macromolecular complex, and that CK2 phosphorylation of SK2-bound calmodulin (CaM) on threonine 80 (T80) decreases SK channel Ca2+ sensitivity by destabilizing the open state of the channel.

The work detailed in this thesis extends the initial findings in a number of ways: First, through the use of 4,5,6,7-tetrabromo-2-azabenzimidazole (TBB), a CK2-specific inhibitor, it demonstrates that CK2 is, *in vivo*, the kinase responsible for T80 phosphorylation. Second, it establishes that CK2 can only phosphorylate SK2-associated CaM when the channel is closed. Third, it defines the physical regions of interaction between the channel and itself, the channel and CK2, and the channel and

the protein phosphatase, PP2A. Fourth, it identifies a mutant SK2 channel (E_RK ala) that no longer binds PP2A. Fifth, it identifies a single lysine residue in the N-terminus of the channel, K121, that serves as an *in vivo* activator of CK2. Sixth, it demonstrates that mutation of this residue to alanine eliminates CK2 activation and shifts the deactivation time constant (τ_{off}) of the channel to a level identical to that observed when the CK2 specific inhibitor TBB (10μM) is added to the WT channel. Seventh, it demonstrates that SK2-floxed mice have small amounts of apamin sensitive current, a result consistent with an important role for the long form of SK2 (SK2-L) in production, targeting and/or trafficking of the SK2 channels. Using this information a model is proposed for how the Ca2+ sensitivity of SK channels is directly regulated by CK2 and PP2A and indirectly regulated through Ca2+ itself, via the state-dependence of CK2. This exquisite system promotes Mg2+ block of NMDA receptors, thus decreasing Ca2+ entry and generating negative feedback on the excitability of dendritic spines and shafts.

Through a collaboration with the laboratory of Patrick Delmas the *in vivo* relevance of our model was validated in a system outside of the hippocampus, noradrenalin (NE) induced modification of SK2 channel Ca2+ sensitivity in superior cervical ganglion (SCG) cells, using our K121A and E_RK ala mutants. Because excitability in hippocampal CA1 neurons is also modulated by NE, and because SK2 channels are closely coupled to NMDA receptors (a Ca2+ source) in the spines of these neurons, it is reasonable to

expect that future studies will identify an *in vivo* role in hippocampal based learning and memory formation for CK2 and PP2A modulation of SK2 channel Ca2+ sensitivity.

Chapter I

Introduction to the hippocampus, plasticity at the CA3-CA1 synapses, and the known components of the SK2 channel multiprotein complex

A Brief History of Neurophysiology and Ion Channels

Living neurons are amazingly complex machines that receive, integrate, and propagate a vast assortment of biochemical and electrical signals. The precisely coordinated output of billions of neurons manifests itself as normal animal behavior. In contrast, even a single point mutation in a single gene can lead to pathological signaling and, potentially, to an untimely death for the organism. A fascination with how normal nervous systems function, and how they can malfunction, has driven generations of scientists to understand neurons and the physiological systems they comprise.

Despite the complexity of neurons a few basic structural features and physical principles govern much of the basic workings of neurophysiology. Arguably the most important of these features is that different concentrations of many ions (most importantly Na^+, Ca^{2+}, Cl-, and K^+) exist inside versus outside of a neuron. These different ion concentrations are separated by a structural feature of unparalleled importance, the neuron's semi-permeable plasma membrane. Within this membrane reside the transporters, pumps, and exchangers that maintain the ionic gradients.

The relationship between the electric potential and the chemical gradient for a single ion can be expressed by the Nernst Equation, which is illustrated below. In this equation E is the electric potential, R is the gas constant, T is the temperature in Kelvin, z the valance of the ion, F the

Faraday constant, X_o is the concentration outside, and X_i is the concentration inside.

Nernst Equation = $$E = \frac{RT}{nF} ln \frac{[X_o]}{[X_i]}$$

When this equation is expanded to include all the relevant ions distributed across a neuron's semi-permeable plasma membrane, a single weighted average of the electrical potential can be computed. This value is the resting membrane potential (Vm). The equation that illustrates this relationship is the Goldman-Hodgkin-Katz Equation[1]. It is depicted below for a plasma membrane that separates differing concentrations of Na^+, K^+, and Cl-. To use this equation the membrane permeability of the different ions must be known, and they are illustrated in this example as P_{Na^+}, P_{K^+}, and P_{Cl-}.

$$V_m = \frac{RT}{F} \ln \left(\frac{P_{Na+}[Na^+]_{out} + P_{K+}[K^+]_{out} + P_{Cl-}[Cl^-]_{in}}{P_{Na+}[Na^+]_{in} + P_{K+}[K^+]_{in} + P_{Cl-}[Cl^-]_{out}} \right)$$

Maintaining these distinct ion concentrations across the semi-permeable membrane is very energy intensive for the neuron, but it is rewarded for this through the generation of an extremely sensitive mechanism for converting changes in ion concentrations and ion permeability into electrical signals.

Theoretically, there are two ways in which a neuron could regulate its Vm, 1) by altering the concentration of the ions across its semi-permeable membrane or 2) by altering the permeability of those ions. However, it turns out that it is faster to alter the permeability than the concentrations. Consequently, to optimize the speed of neuronal communication, most electrical signal propagation is done by altering ion permeability. The prototypical system in which to observe this phenomenon is the action potential of the squid giant axon.

The neuronal action potential was first described by Hodgkin and Huxley in 1939 [2]. A quantitative description of the nonlinear changes in permeability that give rise to the action potential was subsequently described by Hodgkin and Huxley in 1952 [3]. In those experiments squid giant axons were subjected to manipulations of ionic concentrations and currents were recorded using the voltage-clamp technique previously described by Curtis and Cole (1939)[4]. Hodgkin and Huxley's quantitative descriptions of the action potential have remained central to our understanding of how these changes in ion permeability can result in changes in neuronal membrane potential and macroscopic physiological phenomena such as action potentials.

Since that time, further work by Bernstein, Hermann, Cole, Curtis, Katz and others has demonstrated that the permeability changes in the Hodgkin and Huxley equations result from the orchestrated opening and closing of tiny protein pores in the neuronal plasma membrane. These pores

have become known as ion channels. Variation among these ion channels has resulted in each protein evolving a specific role in neurophysiology [5]. Currently, many of these roles are still in the process of being identified.

Additional milestones in ion channel physiology are the following: 1) the development of patch-clamping and single-channel recording [6], which made it possible to study and characterize the properties of ion channels at the level of a single molecule; 2) the cloning of the Na [7] and K channel [8] genes, which led to biochemical and molecular biological descriptions of these ion channels; 3) the crystal structure of the K channel KcsA [9], which has given great insight into what ion channels look like, how they conduct ions through their pores, and how they are gated.

Yet despite these, and other, major advances in our understanding of ion channels and their associated proteins, many questions surrounding the basic physiology of ion channels remain to be answered. The work contained within this thesis aims to detail one basic physiological mechanism of the small conductance Ca^{2+} activated K channel SK2 (KCa2). The primary goal of this research is to more completely understand the role of SK2 channels in hippocampal dependent learning and memory.

The Hippocampal Formation

The hippocampal formation is a collection of brain structures that has been demonstrated to be involved in the generation of episodic memories both in animals and humans. The most famous human case was that of H.M., a patient who had anterograde amnesia after his medial temporal lobes were removed bilaterally in order to prevent epilepsy [10].

Historically the components of the hippocampal formation have been loosely defined, although more recent work indicates that the functional unit of the hippocampal formation is comprised of brain areas Cornu Ammonis 1 (CA1), Cornu Ammonis 2 (CA2), Cornu Ammonis 3 (CA3), dentate gyrus, subiculum, presubiculum, parasubiculum, and entorhinal cortex [11]. A representation of the hippocampal formation and its wiring is illustrated in figure 1. The most notable feature of the hippocampal pathways is that the excitatory connections are unidirectional. Of the major connections illustrated in figure 1, the most frequently studied for N-methyl D-aspartate (NMDA) receptor dependent long-term potentiation (LTP) is the Schaffer collaterals of the CA3 neurons and their synapses onto the dendrites of the CA1 neurons.

SK channels are robustly expressed in both the pre-synaptic CA3 neurons and the post-synaptic CA1 neurons [12,13]. The work contained within this thesis details a mechanism of SK channel Ca^{2+}-sensitivity modulation, which is interpreted in the context of LTP modulation at the CA3 to CA1

synapse. Nevertheless, this phenomenon is clearly relevant to SK channel physiology outside of the hippocampal formation.

Figure 1 Legend.

Basic anatomy and wiring of the hippocampal formation.

The wiring diagram of the hippocampus is traditionally presented as a trisynaptic loop. The major input is carried by axons of the perforant path, which convey polymodal sensory information from neurons in layer II of the entorhinal cortex to the dentate gyrus. Perforant path axons make excitatory synaptic contact with the dendrites of granule cells: axons from the lateral and medial entorhinal cortices innervate the outer and middle third of the dendritic tree, respectively. Granule cells project, through their axons (the mossy fibers), to the proximal apical dendrites of CA3 pyramidal cells that, in turn, project to ipsilateral CA1 pyramidal cells through Schaffer collaterals and to contralateral CA3 and CA1 pyramidal cells through commissural connections. In addition to the sequential trisynaptic circuit, there is also a dense associative network interconnecting CA3 cells on the same side. CA3 pyramidal cells are also innervated by a direct input from layer II cells of the entorhinal cortex (not shown). The distal apical dendrites of CA1 pyramidal neurons receive a direct input from layer III cells of the entorhinal cortex. There is also substantial modulatory input to hippocampal neurons. The three major subfields have an elegant laminar organization in which the cell bodies are tightly packed in an interlocking C-shaped arrangement, with afferent fibers terminating on selective regions of the dendritic tree.

Nature Reviews Neuroscience (2008) 9: 65-75

Figure 1.

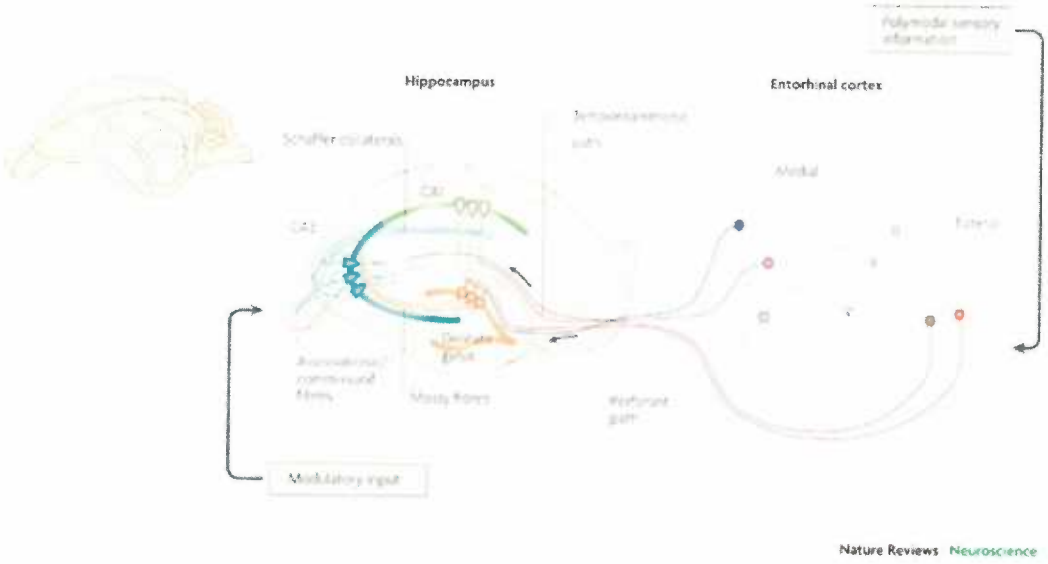

Nature Reviews Neuroscience (2008) 9: 65-75

A Brief History of Synaptic Plasticity and LTP

Overview

Interest in the hippocampal formation intensified in 1973 when Bliss and Lomo published a landmark paper demonstrating that long-term potentiation (LTP) could occur in dentate granule cells after the perforant pathway was electrically stimulated in anesthetized rabbits [14]. LTP seemed to be an obvious candidate for the physical mechanism underlying memory formation, and since 1973 literally thousands of primary research papers, as well as hundreds of review articles [15], have been written on the topic of LTP and its negative correlate, long-term depression (LTD). Amazingly, even with this volume of research it has not been unambiguously established that LTP is both necessary and sufficient for learning and memory [16]. In fact, despite more than 30 years of research on LTP it has only recently been shown that a hippocampal-CA1, NMDA-receptor dependent learning trial (inhibitory avoidance) will actually induce LTP in CA1 neurons [17]. Nevertheless, LTP is clearly important for normal declarative memory, and many important aspects of LTP have become clear over the years: first, there are several different mechanisms for generating LTP (and LTD), and the specific biochemical details of this process differ among brain regions as well as between the specific synapses within a brain region; second, LTP can be mediated by both pre-synaptic and post-synaptic effects, and this differs both with brain region and time scale; third, transcription and new protein synthesis is required for the later stages of LTP.

For the remainder of this document I will focus primarily on LTP, as opposed to LTD, and, furthermore, I will focus on the type of LTP that requires the NMDA receptor and occurs at the CA3 to CA1 synapses in the hippocampal formation.

LTP is most commonly induced using a tetanus, which is a brief, high frequency train of electrical stimuli. Although LTP was first described using a tetanus of 100Hz, the *in vivo* event that is thought to promote LTP is the simultaneous, or near simultaneous, pairing of a postsynaptic back-propagating action potential (bAP) with a pre-synaptic theta-burst [18,19]. A theta-burst is one of two very different types of signals the hippocampus is involved in processing and consists of 5-10Hz electrical 'waves' that occur when the animal is awake and actively exploring or during rapid eye movement (REM) sleep. The second type of input to the hippocampus is irregular, large amplitude sharp waves (SPWs) [18].

One of the most quoted statements concerning biological learning is Hebb's postulate which states: "*When an axon of cell A is near enough to excite a cell B and repeatedly or persistently takes part in firing it, some growth process or metabolic change takes place in one or both cells such that A's efficiency, as one of the cells firing B, is increased*" [20]. The desire to understand the physiological and biochemical mechanisms behind this statement has driven much of the research on learning and memory, and ultimately the modification of the efficiency by which neuron A fires neuron

B, otherwise known as synaptic plasticity, is at the heart of the LTP question.

Synaptic plasticity reflects the ability of a neuron to change the effectiveness at which a pre-synaptic neuron fires a post-synaptic neuron, i.e. synaptic strength. In LTP this is a long-term change. In contrast, a short-term plasticity will arise at a synapse as the result of synaptic facilitation, which occurs when two or more action potentials (APs) invade the presynaptic terminal in close succession. If the excitatory postsynaptic potentials (EPSPs) of the first and second events are compared, the second AP generates a larger post-synaptic response. This facilitation occurs because residual Ca^{2+} in the pre-synaptic terminal generates a larger amount of vesicle release. This is the basis for paired-pulse facilitation, a common protocol used to determine whether a manipulation of the synapse causes pre- or post-synaptic effects. However, this form of potentiation returns to baseline fairly quickly. Consequently, something quite different is occurring during LTP.

So what other features define LTP? LTP most frequently occurs when synaptic inputs arrive synchronously and are spatially clustered in a dendritic branch. This generates a large influx of Ca^{2+} in the dendrite, which performs a nonlinear integration and results in an increase in synaptic strength. When dendritic inputs arrive asynchronously or are highly distributed in space, on the other hand, a linear integration occurs, which generates a small influx of Ca^{2+}. This limited amount of Ca^{2+} generates LTD

and the accompanying decrease in synaptic strength [21] [22]. Furthermore, in 1983 Levy and Steward demonstrated that pairing a weak stimulation with a strong stimulation generates LTP or LTD depending upon the timing of the two stimuli [23]. Since that time, much work has been done to characterize this spike-timing dependent plasticity (STDP). What has been found is that STDP is essentially a higher-order phenomenon that depends on the specifics of intracellular Ca^{2+} dynamics, especially the Ca^{2+} flowing through NMDA receptors. Like LTP, the precise details of STDP vary from one type of synapse to another. This variability is due to a number of factors including 1) the length of time the glutamate-bound NMDA receptors are free from their Mg^{2+} block, 2) the non-linear Ca^{2+} dependence of many post-synaptic proteins, especially CaMKII and calcineurin; 3) the kinetics of EPSP-activated dendritic conductances that modify the shape of the bAP, 4) the density of K currents, such as IA and, BK and SK channels which contribute to, or modulate, bAP shape and Ca^{2+} influx [24]. The STDP profile can also altered by neuromodulators such as noradrenalin (NE) [25].

So how does the coincidence between a bAP and an EPSP lead to LTP? Remarkably the mechanism begins with the biochemistry of only a few different molecules, the most important being Ca^{2+}, NMDA receptor, the alpha-amino-3-hydroxy-5-methyl-4-isoxazole propionic acid (AMPA) receptor, and calcium/calmodulin-dependent protein kinase II (CaMKII). However, many other proteins significantly regulate LTP. Some of the most important are A-kinase anchoring proteins (AKAPs), membrane-associated

guanylate kinases (MAGUKs), and transmembrane AMPA receptor regulatory proteins (TARPs). Also, gradients of many ion channels exist between proximal and distal dendrites. The contribution of each of these factors to LTP is subsequently reviewed.

Calcium (Ca^{2+})

The calcium concentration between the extracellular environment and the intracellular environment differs between four orders of magnitude, from $1x10^{-3}$M outside the dendrite to $70x10^{-9}$M inside the dendrite [26] [27]. This exquisite opportunity for signal generation has been taken advantage of by nearly every important biological system, including synaptic plasticity. Information from Ca^{2+} entry is conveyed by the spatial location, amplitude, duration and frequency of individual Ca^{2+} transients [28], and, remarkably, an increase in intracellular Ca^{2+} is all that is needed to obtain LTP or LTD, as demonstrated through the use of the caged calcium compound nitr-5 to circumnavigate pre-synaptic activity [29].

Ca^{2+} generally enters the cytoplasm of a hippocampal CA1 neuron from three different sources: voltage sensitive Ca^{2+} channels (VSCC), release from intracellular stores, and through the NMDA receptor. Importantly, the interpretation of this Ca^{2+} signal depends on the microdomain in which it occurs. Of the three sources, the Ca^{2+} entering through the NMDA receptor is the most important for LTP. The time course of this Ca^{2+} influx through the NMDA receptor is due to the slow dissociation

of glutamate from the NMDA receptor and the fast reblocking of the channel by extracellular Mg^{+}, which is controlled by the voltage across the membrane [30].

Ca^{2+} is extruded from small dendrites and spines in CA1 hippocampal primarily from plasma membrane Ca^{2+} pumps (PMCAs) and Na^{+}/Ca^{2+} exchangers. Extrusion is slowed in an activity-dependent manner, an event that is, at least partially, controlled by Ca^{2+}-dependent inactivation of the PMCAs. This generates a positive feedback loop that amplifies small Ca^{2+} influxes [31], and may be why R-type VSCC's have been shown to be depressed for at least 30 minutes after a train of bAPs [32].

Biochemical Memory through CaMKII

CaMKII is a synapse-enriched kinase that is one of the few molecules that is an indispensable mediator of Schaffer collateral, CA3 to CA1 LTP [33]. CaMKII consists of a double layered, hexameric ring of either hetero- or homomeric complexes of α and β CaMKII. CaMKII is activated by Ca^{2+}/CaM binding, which enables the kinase to phosphorylate its substrates and promotes intersubunit Thr286 autophosphorylation. Both the affinity of CaMKII for CaM and the time-to-release of CaM increase threefold after autophosphorylation of Thr286. The result is that CaM is trapped and, consequently, the CaMKII remains activated even after the Ca^{2+} has dissociated from CaM [34]. This ability of CaMKII to 'remember' that a Ca^{2+} signal has occurred is a key feature of LTP.

Three factors contribute to deactivation of CaMKII: 1) CaMKII, once activated by Ca^{2+}/CaM, can also autophosphorylate residues Thr305 and Thr306, which serve to block Ca^{2+}/CaM rebinding. 2) A slow autophosphorylation of Thr306 occurs in the absence of Ca^{2+}/CaM binding. 3) Activation of protein phosphatase 1 (PP1) dephosphorylates and inactivation the kinase.

Activity of a synapse leads to the translocation of diffusible CaMKII to the postsynaptic density. CaMKII then becomes trapped at the postsynaptic density (PSD), an effect mediated by Thr286 autophosphorylation and kinase activation. There it forms multiprotein deposits or "towers" on the PSD-95 meshwork [35]. Dissociation from the PSD only occurs after several minutes and requires both CaMKII autophosphorylation on Thr305 and Thr306 and PP1 activity. However, even after it has dissociated, recently activated CaMKII shows an increased propensity to reassociate with the synapse, a phenomenon labeled 'translocation priming' [36]. This likely occurs because a few of the 12 CaMKII subunits remain phosphorylated on Thr286.

CaMKII activation promotes LTP in at least two ways: 1) It phosphorylates the GluR1 subunit on S831, which increases unitary conductance of homomeric GluR1 AMPA receptors [37]. 2) It leads to AMPA receptor insertion [38]. These events are both promoted by the binding of CAMKII to two sites on the NMDA receptor. The first site is dependent upon

Ca^{2+}/CaM being bound to CaMKII, but not on CaMKII being autophosphorylated. The second site requires both events [39] [40].

CaMKII is amazingly sensitive to Ca^{2+} concentrations and can go from totally inactive to completely active within a 300nM range of Ca^{2+}. This extreme sensitivity is due to cooperativity between Ca^{2+}/CaM binding, Ca^{2+} sensitivity of autophosphorylation and dephosphorylation by PP1, all of which serve to increase the hill coefficient of the Ca^{2+} dose-response curve [41].

NMDA receptors and their coincidence detection function

NMDA channels are ionotropic glutamate receptors that are non-selective cation channels. They are tetrameric and are most likely composed of two adjacent NR1 subunits and two adjacent NR2A and/or NR2B subunits [42]. This subunit composition of NMDA receptors changes both with the age of an animal and with activity of a synapse from NR2B containing receptors to NR2A containing receptors [43]. It has been reported that the subunit composition of the NMDA receptor is important for mediating LTP (NR2A) and LTD (NR2B)[44]. However, this is still a topic of controversy because, among other reasons, an NR2A subtype specific inhibitor does not impair LTP in mouse hippocampal slices [45].

Two extraordinary properties of the NMDA receptor are responsible for its central role in the LTP of the CA3 to CA1 synapse. These two properties are the following: 1) during regular synaptic transmission Mg^{2+}

blocks the pore of the channel [46], thus preventing glutamate from opening it; 2) unlike GluR2-subunit-containing AMPA receptors, NMDA receptors are permeable to Ca^{2+}. Consequently, any pre-synaptic release of glutamate that coincides with depolarization of the post-synaptic neuron will result in Ca^{2+} influx through the NMDA receptor. As previously mentioned, this Ca^{2+} influx is the mediator of plastic changes in the synapse.

Ca^{2+} influx through NMDA receptors is primarily important because of the other, Ca^{2+}-sensitive, proteins in the NMDA receptor microdomain. The two most important are CaMKII and the protein phosphatase calcineurin (PP2B), which is further described in the 'Calmodulin' section of this thesis. Calcineurin, a Ca^{2+}-activated phosphatase, is the primary mediator of LTD. One of the ways it decreases synaptic strength is by decreasing the mean open time, burst duration, cluster duration and overall P_o of the NMDA receptor [47].

NMDA receptors are trafficked through the endoplasmic reticulum (ER) and Golgi apparatus to the synapse where they bind to post-synaptic density-95 (PSD-95) through their C-terminal, post-synaptic density 95, disk large, zona occludens-1 (PDZ) binding domains. During this trafficking process they are bound to synapse-associated protein 102 (SAP102), which is in turn bound to the PDZ binding domain of sec8 of the exocyst complex. This protein complex is bound to intracellular membrane vesicles that target proteins to sites of fusion with the plasma membrane [48].

The Plasticity of AMPA Receptors

AMPA receptors are ionotropic glutamate receptors that are responsible for most of the excitatory transmission in the nervous system. There are four different subunits that can be contained in the tetrameric channel: GluR1, GluR2, GluR3 and GluR4. In hippocampal CA1 neurons AMPA receptors are usually composed of GluR1/2 or 2/3 subunit combinations, although GluR 1/1 homomers are present and may play an important role in LTP [49]. The subunit composition of AMPA receptors is important because GluR2 subunits undergo RNA editing (Q607R) that makes them impermeable to Ca^{2+}, among other changes [50].

AMPA receptors undergo a constant recycling into and out of the plasma membrane, and at least some of this recycling is dependent upon Ca^{2+} influx through the NMDA receptor (for review see Derkach et al, 2007 [51]). Once in the membrane AMPA receptors either remain extrasynaptic or become clustered at the PSD. Delivery of AMPA receptors to the extrasynaptic plasma membrane is controlled by PKA mediated phosphorylation of S845 of AMPA receptor subunit GluR1 [52]. This phosphorylation event is enhanced following LTP and serves to increase the pool of AMPA receptors available for synaptic incorporation [53].

When AMPA receptor insertion occurs at synapses that have previously only contained NMDA receptors these previously 'silent' synapses will now fire during normal excitatory transmission; hence, presynaptic activity alone will now generate an EPSP [54].

AMPA receptor insertion is primarily controlled by the subunit GluR1, and LTP-driven insertion of GluR1 is entirely controlled by its C-terminus. Consequently, delivery of the C-terminus of GluR1, and its associated cargo, is another essential mediator of LTP[55]. The importance of the GluR1 subunit is demonstrated by GluR1 knockout mice, which show very little LTP and LTD[56]. Mutant mice that lack both GluR2 and GluR3, on the other hand, (GluR1 and GluR4 expression remained normal) have essentially normal LTP and LTD [57]. Recently GluR1 subunits have been shown to be specifically targeted to mushroom-type spines, following fear-conditioning [58]. This data supports the theory of synaptic tagging in which only certain "tagged" synapses have the machinery to capture plasticity enhancing molecules, in this case GluR1 [59].

AKAPs, MAGUKs and TARPs

In addition to the aforementioned "essential" molecules of LTP, there are many additional modulatory components that are important for proper synaptic plasticity. Three of the most important are the A-kinase anchoring proteins (AKAPs), the membrane-associated guanylate kinases (MAGUKs), and the transmembrane AMPA receptor regulatory proteins (TARPs). Each of these is reviewed below.

Scaffolding proteins connect AMPA and NMDA receptors to a variety of signaling proteins, the actin cytoskeleton, and synaptic adhesion

molecules. Probably the most important for synaptic plasticity is AKAP, which binds the protein kinase A (PKA), the protein phosphatase calcineurin (PP2B), the actin cytoskeleton, and the MAGUKs PSD-95 and SAP97. AKAPs, especially AKAP79/150, use these interactions to organize and choreograph the biochemical events that occur during synaptic plasticity [60]. Furthermore, AKAP79/150 may contribute to LTD by redistributing itself away from the PSD after brief NMDA receptor activation, at the magnitude that results in a low level of Ca^{2+} influx [61].

The question of how glutamate receptors become clustered at the PSD is central to the physiology of synaptic plasticity, and certainly a group of proteins known as the MAGUKs play a major role. The MAGUK family shares a common domain organization consisting of three PDZ domains followed by an SH3 domain followed by a kinase dead, guanylate kinase-like domain. The most important role of the MAGUK family is that they facilitate receptor clustering through their PDZ domains. These are ~90 amino acid protein/protein interaction domains that bind short, usually C-terminal, peptide sequences known as PDZ-binding domains, the classic version being (T/S)XV. Notably, both the NR2A and NR2B subunits of the NMDA receptor contain PDZ binding domains that bind the MAGUK scaffolding protein PSD-95. This interaction mediates clustering of the NMDA receptors and is essential for signal transduction and normal synaptic plasticity [62]. In fact, in two different KO mice of PSD-95, LTP is enhanced while LTD is decreased. Furthermore, over-expression of PSD-95

prevents LTP and enhances LTD[63]. The MAGUK family member SAP-97, on the other hand, binds to AMPA receptor subunit GluR1 and mediates AMPA receptor clustering in mature synapses [64].

Despite the huge volume of literature on the MAGUK family, dissecting out distinct functions of MAGUK family members is proving to be difficult. Even in a double KO of PSD-95 and PSD-93, compensation occurs via up-regulation of SAP-102; hence, AMPA and NMDA receptor can still be trafficked and inserted. A promising approach to combat this problem is to use short hairpin RNAs (shRNAs) to silence PSD-95 or PSD-93. This has led to largely non-overlapping patterns of silencing [65] [63].

It is still not entirely clear what controls the dynamic process of AMPA receptor insertion. However, stargazin (γ-2) and other TARPs γ-3, γ-4, and especially the hippocampal enriched γ-8 [66], clearly play a major role. TARPs physically associate with AMPA receptors and permit them to be trafficked from the ER to the synaptic membrane. This trafficking feature is wholly contained within a domain that is near, but not at, the C-terminus (aa 203-269) of stargazin and provides not only a signal for surface expression, but also a synaptic targeting function as well [67]. The very C-terminus of stargazin contains a PDZ binding domain that mediates its interaction with PSD-95 and SAP-97[68]. Stargazin can be highly phosphorylated at nine serine residues in the C-terminus, possibly in a 'rheostat'-like manner. This phosphorylation occurs through the Ca^{2+}-sensitive kinases PKC and CamKII[69]. Interestingly enough, the nine serine residues are completely

contained within the 203-269 region that is both necessary and sufficient for the AMPA receptor trafficking signal. Dephosphorylation of the nine serines is mediated primarily by PP1 with some contribution from PP2B and is activity dependent, since the presence of TTX or APV prevents it [69].

Despite this large quantity of research, the mechanism by which phosphorylation of stargazin enhances synaptic trafficking remains unclear, although the working hypothesis is that phosphorylation makes stargazin more mobile in the membrane and hence easier to recruit to the PSD[69]. To complicate matters, differences have been observed in AMPA receptor trafficking between hippocampal slice cultures and dissociated neuronal cultures. In hippocampal slice cultures AMPA receptors are clustered at the post-synaptic density through their interaction with stargazin, which binds the first two PDZ domains of PSD-95 [70]. This effect is not observed in dissociated neuronal cell cultures[68]. Differences have also been reported by Roberto Malinow's laboratory [71]. Furthermore, like the MAGUKs, redundancy in the TARP family has made establishing a clear role for TARP family members difficult.

Gradients of Dendritic Channels

Dendritic excitability is to a large degree controlled by the specific types of ion channels present and how these channels are regulated. In fact, the membrane concentration and location of many dendritic ion channels is not constant throughout the dendritic arborization, and proximal

to distal ion channel gradients are frequently present. Predictably, this feature modulates the shape of the bAP, Ca^{2+} entry, and overall dendritic excitability [72]. The major ion channel gradients are briefly reviewed below.

Dendrites are essentially long narrow cables bathed in an electrically conductive medium. Consequently, an EPSP further from the soma of a neuron would be expected to have less of an effect on excitability at the soma. This is not the case because a gradient of AMPA receptors exists, increasing from proximal to distal, and this gradient serves to normalize EPSP amplitudes [73].

Na channels in CA1 pyramidal neurons serve as the conductor of both the bAP and forward propagating dendritic spikes. Although Na channels are expressed at a uniform density from the initial segment of the axon to at least three-quarters of the length of the main apical dendrite, Na channels in the distal dendrites activate at more hyperpolarized voltages than those in the proximal dendrites, due to a greater level of phosphorylation at proximal dendrites. The primary effect of this is to maintain a more depolarized Vm in the proximal dendrites [74].

Ca^{2+} channels have a relatively uniform density along the dendrites, but the distribution of the subtypes differs along the dendrite. L- and N- type Ca^{2+} channels have higher concentrations near the soma and in the proximal dendrites while R- and T- type channels are more numerous in the distal dendrites [75].

Hyperpolarization-activated cyclic-nucleotide gated (HCN) channels are important for regulating temporal summation and neuronal excitability at the perforant path in the distal dendrites, but have little effect at more proximal dendritic locations [76]. In accordance with this, it has been observed that HCN channels are distributed in a gradient with the lowest concentration of channels being proximal and the highest concentration being in the distal dendrites [77].

The non-inactivating class of K channels exists in a uniform pattern along the dendrite; however, the concentration of inactivating A-type K channels increases from proximal to distal dendrites [78]. Furthermore, additional levels of regulation may exist: these two groups have been historically classified as separate entities, based on the specific α and/or β subunits involved; yet work from Bernd Fakler's laboratory (2004) has demonstrated that the composition of the membrane lipids can bi-directionally modulate these channels between non-inactivating delayed rectifiers and rapidly inactivating A-type channels [79].

SK2 channels are also maintained in a gradient in CA1 hippocampal neurons. Few SK2 channels are located in the soma, numbers increase in the proximal stratum radiatum, and the concentration peaks in the distal stratum radiatum and stratum lacunosum moleculare. This was demonstrated through immuno-electronmicroscopy (iEM) using a pan-SK2 antibody (Adelman Lab, unpublished data).

Consequently, the exact input-output transformation occurring in a given neuron will depend not only on its specific complement of ion channels, but their proximal to distal gradient, phosphorylation state, and lipid environment, among other modifying variables.

Summary of Synaptic Plasticity

The synaptic strength of most synapses in the brain can be altered for long periods of time after certain types of stimulation. If the efficiency at which a pre-synaptic neuron fires a post-synaptic neuron increases LTP has occurred. If it decreases, LTD has occurred. An increase in synaptic strength is initiated at CA3 to CA1 synapses when a large amount of Ca^{2+} enters through the NMDA receptor. This results in AMPA receptor recruitment to the PSD from extrasynaptic membranes, beginning with Ca^{2+}-permeable, GluR1 homomeric channels. Trafficking of AMPA receptors to the extrasynaptic membrane also increases, following phosphorylation of S845 on AMPA receptor subunit GluR1. Furthermore, an increase in AMPA receptor Po and single channel conductance occurs through S831 and S845 phosphorylation respectively. The kinase that phosphorylates S845 is PKA, which is localized to the PSD by the scaffolding molecule AKAP79. AKAP79 also localizes PP2B, which is the primary mediator of LTD, in part through regulation of PP1. LTD results, in large part, from AMPA receptor internalization.

The Ca^{2+}-sensitive kinase CaMKII is localized to the PSD where it binds to the C-terminus of the NMDA receptor and, among other functions, phosphorylates S831 on AMPA receptor GluR1 subunits. The special biochemical features of CaMKII provide a 'memory' of Ca^{2+} entry through the NMDA receptors. TARPs link AMPA receptors to the PSD-95 and other MAGUKs and these two protein families contribute to the trafficking and clustering of AMPA and NMDA receptors. Furthermore, gradients of channels in the dendrites shape the bAP and excitability of the dendrite. Together, these and other factors come together to bring about plasticity changes in the synapses between CA3 and CA1 neurons in the hippocampal formation.

So how do SK2 channels fit into this milieu of proteins that create, maintain and modulate synaptic plasticity? There are two ways that have been currently described in the literature. First, SK2 channels form a negative feedback loop with the NMDA receptor, where their hyperpolarizing K currents promote $Mg^{+}2$ block of NMDA receptors and limit Ca^{2+} influx. Second, SK2 channels actively contribute to synaptic plasticity itself, and this value has been calculated to be ~13% of the total. They do this by being removed from potentiated synapses through PKA phosphorylation of the SK2 C-terminus. This thesis details a mechanism of SK channel regulation that may prove to be a third method by which SK2 channels influence synaptic plasticity and memory formation.

Calmodulin

The waveforms of transient, intracellular Ca^{2+} signals encode information that is decoded by a variety of intracellular Ca^{2+} sensing proteins. Perhaps the most important of these is calmodulin (CaM). CaM is part of the EF-hand family of Ca^{2+}-binding proteins which get their name from an N-terminal helix (E-helix) followed by a Ca^{2+} coordination loop, followed by a C-terminal helix (F-helix), which, structurally, resembles the thumb, index and middle fingers of a hand. Members of this family include the Ca^{2+} buffers parvalbumin and calbindin and the Ca^{2+} sensors troponin C, recoverin and the S100 family of proteins.[26]

There are four EF-hands contained within CaM, two in the N-terminal lobe and two in the C-terminal lobe. The Ca^{2+} sensitivity of the C-terminal lobe EF-hands is 3-5 fold higher than the N-terminal lobe EF-hands, which extends the dynamic range of this Ca^{2+} sensor. These two domains adopt different structures in the absence of Ca^{2+}; the more sensitive C-terminus adopts a 'semi-open' structure while the N-terminus adopts a 'closed' conformation. Binding of Ca^{2+} causes major changes in the structure of CaM. The central α-helix is stabilized and the EF-hands transition from their 'semi-open' or 'closed' state to 'open' states. As a result of these conformational changes methionine-rich crevices and hydrophobic residues are exposed which mediate CaM's interaction with its target proteins. These structural changes essentially convert a Ca^{2+} signal into free energy that can alter the structure of interacting protein partners. One

example of this is the conversion of an intracellular Ca^{2+} signal into gating of the SK channel via associated CaM.

One of the most important features of CaM is that its Ca^{2+} sensitivity is modulated by its protein-binding partners. The most important examples of this for plasticity are CaMKII, PKC, the CaM-stimulated adenylyl cyclases, calcineurin (PP2B), and the SK channels. For example, the central importance of calcineurin to LTD is derived from the fact that it has a Ca^{2+} sensitivity that is lower (Kd = 0.1-1nM) than any LTP promoting, Ca^{2+} sensing protein. This feature is of the utmost importance for plasticity because it allows increases in intracellular Ca^{2+} levels to mediate signals that both enhance and weaken synaptic strength. Furthermore, it allows the NMDA receptor to serve as the Ca^{2+} source for both LTD and LTP. This effectively transduces coincidence, or discordinance, of post-synaptic depolarization and presynaptic activation into a modification of synaptic strength. One of the key targets of calcineurin is the phosphorylated form of protein phosphatase inhibitor 1 (I1). This protein is a potent inhibitor of protein phosphatase 1 (PP1) [80] and serves a crucial role in dephosphorylating CaMKII and the AMPA receptors and promoting LTD. Another important event following calcineurin activation is a decrease in the mean open time, burst duration, cluster duration and overall Po of the NMDA receptor [47].

Further adaptability of the Ca^{2+} sensor CaM results from phosphorylation, which has been reported on eight of its 149 residues. Not

surprisingly, these modifications have been demonstrated to regulate CaM's Ca^{2+} sensitivity and its affinity for its protein binding partners[81].

SK channels

The first reported dependence of a potassium permeability on Ca^{2+} was made in 1958 by G. Gardos, who demonstrated that EDTA could prevent a rise in extracellular potassium concentration in solution containing human erythrocytes [82]. It took until 1972 for a paper to follow this up with a demonstration that by injecting Ca^{2+} into a neuron (giant neurons of *Aplysia californica* abdominal ganglion) a hyperpolarization occurred that was due to an increase in potassium conductance [83]. This effect was reversibly blocked by 50mM TEA, a concentration that is sufficient to block SK channels [84].

Three SK channel family members (SK1, SK2, SK3) were cloned during the 1990's by searching for structures resembling K channel pore regions in the available sequence databases, followed by screening both a human hippocampal and a rat brain cDNA library with radio-labeled probes [85]. The SK channel family member IK1 was cloned a short time later using similar methods, but from a human pancreas cDNA library [86].

Work with antibodies for SK1, SK2 and SK3 demonstrate that SK channels are expressed in distinct, but overlapping patterns in the central nervous system [87], as well as in many tissues of the periphery. The fourth SK channel family member (IK1) is only expressed in the periphery [86]. SK1, SK2, and SK3 are expressed in all structures in the hippocampus, but to varying degrees [12]. RT-PCR and *in situ* hybridization results also demonstrate that SK channels are expressed in many tissues throughout the body [88].

SK1 undergoes extensive alternative splicing [89], whereas only one splice variant has been reported for SK2 (generating SK2-long and SK2-short) and no splice variants have been described for SK3 or IK1. SK channels are generally believed to be homomultimers *in vivo*, but one laboratory has reported the formation of heteromultimers *in vitro* [90]. Also, SK2-long and SK2-short have been shown to heteromultimerize *in vitro* and *in vivo* [91]. Recently, it was demonstrated there was no effect of the selective SK channel inhibitor apamin on EPSP amplitude in transgenic mice that express only SK2-short. Appropriately, immuno-electronmicroscopy (iEM) data indicate that these animals lack SK2 channels on dendritic spines and shafts. These data demonstrate that SK2-long controls trafficking of SK2 channels to the dendrites (Adelman lab. unpublished).

SK channels have a similar overall structure to the voltage-sensitive Kv channels in that they are tetrameric and each subunit consists of six membrane-spanning domains that leave the channels with intracellular N- and C- termini. SK channels are solely gated by intracellular Ca^{2+} ions with EC_{50}s of between 0.3 and 0.5 μM [85]. Calmodulin (CaM) is constitutively bound to a region on the intracellular C-terminus of all SK channel family members and the binding of Ca^{2+} to the N-lobe EF-hands of SK-bound CaM induces conformational changes that open the gate of the channel [92-94] and allow K ions to flow through the pore of the channel. Notably, the activation gate of SK2 is not located at the S6 bundle-crossing like the voltage-gated

(Kv) channels. Instead it is located in the vestibule of the channel either in, or very close to, the selectivity filter [95] [96].

The Ca^{2+} sensitivity of the SK channel family is modulated by the small molecule 1-ethyl-2-benzimidazolinone (1-EBIO). 2mM 1-EBIO shifts SK channel Ca^{2+} sensitivity from 0.3-0.5μM to 0.07-0.08μM and slows channel deactivation by approximately 10-fold [97]. More potent inhibitors of SK channels are DCEBIO (EC50 = 27μM) and NS309 (EC50 = 0.62μM) whereas the EC_{50} of 1-EBIO was 453μM in the same data set. Recently an SK channel subtype specific modulator (CyPPA) was demonstrated to be a positive modulator of hSK3 and hSK2, but was inactive towards hSK1 and hIK1 [98].

The constitutive, Ca^{2+} independent interaction between the α-pore forming subunits of SK channels and CaM is also necessary for controlling surface expression of SK channels [99]. Interestingly, the constitutive interaction is not absolutely required for gating [99].

In the periphery, SK channels have been reported to contribute to the regulation of respiration and parturition [100], the regulation of urinary bladder smooth muscle contractions [101], regulation of the glucose response in pancreatic β-cells [102], and in modulation of arterial tone and blood pressure [103]. SK channels also have a role in pathology, as their expression increases after skeletal muscles are denervated, an event that results in hyperexcitability of the denervated muscle [104]. This pathological role of SK channels is potentially important for treating patients with myotonic muscular

dystrophy [105]. There is also one report associating the expression of an SK3 N-terminal fragment with schizophrenia [106].

In addition to a wide variety of functions in the periphery, several important roles have been described for SK channels in the central nervous system. These include modulation of gonadotropin-releasing hormone (GnRH) induced current oscillations in anterior pituitary [107], the control of excitation and synaptic integration in hippocampal and cortical neurons [108,109], pacemaking in the substantia nigra, rapid firing and mode switching in the cerebellum and inhibition in the organ of Corti [110,111]. They have also been shown to control oscillations in the nucleus reticularus in the dorsal thalamus, which helps control sleep (Cueni et al, unpublished work).

The role of SK channels in the hippocampal formation is especially intriguing due to the fact that intraperitoneal injections of the specific SK channel inhibitor apamin (which then crosses the blood-brain barrier) improves performance in hippocampal-dependent memory tasks [112]. All three SK family members are present in the hippocampal formation will large apamin-sensitive currents found in CA1 and CA3 neurons (80-170pA), and small currents found in the dentate granule cells (<50pA) [12,113]. Historically it was believed that SK channels were responsible for generating the mAHP and contributing to spike-frequency adaptation [114] in the hippocampal CA1 neurons. However, recent work from Johan Storm's laboratory (and others) suggests that the M-current is responsible for the mAHP [115]. Indeed, recent evidence points to a role for SK channels in both

the dendrites and the axons [116-118](Adelman lab, unpublished data), and recent electron-micrograph (EM) studies have demonstrated that SK2 channels are colocalized to the PSD with the NMDA receptor in the spines of native CA1 neurons [119]. In this dendritic location they serve to control excitability in the shafts of CA1 neurons by controlling the duration of dendritic plateau potentials [120] Most importantly however, SK channels have a role in modulating synaptic plasticity through a negative-feedback loop with the NMDA receptor [118,121] and they contribute to LTP itself (~13% of total LTP) through PKA mediated internalization of SK2 channels from potentiated spines [119]. Three adjacent C-terminal serine residues Ser568,569,570 in the SK2 C-terminus control this internalization, as demonstrated by a previous study in COS7 cells [122].

The Ca^{2+} source for SK channels in CA1 neurons is still a matter of debate, and likely depends on the precise location of the channels in question. Although in acutely dissociated CA1 hippocampal neurons the Ca^{2+} source was found to be L-type calcium channels [123], the Ca^{2+} source seems to be either R-type calcium channels [124] (also, Adelman Lab. unpublished data) or the NMDA receptors themselves [118]. Indeed, it may turnout that, like AMPA receptors, important differences exist between cultured neurons and slices.

Modulation of SK channels has been linked to the neurotransmitters NE in the preoptic area [125] and somatostatin in medium spiny neostriatal neurons [126]. It has also been demonstrated that a sigma

receptor-1 agonist, (+)pentazocine, potentiates NMDAR responses and LTP by "preventing a small conductance Ca^{2+}-activated K^+ current (SK channels)...to open" [127]. It is likely that this effect is through the CK2 and PP2A mediated regulation of SK channel Ca^{2+} sensitivity that is detailed within this thesis.

Protein Kinase CK2

Protein kinase CK2 (formerly known as casein kinase 2) is likely the most active and pleiotropic kinase in Eukaryotic cells (for reviews see the following: [128,129]). Not surprisingly, CK2 is essential for life and eliminating all isoforms of CK2 is lethal in yeast, Dictyostelium and mice [130]. CK2 phosphorylates serine and threonine residues, and may even be able to phosphorylate tyrosine residues in some instances [131], although *in vivo* evidence of this is lacking. The consensus sequence for CK2 has been reported as S/TXXD, but many variations on this motif can be phosphorylated by the kinase, with the presence of acidic residues between n-4 and $n^{+}7$ enhancing phoshorylatability of the substrate. Currently more than 300 substrates have been identified [129]. In the process of identify these substrates it has become clear that charge and shape play as much of a role in controlling the binding and activity of CK2 as a consensus sequence [132].

The majority of CK2 is found as heteromultimers composed of two catalytic α subunits, one α and one α' subunit, or two α' subunits bound to a dimer of CK2β [129], although they may have functions independent of the holozyme. Remarkably, α' subunits are found in neither *Drosophila* nor *Xenopus* [133]. CK2α' is more associated with dendrites than CK2α, furthermore CK2α' is expressed to a greater degree in brain than CK2α [134]. Knocking out CK2α' in mice results in globozoospermia and infertility in male mice. This makes sense on one hand, since CK2α' is preferentially

expressed in the brain and testis. However, the absence of a brain phenotype is puzzling, unless CK2α is completely redundant with CK2α' in the brain. A more likely scenario is that the brain phenotype has yet to be found [135].

Two proteins have been identified that have isoform specific interactions with CK2. One is the protein (CKIP-1), which interacts with CK2α but not CK2α' and was identified using a yeast 2-hybrid assay [136]. The other, provocatively, is PP2A [137]. This CK2/PP2A complex has been shown to directly regulate transcription of endothelial nitric-oxide synthase [138].

The crystal structure of CK2α in complex with CK2β has been solved [139]. This has generated an image of the CK2 holoenzyme as a butterfly shaped molecule with dimensions of 155 x 90 x 66 Å in which the two CK2α subunits are not in contact with one another, yet associate with a dimer of CK2β subunits. CK2β was shown neither to block the active site of the kinase nor affect the active segment in the crystal structure. Furthermore, the crystal structure demonstrates that the acidic loop in CK2β is more than 30 Å away from the nearest basic cluster in CK2α. The crystal structure also demonstrates that the acidic loop of CK2β forms a wedge-like structure that limits the access of substrates to the active site of the kinase. It could also bind to the basic cluster on another CK2 holoenzyme, thus forming a higher order aggregate. This has been observed in vitro [140], and opens up the possibility for CK2 to generate large deposits like CaMKII [35].

Collectively, these data are consistent with a role of CK2β in targeting and modulation of the CK2 holozyme.

The CK2 heteromultimer has also been reported to undergo autophosphorylation on Ser2 and Ser3 of the CK2β subunits and an unidentified site in the α subunits [141]. However the phosphorylation status of CK2β has not been reported to have a significant effect on the kinase activity of CK2 towards several different substrates, including CaM [142]. Hence it is still unclear what role, if any, CK2 autophosphorylation plays *in vivo*.

CK2 has many cellular roles including the regulation of cell cycle, signaling and transcription; however, CK2 is more abundant in brain than in any other tissue. "This begs the question: what is all that CK2 doing in the central nervous system" [143]? One of the initial studies describing a role for CK2 in the nervous system looked at the activity of the kinase at various time points after high-frequency (2 trains of 100 Hz, each train 500ms) stimulation. What was observed was that CK2 activity increased within 2 minutes after LTP induction, reached a peak of ~2x baseline activity at 5 minutes, then returned to baseline within 15 minutes [144]. CK2 has also been linked to NMDA receptor function in two different ways. First, in 1999 David Lieberman and Istvan Mody demonstrated that the activity of NMDA channels in cell-attached and inside-out patch recordings from dissociated rat dentate granule cells was enhanced by the application of purified CK2 or spermine and decreased by specific inhibitors of CK2. Furthermore, when

field recordings were made from dentate neurons in rat slices NMDA receptor, but not AMPA receptor, mediated EPSPs decreased in the presence of specific CK2 inhibitors [145]. The second way CK2 has been linked to NMDA receptors is through data showing that trafficking of the NR2B subunit is regulated through CK2 phosphorylation of the PDZ ligand IESDV on serine 1480. This was shown to disrupt the interaction of NR2B with the PDZ domains of PSD-95 and SAP102 and decrease NR2B surface expression [146]. In another suggestive experiment, a group reported that transfection of kinase-dead CK2 into CA1 neurons both decreased CK2 activity and enhanced spatial memory formation. Furthermore, application of an inhibitor of protein phosphatase 2A (PP2A), an antagonist of CK2 phosphorylation in many systems, enhanced memory formation [147]. However, with the pleiotropic nature of both CK2 and PP2A it is difficult to determine what biochemical systems were actually affected in these experiments.

One of the hallmarks of CK2 activity is its activation by polybasic compounds such as spermine and poly-K. The extent to which this activation occurs depends largely on whether or not CK2α is bound to CK2β and what substrate is being phosphorylated. In fact, substrates that are preferentially phosphorylated by free-CK2α are inhibited by poly-K [148]. The majority of the evidence suggests that the effects of poly-basic compounds are through a direct effect on the CK2 holoenzyme, most likely through the binding of the poly-basic compound to the acidic loop in CK2β (Asp55-

Asp64)[139,149]. However, one report found a 3-fold increase in CK2 transcripts, suggesting that polyamines were acting on CK2 through an indirect mechanism that regulates CK2 transcription [150].

The most extreme example of poly-basic compound regulation of CK2 activity is the substrate CaM, where phosphorylation is completely dependent on the presence of poly-basic compounds, and this dependence is imparted to the CK2α subunit by the CK2β subunit [151]. From the perspective of CaM, inhibition is mediated by the central helix and Ca^{2+}-binding loop-III [152]. The mechanism for this effect is the following: negative charges on the C-terminus of CaM and the N-terminus of CK2β strongly repel one another in the absence of poly-K. In its presence, however, the repulsion is masked and the two proteins can interact, which leads to CaM phosphorylation [153].

A specific inhibitor of CK2 exists, 4,5,6,7-tetrabromo-2-azabenzimidazole (TBB), that has an IC_{50} of 0.9μM [154]. Furthermore, a crystal structure of the CK2α subunit in complex with TBB has been solved, demonstrating that TBB mediates its inhibition of the kinase by binding to the ATP binding site and maintains its selectivity by being too large to fit into the binding sites of other kinases [155].

Protein Phosphatase 2A (PP2A)

PP2A is one of only a few protein phosphatases that exist to dephosphorylate and antagonize the activity of the hundreds of kinases in eukaryotic organisms. Not surprisingly, a role for PP2A has been described in a broad range of physiological processes including apoptosis, transcription, translation, DNA replication, signal transduction, cell division and ion channel function [156,157].

Classically, protein phosphatase 2A (PP2A) is described as a hetero-trimeric phosphatase that consists of scaffolding ($PP2A_A$/PR65), catalytic ($PP2A_C$/PR36), and regulatory domains ($PP2A_{B/B'/B''/B'''}$PR55/PR61/PR72/PR93 &110). The scaffolding and catalytic subunits bind quite strongly to one another (Kd ~0.1nM) [158] and are almost always found associated with one another to form the core dimer of the phosphatase ($PP2A_D$). The various regulatory B subunits, on the other hand, associate with the core dimer to control substrate specificity and targeting of the complex. Recent evidence suggests that at least 1/3 of the PP2A in the cell exists in the absence of a B regulatory subunit as $PP2A_D$ and at least one example exists where a protein other than $PP2A_A$ serves as the scaffold for the catalytic subunit [159]. At least 75 combinations of PP2A isoforms can occur due to the existence of 2 isoforms of both $PP2A_A$ and $PP2A_C$ (termed α and β) and at least 16 isoforms of $PP2A_B$ [156]. The nomenclature for the B isoforms has become rather complicated with at least two different names for each group of B subunits and several isoforms

within each group. Essentially, four groups of proteins have been established to identify PP2A B subunits: B/PR55, B'/PR61, B"/PR72, and B"'/PR 93 and PR110.

The crystal structure of the PP2A hetero-trimeric complex was recently solved by two groups using $PP2A_{A_\alpha}$, $PP2A_{C_\alpha}$ and $PP2A_B$ subunit B'/PR61 [160]. The results illustrate several interesting features of the complex. First, binding of $PP2A_{C_\alpha}$ to $PP2A_{A_\alpha}$ on HEAT (huntingtin-elongation-A subunit-TOR-like) repeats 11-15 induces a 40 degree bend and 25 degree twist in the scaffolding subunit that serves to alter its shape from "fishhook" to "twisted-horseshoe." Second, despite no amino acid similarity, B' forms a "C-shaped" structure containing 8 repeating "pseudo-HEAT"-domains similar to the 15 repeating HEAT domains found in the PP2A scaffolding subunit [161]. The interaction with the scaffolding subunit occurs through the convex side of the "C" and the concave side of the scaffolding subunit "horseshoe". Third, the methylation sensitive C-terminus of the PP2A catalytic subunit was shown not to be essential for binding, but to stabilize the association of B' with $PP2A_D$.

PP2A is regulated by three different modifications, all of which involve amino acid residues on the catalytic domain. They are the following: phosphorylation of tyrosine residue Y307, phosphorylation of threonine residue T304, and methylation of the terminal leucine residue L309. The phosphorylation events have both been shown to inactivate PP2A while methylation appears to regulate B subunit binding and hence trafficking and

substrate specificity. Recent work from Longin et al (2007) on the role of the $PP2A_C$ C-terminus in PP2A physiology agrees with the PP2A holoenzyme crystal structures that show that binding of B' subunit to the $PP2A_D$ does not require a methylated C-terminus. Longin and co-investigators extended this work to demonstrate that, like the B'/PR61 subunits, B"/PR72 subunits can bind without methylation. However, B/PR55 binding does require methylation in order to bind [162]. Methylation of the C-terminus of $PP2A_C$ is catalyzed by a unique S-adenosylmethionine-dependent leucine carboxyl methyltransferase 1 (LCMT1). Demethylation is catalyzed by a specific phosphatase methylesterase (PME-1).

Bildl Paper

The impetus for much of the work contained in this thesis is a paper published in 2004 [163], that details experiments performed as a collaboration between our laboratory and the laboratory of Bernd Fakler in Freiburg, Germany. Findings from that paper that are essential to the work contained within this thesis are subsequently reviewed.

To perform the initial proteomics experiments cytoplasmic N- and C-termini of SK2 and SK3 were coupled to a solid support and then exposed to cytosolic rat brain homogenate. After washing in 2M urea, specifically retained SK channel binding proteins were eluted, separated on 2-D gels, and subsequently identified using tandem mass-spectrometry. Among the proteins identified by this method were CaM (a crucial positive control for these experiments), protein kinase CK2α and β subunits, the scaffolding subunit (PR65) of protein phosphatase 2A (PP2A), and the β-regulatory subunit (PR55) of PP2A.

To further confirm these interactions the binding between the SK2 C-terminus and PR65, CK2α and CK2β was recapitulated using cloned components in an *in vitro* binding assay. Furthermore, it was demonstrated that CaM, CK2α, CK2β, and PR65 could all bind simultaneously, not merely to the entire C-terminus, but specifically to the CaMBD (amino acids 395-487), see figure 2 panel A. Surprisingly, it was also demonstrated that the CK2α and CK2β subunits could both bind simultaneously to the SK2 N-terminus. This suggests that a more complex interaction exists between

SK2 and CK2. Evidence for an *in vivo* association between these proteins was obtained when Tim Strassmaier demonstrated that CK2α could be co-precipitated along with SK2 and CaM from mouse brain homogenate (fig.2B). Appropriately, the interaction was enhanced in a transgenic mouse that over expresses SK2 and was absent from an SK2-null mouse. This is somewhat surprising since CK2α' is the isoform enriched in brain and dendrites. It remains to be determined whether SK2 also interacts with CK2α'.

Figure 2 Legend.

CaM and CK2 Co-assemble at the CaMBD of SK2 Channels

a, Binding assay, with CaMBD as a bait protein; proteins indicated bind to the CaMBD whether applied alone or in combination. The CaMBD is located in the proximal C terminus and comprises amino acids 395–487 in SK2 channels. **b**, Coimmunoprecipitation of SK2, CaM, and CK2 protein from mouse brain plasma membranes. Proteins precipitated with anti-SK2 (eluate) from brain plasma membrane preparations (lysate) of wt, SK2 null, and SK2 over-expressing mice (SK2tTA $^{+}$/T). Separated by SDS-PAGE, blotted to a nitrocellulose filter, and probed with anti-SK2, anti-CaM, or anti-CK2 (this rabbit antibody from Upstate specifically recognizes the CK2α isoform of CK2) antibodies. Note that CaM and CK2 were coprecipitated with SK2 from wt and SK2tTA /T preparations, whereas neither protein was precipitated from SK2 null mice although CaM and CK2 were present in the lysates at equal amounts.

Bildl, Strassmaier et al. 2004[163]

Figure 2.

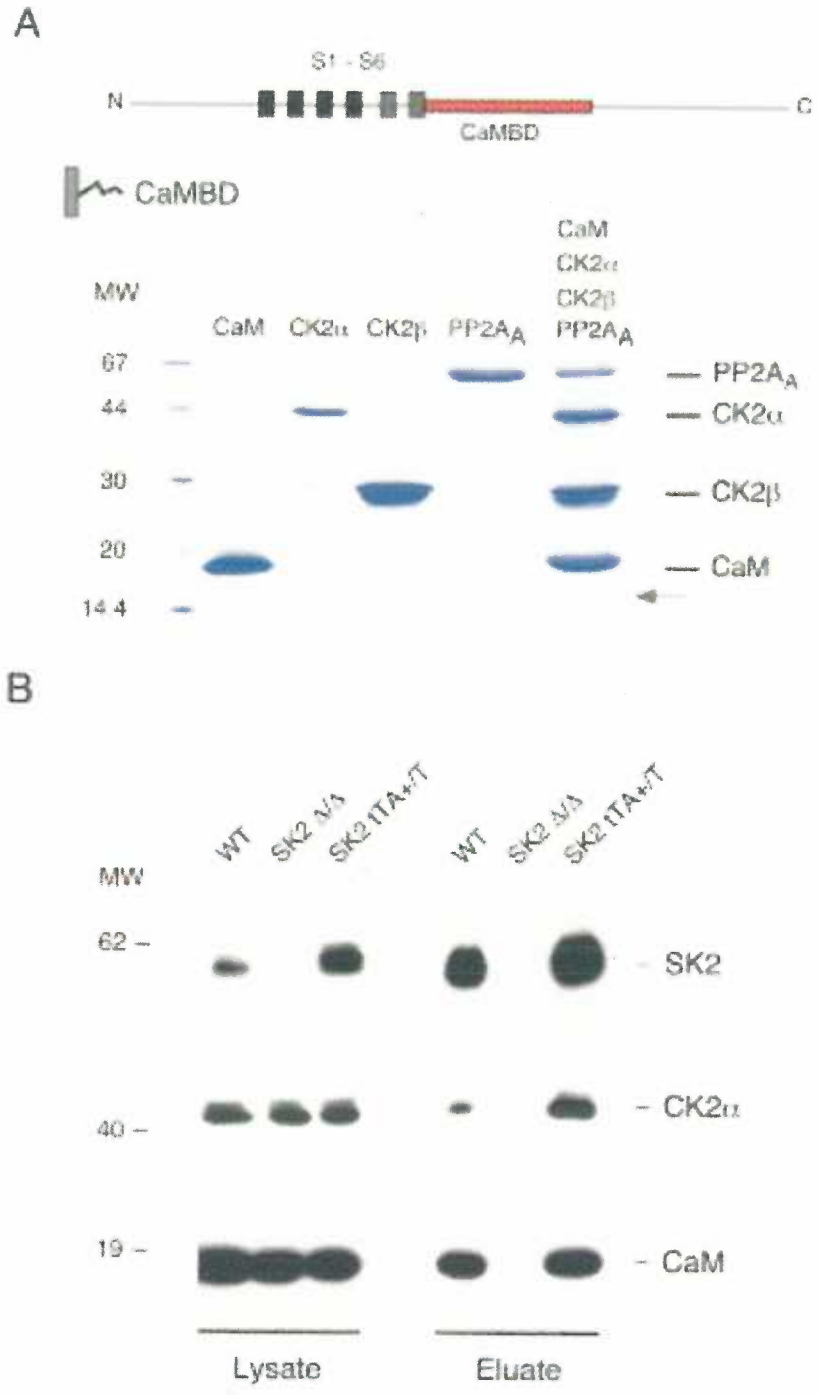

Bildl, Strassmaier et al. 2004[163]

To examine the function of the association between CK2 and SK2, all four residues in CaM that had been previously reported to be phosphorylatable by CK2 were mutated to alanine and aspartate residues to mimic the dephosphorylated and phosphorylated states. These CaM surrogates were then co-expressed with WT SK2 in Xenopus oocytes and Ca^{2+} sensitivity and gating kinetics were assessed. Only one mutant was shown to have an effect, CaMT80D. When co-expressed with WT SK2, Ca^{2+} sensitivity decreased and gating kinetics, as measured by the deactivation time constant (τ_{off}), speeded up (figure 3a,b).

In the steady state-dose response experiments, which were recorded using macropatches from Xenopus oocytes, it was observed that the WT data was better fit by a Hill equation with two components. In contrast, when CaM(T80A) or CaM(T80D) was coexpressed with the WT SK2 channel the data was well fit by a Hill equation containing a single component (figure 3b). This phenomenon was never observed in my own experiments using transfected CHO cells. All τ_{off}s from SK channel mutants and CaM surrogate coexpression experiments were adequately fit by a Hill equation containing a single component ($I_{relative} = 1/(1+(EC_{50}/[Ca^{2+}]_i)^k)$, where k = the Hill coefficient).

Figure 3 Legend.

CaM surrogate T80D alters SK2 channel gating kinetics and Ca^{2+} sensitivity

a, Currents recorded at -80 mV in response to rapid application of 3 μM $Ca^{+}2$ to excised inside-out patches with either SK2-CaM(T80D) (black) or SK2 CaM(T80A) channels (gray) held at 0.1μM $Ca^{+}2$ prior to the step increase. Recordings were made in symmetrical 120 mM K. (Lower panel) Time constants obtained from mono-exponential fits to the onset and decay of currents from experiments as in the upper panel. Values are given as mean $^{+}$/- SD of 13 to 15 experiments. **b**, Steady-state $Ca^{+}2$ response relations obtained from SK2 channels co-expressed with CaM wt or the indicated CaM mutants in excised inside-out patches with [Ca2]i of 0.08, 0.2, 0.4, 1.1, 3, 10, and 30

μM $Ca^{+}2$. Recordings were made with K concentrations of 120 mM on either side of the membrane. Lines represent fits of a single Hill equation (CaM mutants) or the sum of two Hill equations (CaM wt). The double component fit curve obtained for coexpression with CaM wt was added to the left panel for better comparison. The values for the EC50 and Hill coefficient were 1.85μM and 2.1 for CaM (T80D) coexpression and 0.38μM and 3.9 for CaM (T80A) coexpression. For coexpression with CaM wt, the respective values of the mono-component fit were 0.53μM and 1.8 (grey line). In the double component fit, the EC50 and Hill coefficient of SK2-CaM (T80D) channels were used for the low-affinity component, while its relative contribution and the values for the EC50

and Hill coefficient of the high-affinity channel population were fitted yielding values of 0.32 (relative contribution), 0.35μM, and 4.1.

Figure 3.

a.

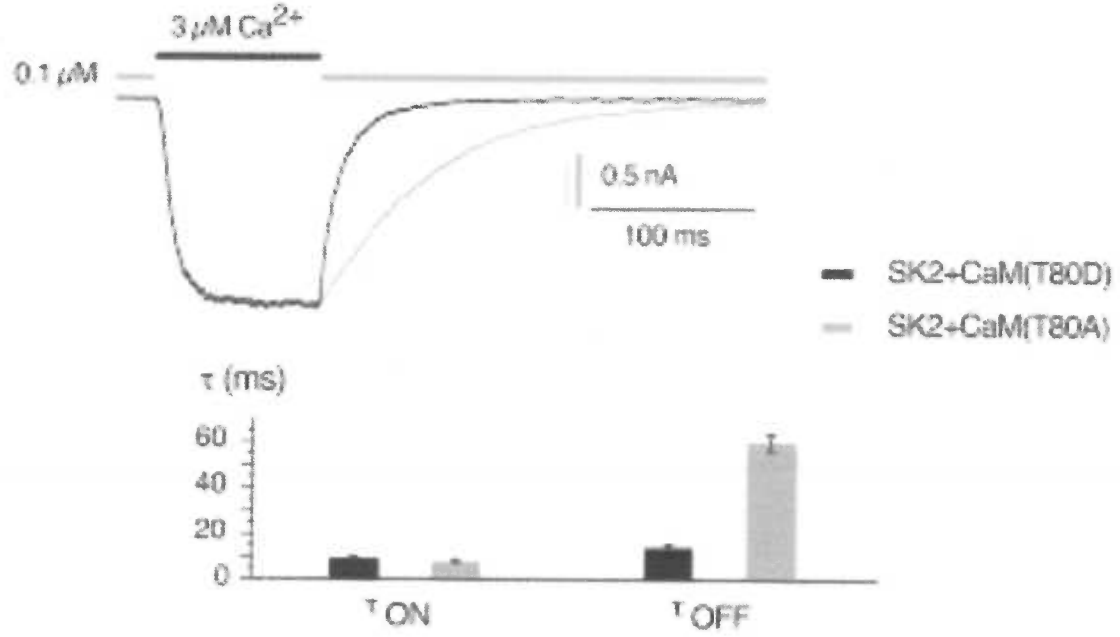

b.

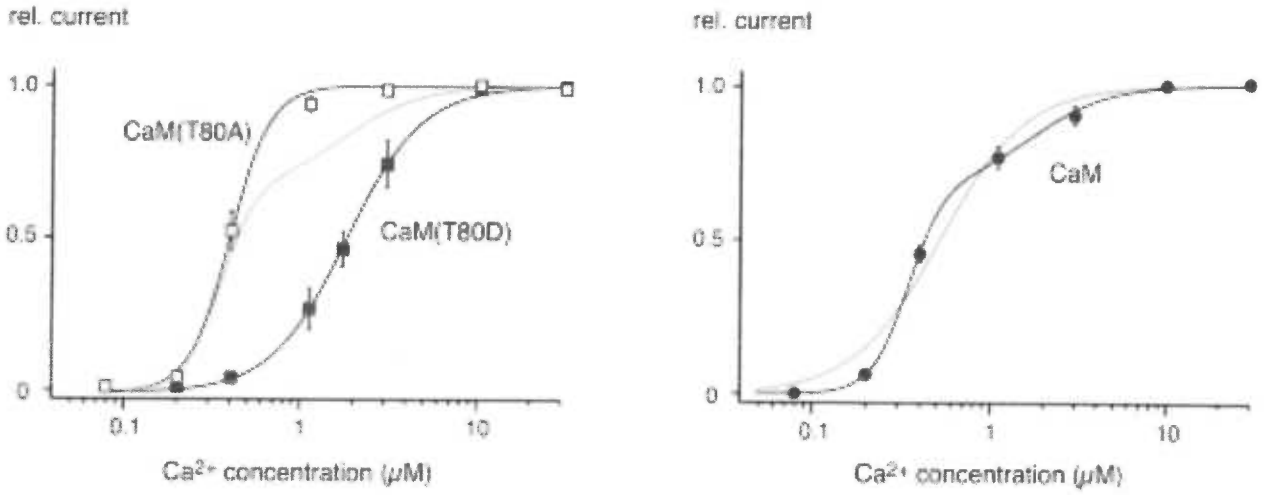

Bildl, Strassmaier et al. 2004[163]

Chapter II

The structural and functional relationship between SK2, CK2 and PP2A

Introduction and Background

In many neurons, SK channels influence somatic excitability by contributing to afterhyperpolarization [121,164]. In hippocampal CA1 neurons SK2 channels modulate synaptic plasticity by controlling Ca^{2+} influx through NMDA receptors [112,118] and regulate dendritic excitability [120] in dendritic shafts. SK channels effectively form a Ca^{2+}-mediated feedback loop with their Ca^{2+} sources by exerting a repolarizing conductance in response to increased intracellular Ca^{2+}.

Three homologous SK channels, SK1–3, are expressed in the CNS, exhibiting overlapping yet distinct spatial profiles [114]. SK channels are gated solely by intracellular Ca^{2+} ions, show very similar sensitivities to Ca^{2+} (EC50 values of ~0.3–0.5 μM) [85], and share a common Ca^{2+}-gating mechanism. Calmodulin (CaM) is constitutively bound to a domain in the proximal region of the intracellular C terminus, the CaM binding domain (CaMBD). Each of the four SK subunits harbors a bound CaM, and binding of Ca^{2+} ions to the N-lobe E–F hands of CaM initiates a conformational rearrangement that results in channel gating [92-94]. Thus, the structure and function of SK channel Ca^{2+}-gating are highly conserved, and all three SK channels expressed in brain show almost identical Ca^{2+} sensitivities.

Despite their similar gating mechanisms, the SK channels appear to serve distinct physiological roles. For example, SK2 channels are largely postsynaptic, whereas at least some SK3 channels are presynaptically located [117] [12,116,118]. Consistent with distinct roles, disruption of any one of

the SK genes does not result in altered expression levels of the other, intact genes [109]. Nevertheless, heteromeric channels have been detected [91], and overlapping functions cannot be discounted. Their central role in modulating local Ca^{2+} transients and Ca^{2+}-dependent events suggest that Ca^{2+}-independent signaling mechanisms might modulate SK channels, perhaps by tuning their Ca^{2+} sensitivity. Indeed, a proteomics approach identified CK2 and PP2A as SK2 binding proteins. In *in vitro* assays, CK2 did not phosphorylate the SK2 CaMBD but did phosphorylate CaM in complex with the SK2 CaMBD. Subsequent functional analysis showed that coexpression of SK2 channels with a CaM mutant that contained the phosphorylation surrogate, aspartate (D), at the CK2 phosphorylation substrate site, T80 [CaM(T80D)], resulted in a reduction in the steady-state Ca^{2+} sensitivity of SK2 channels and speeded channel deactivation compared with SK2 coexpression with CaM(T80A) [163]. By using native wild-type CaM, CK2, and expressed SK2 channels, the work contained in this thesis demonstrates that both CK2 and PP2A are associated with expressed SK2 channels and provide opposing regulatory activities. In addition, there are multiple points of interaction between the different proteins, as well as interactions between the N- and C-terminal domains of SK2. Furthermore, CK2 activity toward SK2-associated CaM is state dependent and is controlled by a specific lysine residue adjacent to one of the CK2–SK2 interaction domains.

Methods

Molecular biology

Constructs were subcloned into the vector pJPA that contains the cytomegalovirus promoter for protein expression in transfected cells. To generate glutathione S-transferase (GST)-fusion proteins, constructs were subcloned into pGEX-4T2 or pGEX-KG (Amersham Biosciences, Piscataway, NJ) expression vectors. To generate N-terminal 6xHis fusion proteins, constructs were subcloned into the vectors pET16b or pET33b (EMD Biosciences, La Jolla, CA). The short form of CK2 (1–340) was used to create the N-terminally His-tagged CK2α. Full-length proteins were used for all other His-tagged fusion proteins. Site-directed mutagenesis was performed with Pfu turbo DNA polymerase (Stratagene, La Jolla, CA). All sequences were verified by DNA sequence analysis. Protein expression vectors were transformed into BL-21 (DE3) codon$^+$ Escherichia coli (Stratagene) before induction with isopropyl ß-D-1-thiogalactopyranoside.

GST pull-down assays

Glutathione-agarose beads (Sigma, St. Louis, MO) were resuspended according to the manufacturer's suggested protocol, and 250 µl of slurry was used per reaction. Beads were washed one time with 1 ml of pull-down wash buffer (PWB) [20 mM HEPES, pH 7.8, 10% glycerol, 100 mM KCl, 0.1 mM EDTA, 0.1 mM dithiothreitol (DTT), 0.1% Igepal CA-630 (Sigma)] and then incubated at 4°C for 2 h with ~100 µl of crude-bacterial

lysate containing the GST-fusion protein. Lysate was the soluble fraction generated by French pressing 1 L of isopropyl ß-D-1-thiogalactopyranoside-induced bacterial culture that had been pelleted and resuspended in 20 ml of 20 mM HEPES buffer, pH 7.8, 1 mM DTT, and complete protease inhibitor mixture tablets (Roche, Mannheim, Germany). Bead–protein complexes were washed one time with 1 ml of PWB followed by a 5 min wash at 4°C with 1 ml of PWB plus 0.1% BSA to prevent nonspecific binding. This was followed by two 1 min washes with 1 ml of PWB. These "baits" were then exposed to an excess (~250 µl) of 6xHis-tagged "prey" protein added as crude-bacterial lysate, and reaction volume was increased to 1 ml with PWB. Bait and prey were incubated together at 4°C overnight, washed four times with 1 ml of PWB, added to 2x protein loading buffer containing 100 mM Tris-Cl, pH 6.8, 100 mM DTT, 4% SDS, 0.2% bromophenol blue, and 20% glycerol, heated to 95°C for 5 min, and run on SDS-PAGE gels. Western blots were prepared from the gels, and specifically retained prey proteins were identified with an anti-6xHis horseradish peroxidase-coupled monoclonal antibody (Clontech, Mountain View, CA).

Electrophysiology

Chinese hamster ovary (CHO) cells were grown in F-12 media supplemented with penicillin–streptomycin and 10% heat-inactivated fetal bovine serum (Invitrogen, Carlsbad, CA). Cells were transfected with pJPA

expression plasmids and pEGFP-N1 (Clontech) in a ratio of 10:1 by using Lipofectamine 2000 (Invitrogen). Recordings were performed at room temperature 1–2 d after transfection. Transfected cells were identified by enhanced green fluorescent protein. When filled, pipettes prepared from thin-walled borosilicate glass (World Precision Instruments, Sarasota, FL) had resistances of 2–3 MΩ. For excised patch recordings, the pipette solution contained (in mM): 140 KCl, 10 HEPES, 1.0 EGTA; pH was adjusted to 7.2 with KOH. As calculated according to Fabiato and Fabiato (1979) Go, 0.9943 mM total Ca^{2+} (as CaCl2·2H2O) was added to give 10 μM free Ca^{2+}. Excised patches were superfused with an identical solution or one that contained no calcium with an RSC-200 rapid solution exchanger (Molecular Kinetics, Pullman, WA). Currents were measured at –80 mV and digitized with an EPC9 patch-clamp amplifier (HEKA Elektronik, Lambrecht/Pfalz, Germany). Currents were sampled at 1 kHz and filtered at one-third the sample frequency, and analysis was performed with Pulse (HEKA Elektronik) and Igor (Wavemetrics, Lake Oswego, OR) software. Leak and background currents were measured by changing the bath solution on the inside face of the patch to 0 Ca^{2+} to close SK2 channels. MgATP was applied at a concentration of 5 mM for 2.5 min in the absence of Ca^{2+}, unless stated otherwise.

CK2 activation assay

Protein kinase CK2 assays were performed according to the manufacturer's suggested protocol for the CK2 assay kit (Upstate Biotechnology, Lake Placid, NY). Recombinant, human CK2 was obtained from EMD Biosciences and used at a dilution of 1:20,000.

CK2 phosphorylation assay

Assays were performed as described previously (Bildl et al., 2004Go). Briefly, purified CaM (2.5 µg) or CaMBD–CaM complex (5 µg) was incubated for 2 h at 30°C in a 50 µl reaction mixture containing 50 mM Tris, pH 7.5, 10 mM MgCl2, 1 µM poly-L-lysine (30–70 kDa; Sigma), 200 µM ATP, 20 µCi/ml γ-32P] ATP (PerkinElmer, Boston, MA), 1 KU/ml CK2 (human, recombinant, E. coli; EMD Biosciences), and 1 mM EGTA, 10 µM Ca^{2+}, or 100 µM Ca^{2+}. Then, 2x protein sample buffer containing 100 µM DTT and 1 mM EGTA was added to the reactions. The samples were heated to 95°C for 5 min and run on 18% PAGE gels. Gels were exposed to a phosphoimager, and densitometry was performed on the images with ImageJ (NIH). The densitometry data contained 21 points in each of the experiments presented; thus, 19 degrees of freedom exist and present a target correlation coefficient of 0.433. For the experiment with poly-L-lysine as the CK2 activator, $r = 0.77$; thus $p < 0.001$. For the experiment, with the SK2 N terminus as the CK2 activator, $r = 0.53$; thus $p < 0.05$. Consequently, all the data presented were within the linear range.

Pharmacology

4,5,6,7-Tetrabromo-2-azabenzimidazole (TBB) was obtained from EMD Biosciences and used at a concentration of 10 μM. Phosphatase inhibitor cocktail 1 (PIC1), containing microcystin LR, cantharidin, and (-)-p-bromotetramisole at proprietary concentrations, and phosphatase inhibitor cocktail 2 (PIC2), containing sodium vanadate, sodium molybdate, sodium tartrate and imidazole at proprietary concentrations, were obtained from Sigma.

Data analysis

To determine deactivation time constants, the equation Ibase $^{+}$ (Im – Ibase)e–t/τ_{off} was used (See Appendix B for derivation of time constants). For Ca^{2+} concentration–response experiments, each data point represents the average of three sweeps with the 0 Ca^{2+} background current subtracted. The channel was maximally activated by 10 μM Ca^{2+} in all cases. Data points were normalized to the maximum response in 10 μM Ca^{2+}, and the concentration–response data for individual patches were fit with the logistic equation 1/(1 $^{+}$ (EC50/Ca^{2+})n) and forced through 1 to derive an EC50 value and hill number for each patch. The EC50 values were averaged for all patches for each condition to obtain an average EC50 ± SEM. For display purposes, those concentration–response data from each patch were normalized to 1, and the responses from patches for each condition were averaged to give mean ± SEM for each concentration. The logistic equation

was then fit to the average concentration–response as displayed for visualization. all values are reported as the mean ± SEM of n experiments. Statistical significance was evaluated with a Student's t test or ANOVA, and $p < 0.05$ was considered significant.

Results

The current amplitude and τ_{off} of SK2 channels is stable in CHO cells

Heterologous expression studies with surrogates for phosphorylation or dephosphorylation of CK2 phosphorylation sites on CaM suggested that endogenous CK2 phosphorylates SK2-associated CaM at position T80, resulting in a rightward shift of the apparent steady-state Ca^{2+} sensitivity of the channels and faster channel deactivation [163]. To directly examine protein kinase activity that co-assembled with SK2 channels, SK2 was expressed in CHO cells, relying on endogenous CaM and CK2 to co-assemble into SK2 channel multiprotein complexes. Rapid solution exchange (~2 ms; see Materials and Methods) was used to examine the deactivation kinetics of the channels. Steady-state currents were evoked by application of 10 μM free Ca^{2+} in the bath solution. On switching from 10 μM free Ca^{2+} to 0 Ca^{2+}, the deactivation time constant (τ_{off}) was 54 ± 2 ms (n = 10) (Fig. 6b). Both current amplitude and τ_{off} of SK2 channels were observed to be stable over a period of 5 minutes when patches were held in either Ca^{2+} free bath solution or bath solution containing 10μM Ca^{2+} (Fig. 4 a and b).

Figure 4 Legend.

The current amplitude and τ_{off} of SK2 channels is stable in CHO cells

a, Holding an inside-out patch from CHO cells transiently transfected with SK2 for 5 minutes in bath solution that either contains Ca^{2+} ($^{+}Ca^{2+}$) or does not contain Ca^{2+} (0 Ca^{2+}) before exposing the patch to a rapid change in Ca^{2+} via a rapid perfusion exchange system to assay channel gating kinetics, does not result in a change in the τ-off observed. **b**, Holding an inside-out patch from CHO cells transiently transfected with rSK2 for 5 minutes in bath solution that either contains Ca^{2+} ($^{+}Ca^{2+}$) or does not contain Ca^{2+} (0 Ca^{2+}) results in Ca^{2+}-activated current amplitudes that are stable for at least 5 minutes. 10 Ca^{2+} solution: τ_{off} (msec) = 47^{+}/-3 before, 47^{+}/-4 after, p=1; relative current amplitude = 1 before, 0.98 $^{+}$/-0.4 after, p= 0.95; 0 Ca^{2+} solution: τoff = 51^{+}/-2 before, 50^{+}/-3 after, p=0.99; relative current amplitude = 1 before, 0.89 $^{+}$/-0.05 after, p= 0.07

Figure 4.

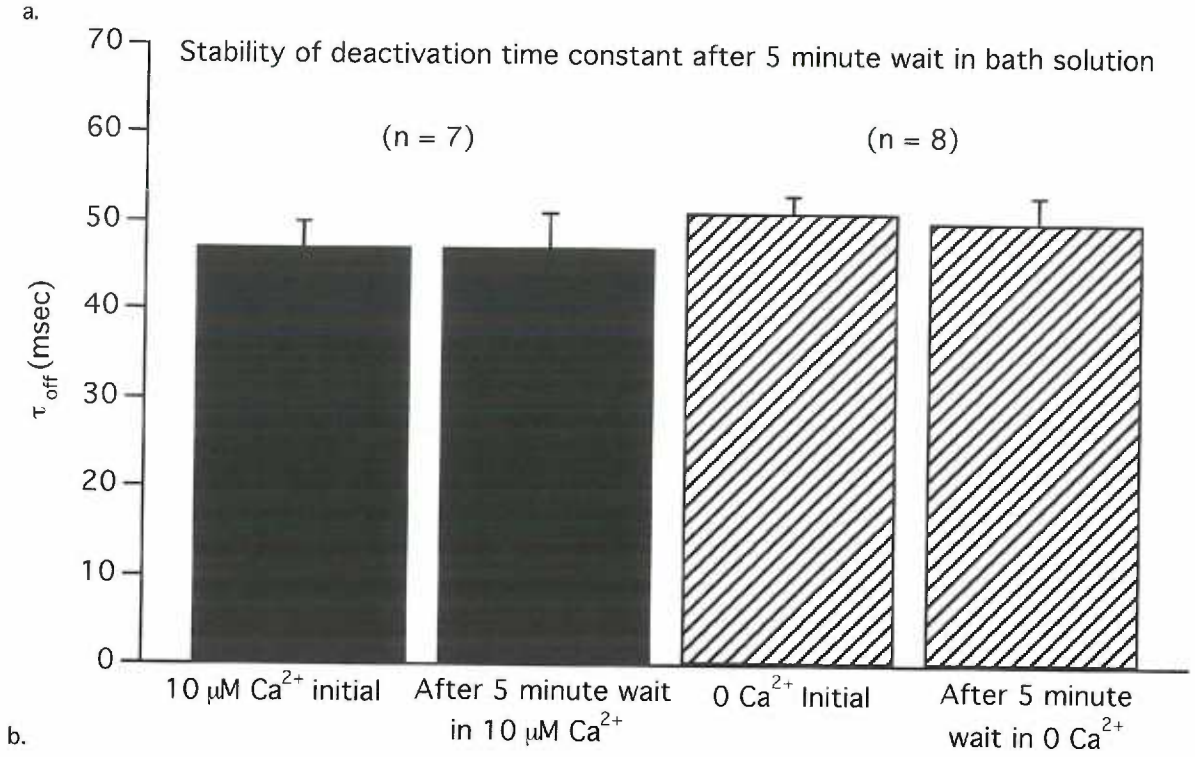
a.
Stability of deactivation time constant after 5 minute wait in bath solution
(n = 7)
(n = 8)
τ_{off} (msec)
70
60
50
40
30
20
10
0
10 μM Ca^{2+} initial
After 5 minute wait in 10 μM Ca^{2+}
0 Ca^{2+} Initial
After 5 minute wait in 0 Ca^{2+}

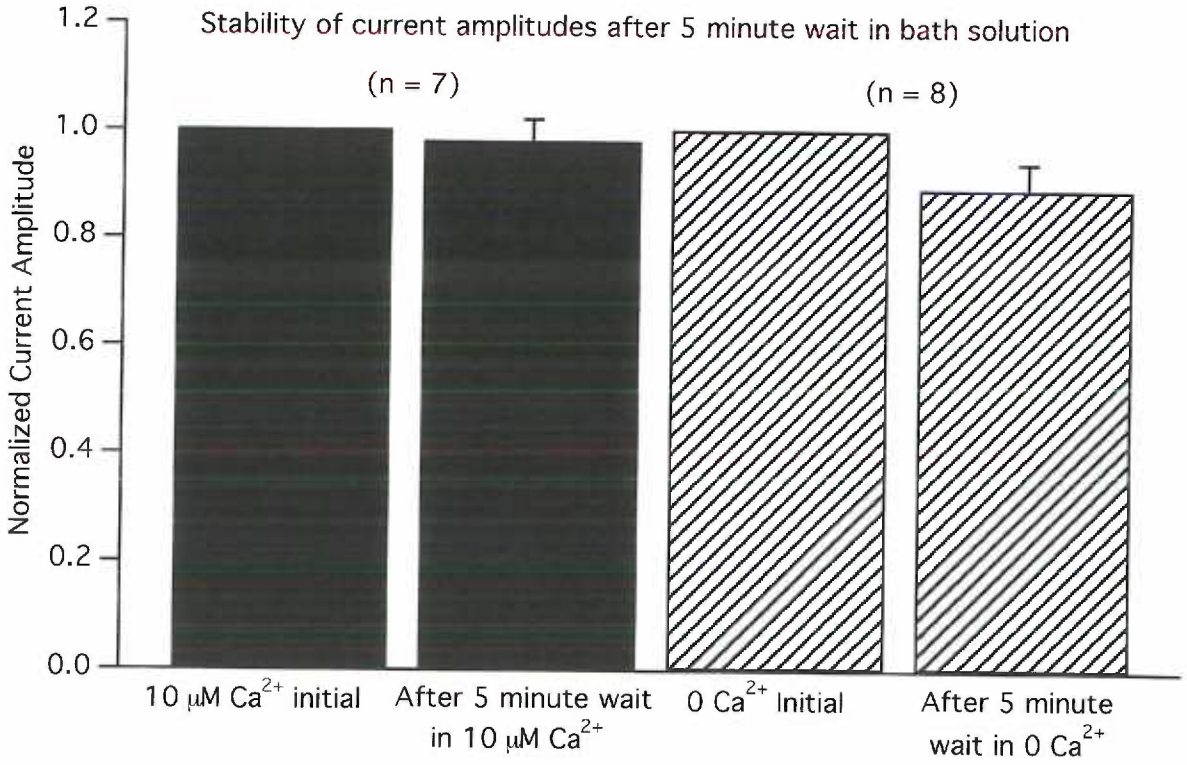
b.
Stability of current amplitudes after 5 minute wait in bath solution
(n = 7)
(n = 8)
Normalized Current Amplitude
1.2
1.0
0.8
0.6
0.4
0.2
0.0
10 μM Ca^{2+} initial
After 5 minute wait in 10 μM Ca^{2+}
0 Ca^{2+} Initial
After 5 minute wait in 0 Ca^{2+}

Description of the effects of MgATP and the CK2 specific inhibitor TBB

To activate protein kinases associated with the SK2 channels, patches were exposed to normal 0 Ca^{2+} bath solution with 5 mM MgATP for 2.5 min. Patches were then exposed to 10 μM Ca^{2+} in the absence of MgATP to evoke a steady-state current before deactivation was examined by rapidly switching to 0 Ca^{2+} solution. The deactivation rate was significantly increased after MgATP treatment, becoming 30.0 ± 0.9 ms (n = 6) (Fig. 5b), and the reaction reached a new steady-state with a $\tau_{MgATP\ effect}$ of 0.5 seconds (Fig. 5d). Consistent with these results, steady-state Ca^{2+} dose–response experiments showed that, after protein kinase activation, the apparent EC_{50} value was shifted from 0.53 ± 0.02 μM (Hill coefficient = 6.0 ± 0.2; n = 15) in control to 0.66 ± 0.03 μM (Hill coefficient = 5.5 ± 0.3; n = 15) (Fig. 5c). The Hill coefficient was not significantly changed by the addition of MgATP. To determine whether the activated kinase was CK2, the specific inhibitor TBB (10 μM) [154] was co-applied to the patches with MgATP in 0 Ca^{2+} for 2.5 min, and deactivation kinetics were reexamined in the continued presence of TBB. Channel deactivation was significantly slowed by TBB, with a time constant of 94 ± 8 ms (n = 9) (Fig. 5b). Consistent with this result, steady-state Ca^{2+} dose–response experiments in the presence of TBB showed an apparent EC_{50} value of 0.28 ± 0.02 μM (Hill coefficient = 7.1 ± 0.3; n = 9) (Fig. 5c). The Hill coefficient was significantly increased by the application of TBB ($p < 0.01$).

Figure 5 Legend.

Activation of CK2 speeds SK2 channel τ_{off} and reduces Ca^{2+} sensitivity.

a, Deactivation of normalized SK2 currents after rapid solution exchange from 10 μM to 0 Ca^{2+}; black trace, control (τ_{off} = 57.0 ms); dark gray trace, after a 2.5 min exposure to 5 mM MgATP in 0 Ca^{2+} (τ_{off} = 29.3 ms); light gray trace, after 2.5 min exposure to 5 mM MgATP in 0 Ca^{2+} and TBB (τ_{off} = 112.4 ms). Single exponential fits are added to traces. Bars in inset indicate relative current amplitudes. Calibration, 50 msec. **b**, Average τ_{off} for the indicated conditions. **c**, Normalized steady-state Ca^{2+} dose–response relationships for SK2 control (open circle), after application of MgATP (closed circle), and additionally in the presence of TBB (triangle). **d**, Time course of MgATP effect. Separate groups of patches were exposed to 5 mM MgATP for 0 min (n = 10), 0.25 min (n = 11), 0.75 min (n = 12), 2.5 min (n = 11), or 5 min (n = 8) to generate paired, before (black circles) and after (open circles) time points. The time constant of MgATP effect = 0.5 s.

Figure 5.

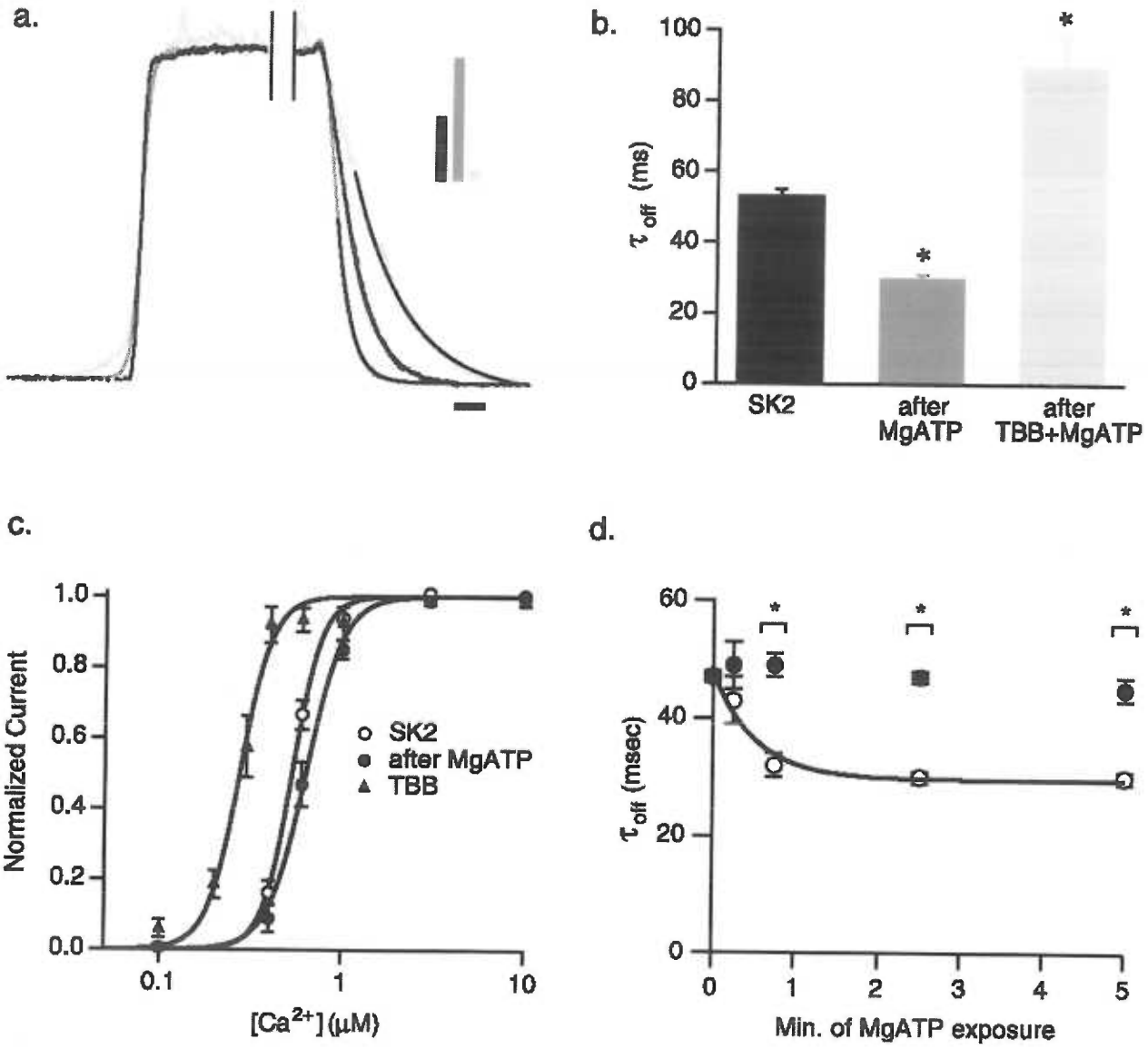
a.
b.
100
80
60
40
20
0
τ_{off} (ms)
*
*
SK2
after MgATP
after TBB+MgATP
c.
1.0
0.8
0.6
0.4
0.2
0.0
Normalized Current
SK2
after MgATP
TBB
0.1
1
10
[Ca2+] (μM)
d.
60
40
20
0
τ_{off} (msec)
*
*
*
0
1
2
3
4
5
Min. of MgATP exposure

Coexpression of SK2 with CaM surrogates T80A and T80D

In the 2004 paper by Bildl et al [163] the CaM surrogates T80A and T80D were co-expressed with WT SK2 channels in Xenopus oocytes to examine the effects of CK2 phosphorylation at this position. We further examined the effects of these CaM surrogates on WT SK2 in CHO cells, both at baseline and in response to 5mM MgATP application (2.5 minutes). Surprisingly, no difference was apparent between baseline SK2 alone and SK^{2+}CaMT80A (p=1.0), nor did the $^{+}$CaMT80A condition attenuate the MgATP effect, although a non-significant trend was observed between these two conditions (WT old $^{+}$MgATP versus WT^{+}T80A old $^{+}$MgATP, n=6, p=0.15, fig.6a). However, further experiments with new DNA preparations and new solutions demonstrated that the values were, indeed, not significantly different (WT new versus WT $^{+}$T80A new, n=10,8, p=1.0; WT new $^{+}$MgATP versus WT $^{+}$T80A new $^{+}$MgATP, n=10,8, p=1.0, fig.6a). To determine whether CaM T80A mRNA was present, rtPCR was performed using primers designed to identical regions in WT CaM, CaM T80A and CaMT80D mRNAs, and rtPCR was performed on CHO cells transfected with either CaM WT, CaM T80A or CaM T80D. What was observed was that a robust rtPCR signal could be obtained from transfections of WT CaM or CaM T80D, but not for CaM T80A. Upon re-sequencing of the T80A construct no errors in the sequence were identified, but to make sure our results were correct the construct was remade using the CaM WT plasmid as the starting template. Again, upon comparison of CaM WT and CaM

T80A containing channels no difference between the two conditions was observed (WT new versus WT^{+}T80A remake, n= 10,5, p=0.95; WT new $^{+}$MgATP versus WT $^{+}$T80A remake $^{+}$MgATP, n=10,3, p=0.88, fig.6a). Furthermore, T80A was, again, undetectable by rtPCR (data not shown). We conclude from this that the mRNA for T80A is destabilized or targeted for degradation by the T80A mutation in CHO cells.

Figure 6 Legend.

CaM surrogate T80D significantly decreases SK2 channel τ_{off}, but CaM surrogate T80A does not alter SK2 channel τ_{off} because it is not expressed.

a, Summary of τ_{off}s from inside-out patches from CHO cells transiently transfected with one of two DNA preps of SK2 (WT old, WT new) and assayed for τoff in two independently made sets of 10μM Ca^{2+} and 0 Ca^{2+} solutions (WT old, WT new). SK2 was co-transfected with either the original DNA preps of WT CaM, T80A CaM or T80D CaM (black), new DNA preps (blue), or a new T80A prep made from a new construct that used the WT CaM construct as a template (green). Recordings were done both before (solid) and after (banded) a 2.5 minute application of 5mM MgATP. Values for τ_{off} (msec.) are as follows: WT old, 53^{+}/-1, n=6; WT old $^{+}$MgATP, 28 $^{+}$/- 0.4, n=6; WT old^{+}CaM T80A, 52 $^{+}$/- 3, n=6; WT old $^{+}$CaM T80A $^{+}$MgATP, 36 $^{+}$/-3, n=6; WT old $^{+}$CaM T80D, 14^{+}/-1, n = 12; WT old $^{+}$CaM T80D $^{+}$MgATP, 10 $^{+}$/- 1, n= 12; WT new, 47^{+}/- 1, n= 10; WT new $^{+}$MgATP, 30 $^{+}$/- 1, n =10; WT new $^{+}$CaM T80A, 45^{+}/- 1, n=8; WT new $^{+}$CaM T80A $^{+}$MgATP, 29^{+}/-1, n=8; WT new $^{+}$CaM T80A remake, 44^{+}/- 5, n=5; WT new $^{+}$CaM T80A remake $^{+}$MgATP, 24^{+}/-2, n=3. * = significantly different by ANOVA, # = significantly different by paired t-test, Δ = significantly different from WT by ANOVA. **b**, rtPCR results using primers specific for plasmid produced mRNA.

Figure 6.

a

.

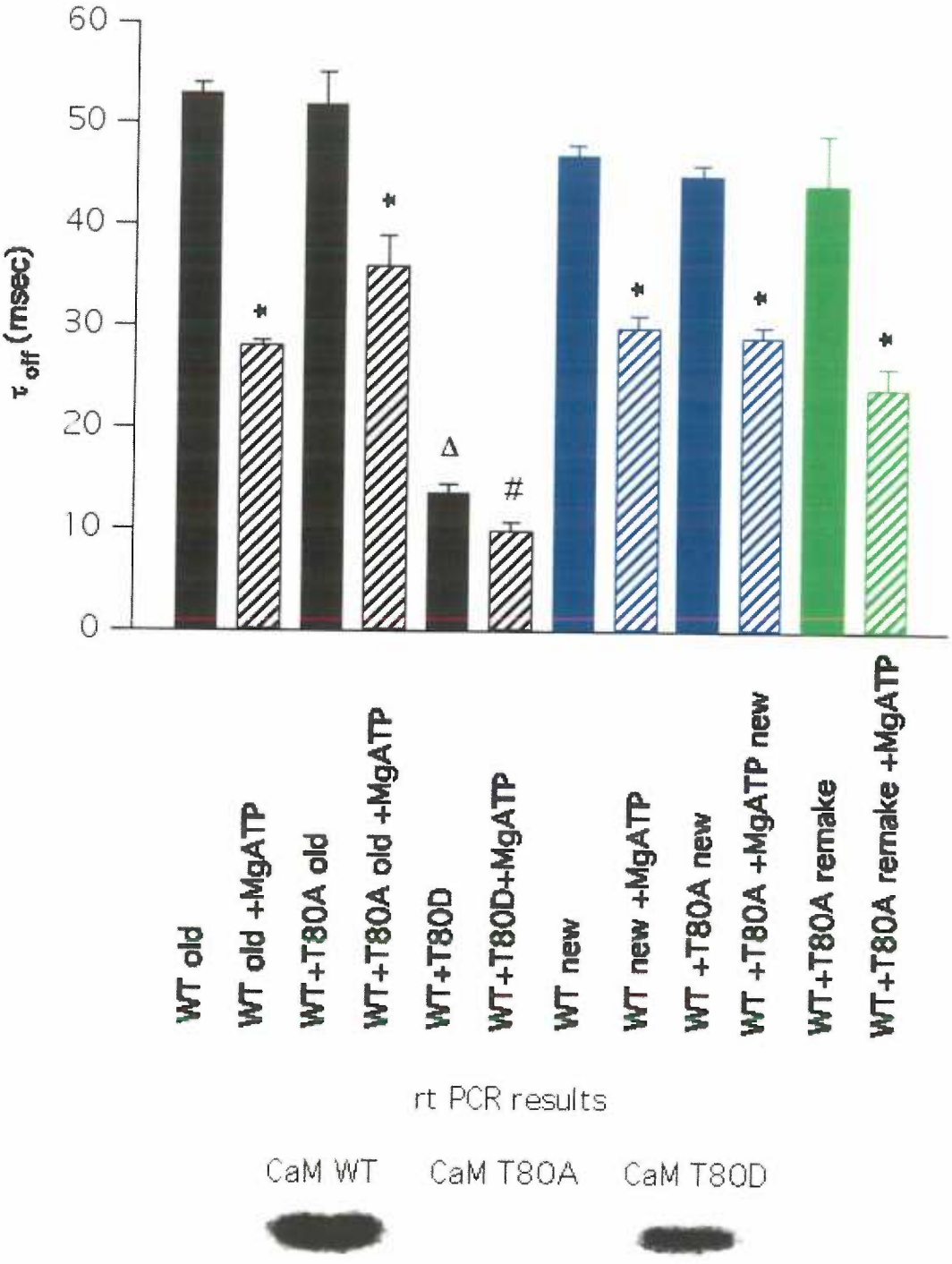
60
50
40
30
20
10
0
τ_{off} (msec)
*
*
Δ
#
*
*
*
WT old
WT old +MgATP
WT+T80A old
WT+T80A old +MgATP
WT+T80D
WT+T80D+MgATP
WT new
WT new +MgATP
WT +T80A new
WT +T80A +MgATP new
WT+T80A remake
WT+T80A remake +MgATP

b

rt PCR results
CaM WT
CaM T80A
CaM T80D

Pre-incubation with TBB blocks the MgATP effect

The structure of the CK2 inhibitor TBB is very similar to the structure of the positive regulator of SK channel family Ca^{2+} sensitivity, 1-EBIO (both are benzimidazolinones). Furthermore, both lead to an increase in the τ_{off} of SK2 channels. To test whether this increase is occurring through a similar mechanism the following time course was performed: first, base-line τ_{off}s were determined both before and after a 5 minute wait in 10μM Ca^{2+} bath solution, then τ_{off}s were again determined after a 20 second application and continued presence of 1-EBIO or TBB, after a 1 minute washout, and after a 20 second pre-incubation of 1-EBIO or TBB followed by a 2.5 minute application of MgATP. What was observed was that the decrease in τ_{off} caused by MgATP application was preserved in the 1-EBIO condition (n=6,6; p=0.03), but was eliminated by the pre-application of TBB (n=8,8; p=1). These data demonstrate that TBB is capable of blocking the MgATP binding site of CK2 while 1-EBIO cannot. Therefore, unlike TBB, the ability of 1-EBIO to increase SK2 τ_{off} is through a non-specific allosteric mechanism.

Figure 7 Legend.

Pre-incubation with TBB blocks the MgATP effect.

Time course plotting the τ_{off} of SK2 channels proceeding through the following steps: Immediately after the inside-out patch is pulled (initial), a 5 minute hold in bath solution containing 10μM Ca^{2+}, 20 second exposure to either 2mM 1-EBIO or 10μM TBB in bath solution containing 10μM Ca^{2+}, 1 minute exposure to a drug-free bath solution containing 10μM Ca^{2+}, 20 second exposure to either 2mM 1-EBIO or 10μM TBB in bath solution containing 10μM Ca^{2+} followed by a 2.5 minute application of 5mM MgATP in the presence of the drug in Ca^{2+}-free bath solution (τoff assayed immediate after in 0 and 10μM Ca^{2+} bath solution containing drug), 1 minute exposure to a drug-free bath solution containing 10μM Ca^{2+}.

Figure 7.

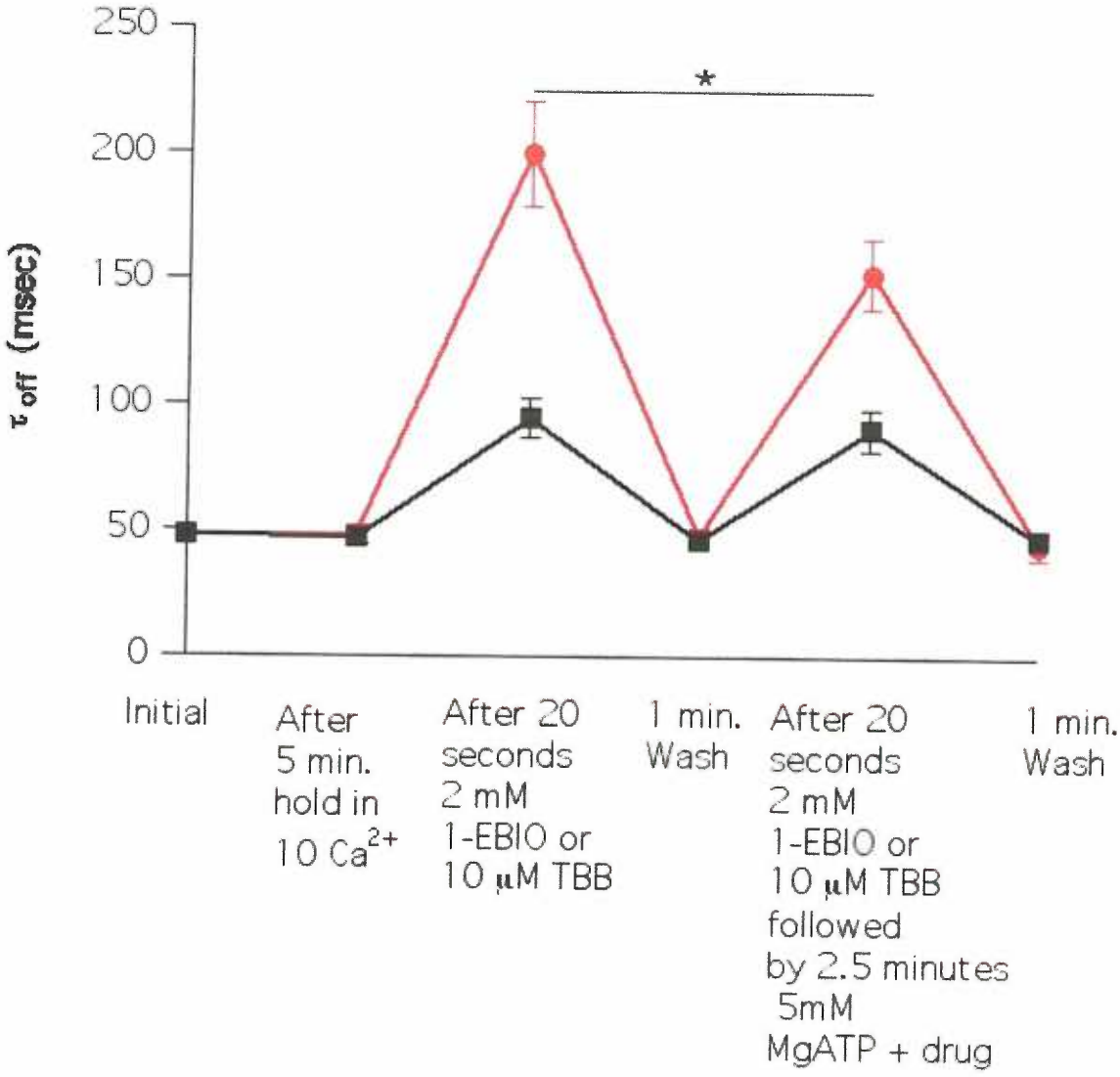
250
200
150
100
50
0
τ_{off} (msec)
*
Initial
After 5 min. hold in 10 Ca^{2+}
After 20 seconds 2 mM 1-EBIO or 10 μM TBB
1 min. Wash
After 20 seconds 2 mM 1-EBIO or 10 μM TBB followed by 2.5 minutes 5mM MgATP + drug
1 min. Wash

CK2 is stably associated with the SK2 channel multiprotein complex

One of the ways CaM is known to be constitutively associated with the SK2 channel multiprotein complex is that an inside-out patch containing SK2 channels can be held in bath solution that does not contain CaM for a long period of time without loss of Ca^{2+}-dependent channel activity. Likewise, an inside-out patch that contains SK2 channels can be held in a bath solution that does not contain CK2 for at least 10 minutes without loss of the MgATP effect (Fig. 8 n=6, p=<0.001). It should be noted, however, that the magnitude of this effect significantly declined over the 10 minute period (n=11,6 p=<0.001). It can be concluded from these data that CK2 is stably associated with the SK2 channel multiprotein complex.

Figure 8 Legend.

CK2 is stably associated with the SK2 channel multiprotein complex.

Summary of τ_{off}s for SK2 channels before (No Wait Initial) and after (No Wait $^{+}$MgATP) the application of 5mM MgATP, or before (10 Min Wait Initial) and after a 10 minute wait in bath solution that contains 10μM Ca^{2+}, but not CK2, both before (After 10 Minute Wait in 10μM Ca^{2+}) and after (MgATP Response After 10 minute Wait in 10μM Ca^{2+}) the application of 5mM MgATP. ** indicates p<.001.

CK2 phosphorylation of SK2-associated CaM is state dependent

To determine whether the activity of CK2 toward SK2-associated CaM was state dependent, MgATP was applied to patches in the presence of 10 μM Ca^{2+} (open channels) or 0 Ca^{2+} (closed channels). Activation of CK2 while the channels were open did not shift τ_{off} (49 ± 4 ms before MgATP; 45 ± 4 ms after MgATP; n = 6) (fig.9a,b). In contrast, CK2 activation while the channels were closed decreased τ_{off} from 54 ± 2 ms before MgATP to 28.1 ± 0.4 ms after MgATP (n = 6) (fig.9a,b). To further test this hypothesis *In vitro,* radiolabeled CK2 phosphorylation reactions were performed with either CaM alone or CaM added as a preformed complex with the CaMBD as substrates. CK2 requires positively charged molecules to phosphorylate CaM [165]; therefore, reactions were stimulated by poly-L-lysine (1 μM) and were performed in the absence or presence of Ca^{2+} (0, 10, or 100 μM). In the absence of Ca^{2+}, CaM was efficiently phosphorylated whether or not it was in complex with the CaMBD. In the presence of Ca^{2+}, CaM alone was phosphorylated equally efficiently, whereas CK2 phosphorylation of CaM in complex with the CaMBD was inhibited, being decreased by 31 ± 6% in 10 μM Ca^{2+} and 55 ± 6% in 100 μM Ca^{2+} (n = 7) (Fig. 9c). Together, these results show that CK2 phosphorylates SK2-associated CaM only while the channels are closed.

Figure 9 Legend.

CK2 activity for SK2-associated CaM is state dependent.

a, SK2 current deactivation as in Figure 1, for control SK2 (black trace) and after application of 5 mM MgATP (gray trace; 45 s) in the presence of 10 μM (left) or 0 Ca^{2+} (right). Calibration, 50 ms. **b,** Average SK2 τ_{off}s for the indicated conditions. **c,** *In vitro* CK2 phosphorylation reactions, stimulated by poly-L-lysine. Autoradiograph of phosphorylated CaM shows representative results for the conditions indicated, and the bar graph shows the average relative phosphorylation of CaM.

Figure 9.

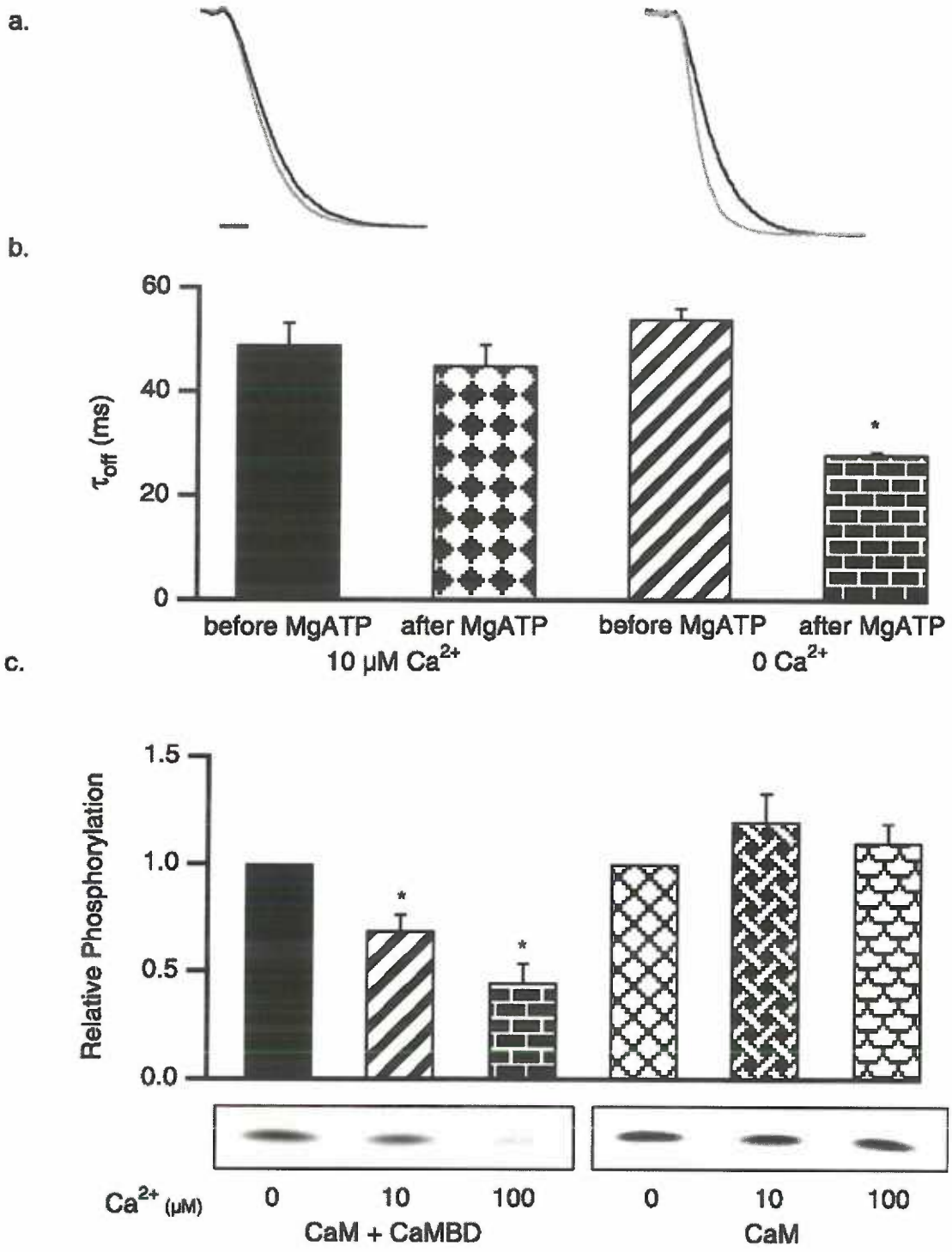
a.
b.
60
40
20
0
τ_{off} (ms)
*
*
before MgATP
after MgATP
before MgATP
after MgATP
10 μM Ca^{2+}
0 Ca^{2+}
c.
1.5
1.0
0.5
0.0
Relative Phosphorylation
*
*
Ca^{2+} (μM)
0
10
100
0
10
100
CaM + CaMBD
CaM

A phosphatase activity that is sensitive to a cocktail containing PP2A inhibitors is associated with the SK2 channel multiprotein complex.

At this point in the project three lines of evidence suggested that a phosphatase was associated with the SK2 channel multiprotein complex and that this phosphatase was PP2A: first, the PP2A scaffolding subunit was specifically retained in the proteomics experiments performed by the Fakler laboratory [163]; second, MgATP application could not shift the τ_{off} to the same level observed when CaM T80D was co-expressed with WT SK2; third, TBB not only eliminated the MgATP effect, but it doubled the τ_{off} of the WT SK2 channel. Collectively, these data suggest that the channel exists in a steady-state between the kinase activity of CK2 and the phosphatase activity of PP2A.

To further examine whether a phosphatase was associated with the SK2 channel multiprotein complex, inside-out patches were pulled from CHO cells expressing SK2 channels, initial τ_{off} was assessed, and then a phosphatase inhibitor cocktail containing PP2A inhibitors (PIC1), or a phosphatase inhibitor cocktail lacking PP2A inhibitors (PIC2), was applied for 2.5 minutes. Afterwards τ_{off} was reassessed. What was observed was that τ_{off} shifted from 53^{+}/-3 msec. before PIC1 application to 31^{+}/-2 msec. after PIC1 application, $p<0.01$ ($n = 5$) while no significant shift in τoff was observed when PIC2 was applied (PIC2 before, 5^{2+}/-7, $n = 4$; after, 56^{+}/-6, $n = 4$, $p=0.86$, fig.10). These data support the hypothesis that PP2A is associated with the SK2 channel multiprotein complex.

Figure 10 Legend.

A phosphatase inhibitor cocktail containing PP2A inhibitors (PIC1) speeds τ_{off} but a phosphatase inhibitor cocktail lacking PP2A inhibitors (PIC2) does not.

a, Example current traces from SK2 WT (black, τ_{off} 49.6 msec.), SK^{2+}PIC1 (blue, , τ_{off} 34.3 msec.), and SK^{2+}PIC2 (green, τ_{off} 52.9 msec.). **b**, Summary plot of τoffs for the following conditions: SK2 channels before application of PIC1 (PIC1 before, black, 53^{+}/-3, n =5), SK2 channels after application of PIC1 (PIC1 after, blue, 31^{+}/-2, n =5), SK2 channels before application of PIC2 (PIC2 before, black, 5^{2+}/-7, n =4), SK2 channels after application of PIC2 (PIC2 after, green, 56^{+}/-6, n =4)

Figure 10.

a

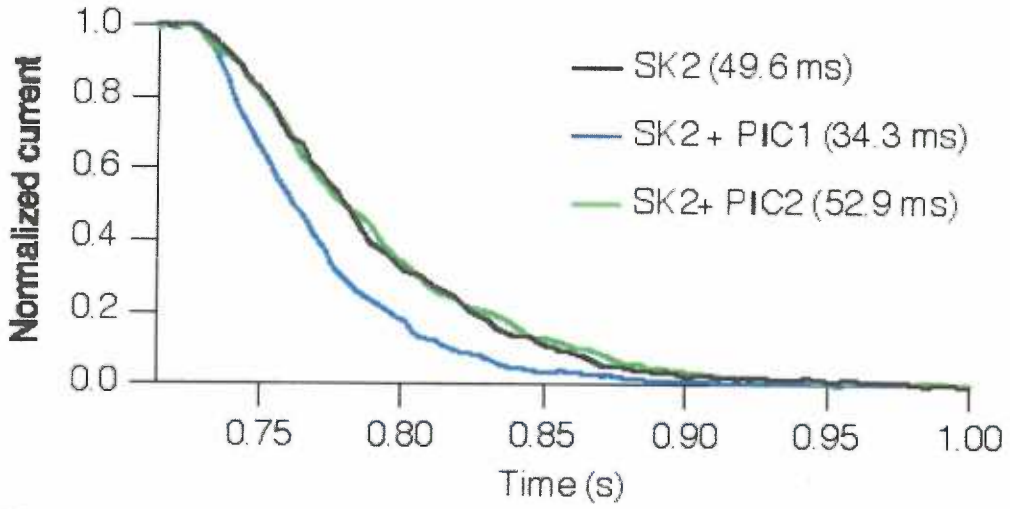
Normalized current
1.0
0.8
0.6
0.4
0.2
0.0
0.75
0.80
0.85
0.90
0.95
1.00
Time (s)
SK2 (49.6 ms)
SK2 + PIC1 (34.3 ms)
SK2+ PIC2 (52.9 ms)

b

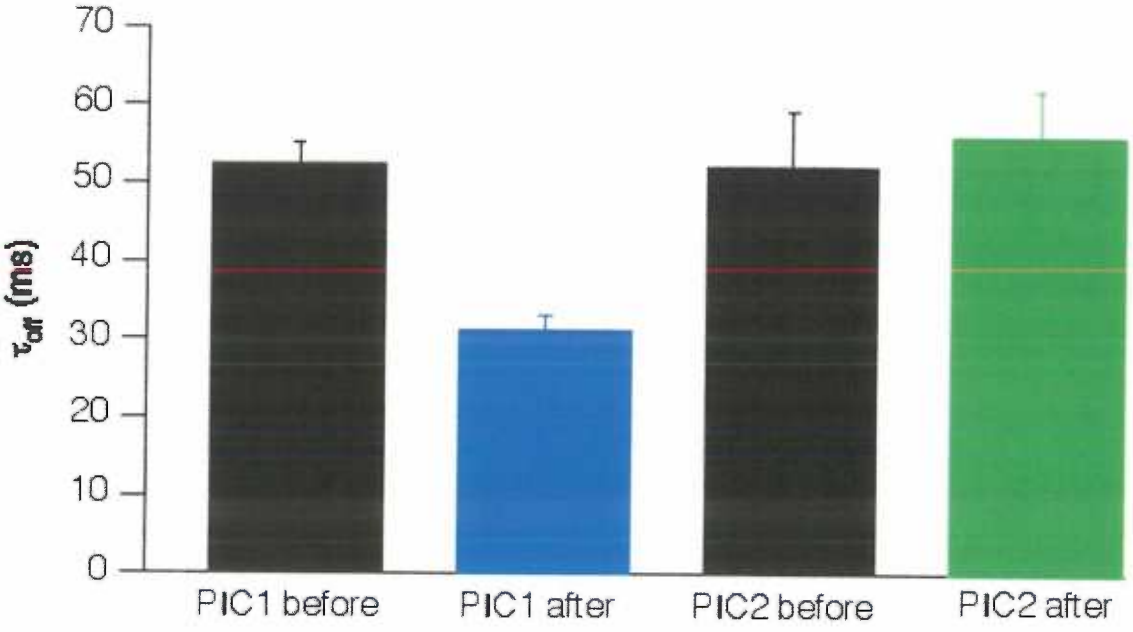
τ_{off} (ms)
70
60
50
40
30
20
10
0
PIC1 before
PIC1 after
PIC2 before
PIC2 after

PP2A is stably associated with SK2 channel multiprotein complexes

Inside-out patches containing SK2 channels were held in a bath solution lacking PP2A for 5 minutes before PIC1 was added for a period of 2.5 minutes. What was observed was that τ_{off} still decreased significantly, even after the pre-incubation step. This suggests that PP2A is stably associated with the SK2 channel multiprotein complex. MgATP was applied to a control group of SK2 channel containing inside-out patches in parallel as a positive control. The τ_{off} also decreased significantly in this group.

Figure 11 Legend.

PP2A is stably associated with the SK2 channel multiprotein complex.

Time course plotting τ_{off} versus minutes for SK2 channels exposed to either a phosphatase inhibitor cocktail containing PP2A inhibitors (PIC1, red line) or 5mM MgATP (black line) applied in 0 Ca^{2+} containing bath solution. Time points are initial, after a 5 minute wait in 0 Ca^{2+} containing bath solution, and after 2.5 minute application of the drug. * = $p<0.05$.

Figure 11.

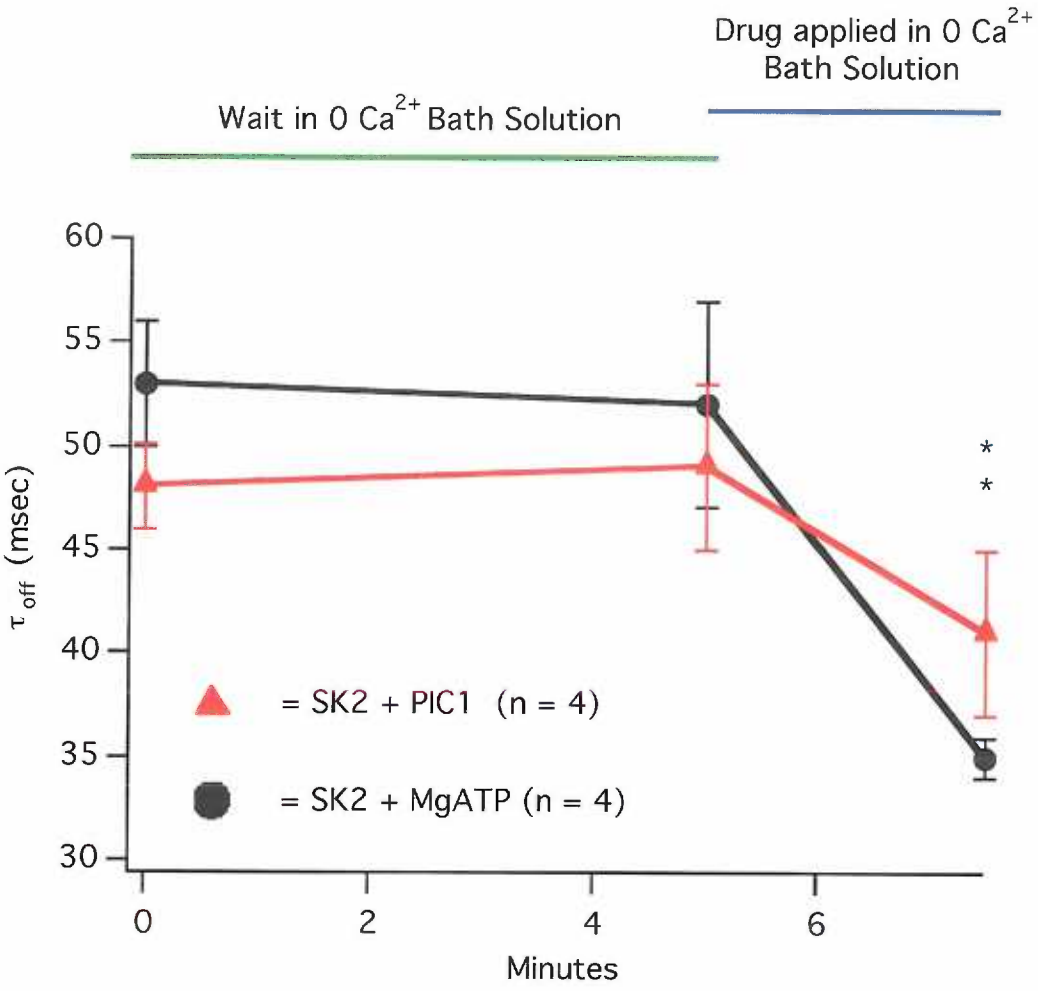
Drug applied in 0 Ca2+ Bath Solution
Wait in 0 Ca2+ Bath Solution
60
55
50
45
40
35
30
τoff (msec)
= SK2 + PIC1 (n = 4)
= SK2 + MgATP (n = 4)
* *
0
2
4
6
Minutes

PP2A activity is not speeded by shrimp-alkaline phosphatase (SAP) nor is it state-dependent

To further investigate the nature of the phosphatase activity associated with the SK2 channel macromolecular complex SK2 channels were exposed to MgATP for 2.5 minutes in order to activate CK2 and speed the τ_{off} of the channel. All groups shifted significantly with this treatment to a similar value of ~30 msec. Afterwards a time course was performed using four separated conditions: 1), bath solution containing 0 Ca^{2+}, 2) bath solution containing 10μM Ca^{2+}, 3) bath solution containing 10U/mL shrimp alkaline phosphatase (SAP) in 0 Ca^{2+}, 4) bath solution containing 10U/mL SAP in 10μM Ca^{2+}. What was observed was that a slow increase in τ_{off} occurred in all conditions. This effect was significant in all groups after an 8.5 minute wait in bath solution (0 Ca^{2+}, n=6,4, $p<0.05$; 10 Ca^{2+}, n=6,6, $P<0.001$; SAP^+ 0 Ca^{2+}, n=8,6, $p< 0.01$; SAP^+ 10 Ca^{2+}, n=9,8, $p< 0.001$). However, when the different groups were compared at each time point in the time course, using ANOVA, a significant group effect was not observed (After MgATP, p=0.95, 0.75 min., p=0.37, 3.25 min., p=0.33, 8.25 min., p=0.66). Although, a significant amount of run-down in current amplitude occurred during this period of time in all conditions (0 Ca^{2+}, n=6,4, $p<0.01$; 10 Ca^{2+}, n=6,6, $P<0.01$; SAP^+ 0 Ca^{2+}, n=8,6, $p< 0.001$; SAP^+ 10 Ca^{2+}, n=9,8, $p< 0.001$), it did not differ between groups (After MgATP, p=0.48, 0.75 min., p=0.66, 3.25 min., p=0.094, 8.25 min., p=0.098). These data

indicate that the activity of PP2A is not state-dependent, nor is the phosphatase activity enhanced by the presence of SAP.

Figure 12 Legend.

SK2 channel associated PP2A activity is slow to reverse changes in the equilibrium caused by MgATP application, is not state-dependent and is not affected by shrimp alkaline phosphatase (SAP).

a, Time course of τ_{off} at the following time points: immediately after inside-out patch is pulled, immediately after 2.5 minute application of 5mM MgATP applied in 0 Ca^{2+} bath solution, 45 seconds after MgATP application, 3.25 minutes after MgATP application, 8.25 minutes after MgATP application. Inside-out patches containing SK2 channels were held in four different conditions, 0 Ca^{2+} bath solution (black circles), 10μM Ca^{2+} bath solution (grey diamonds), 0 Ca^{2+} bath solution containing 10U/mL SAP (blue squares), and 10μM Ca^{2+} bath solution containing 10U/mL SAP (green triangles). **b**, Percentage of initial current amplitude remaining versus total time (minutes) in the conditions shown in **a**.

Figure12.

a.

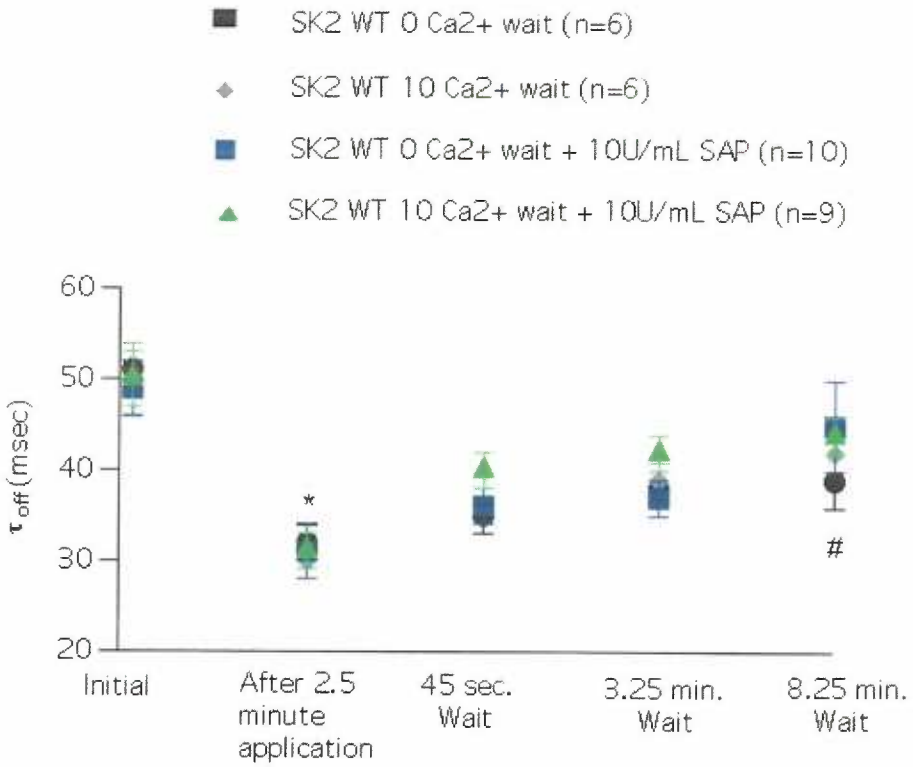
SK2 WT 0 Ca2+ wait (n=6)
SK2 WT 10 Ca2+ wait (n=6)
SK2 WT 0 Ca2+ wait + 10U/mL SAP (n=10)
SK2 WT 10 Ca2+ wait + 10U/mL SAP (n=9)
60
50
40
30
20
τ off (msec)
*
#
Initial
After 2.5 minute application of 5mM MgATP
45 sec. Wait
3.25 min. Wait
8.25 min. Wait

b.

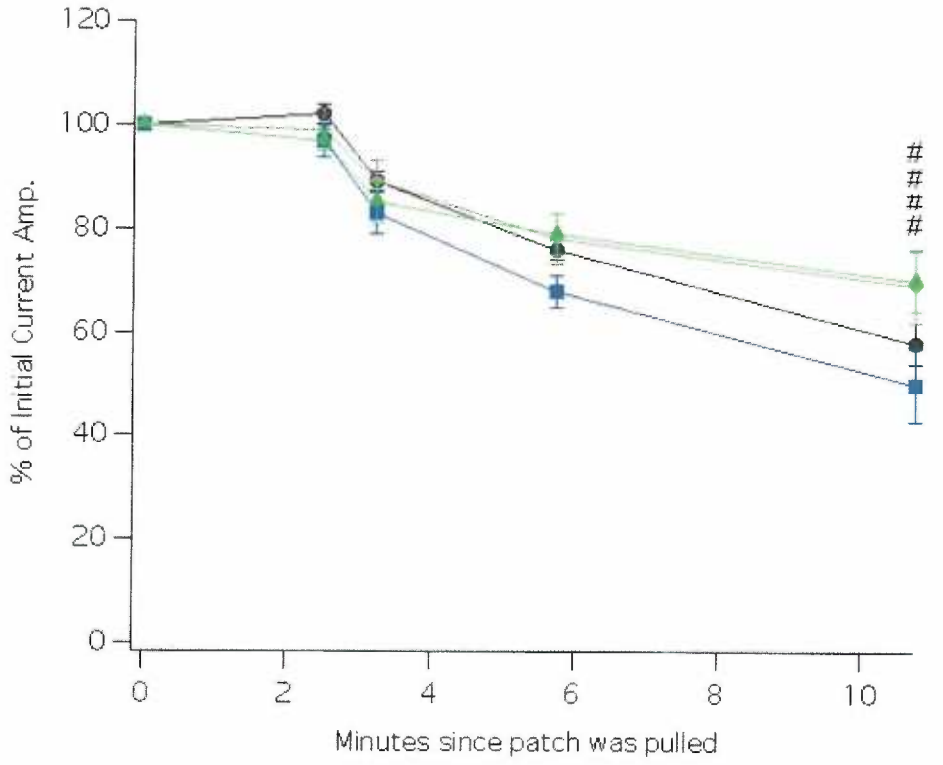
120
100
80
60
40
20
0
% of Initial Current Amp.
#
#
#
#
0
2
4
6
8
10
Minutes since patch was pulled

PP2A is a component of the SK2 channel complex

In previous experiments, activation of SK2-associated CK2 significantly accelerated channel deactivation, but the time constant was not reduced as much as when SK2 was co-expressed with the CaM phosphorylation surrogate CaM T80D (13.7 ± 0.8 ms; n = 12) (Fig. 5a). Moreover, the τ_{off} measured after application of the CK2 inhibitor TBB (94 ± 5 ms, fig. 6b) was much larger than the τ_{off} measured after coexpression of SK2 with the CaM surrogate CaM T80A (45 ± 1 ms; n = 8; fig. 5a). These results, along with others, suggest that a phosphatase is associated with the SK2 channel multiprotein complex. Indeed, two of the binding partners isolated with the SK2 C-terminus in the initial proteomics experiments were the scaffolding and B regulatory subunits of PP2A [163].

To test SK2-associated PP2A activity, a PP2A scaffolding subunit (PR65) dominant-negative mutant (K416E) was co-expressed with WT SK2 channels. This previously described mutation decreases the affinity of PR65 for the catalytic subunit of PP2A by ~100-fold [166]. Consistent with an effect of PP2A on SK2, the τ_{off} was 39 ± 2 ms (n = 4) for cells co-transfected with the mutant PP2A, whereas the τ_{off} from WT control cells was significantly larger: 54 ± 2 ms (n = 6) (Fig. 13c).

Inspection of the C-terminal domain of SK2 revealed a sequence similar to two known PP2A binding sites, one in SV40 small T-antigen and one in protein kinase CK2 (Fig. 13a). Mutation of the sequence EHRK to AHAA in CK2α was shown to abolish binding to PP2A [137]; therefore, the

homologous sequence in the SK2 C-terminal domain, EQRK [amino acids (aa) 469–472], was mutated to AQAA. Bacterially expressed GST-fusion proteins of WT and AQAA (aa 469–472) mutants were tested in pull-down assays for their ability to bind to His-tagged PR65. Western blots of the eluted proteins with the anti-His antibody showed that the WT SK2 C-terminal domain was capable of binding PR65, whereas the triple mutant was greatly diminished in its ability to bind PR65 (Fig. 13b). The triple mutant AEAA (aa 469–472) was introduced into full-length SK2 and expressed in CHO cells. The τ_{off} of AEAA (aa 469–472) was 14.4 ± 0.8 ms (n = 6) (Fig. 13c), not significantly different from the τ_{off} measured from patches co-expressing WT SK2 and CaMT80D (13.7 ± 0.8 ms; n = 12), nor was it different from the time constant measured for a truncation at position 471 (SK2 471*; 11.9 ± 1.7 ms; n = 6) (Fig. 13c). Together, the results show that SK2 channels are co-assembled complexes with PP2A and protein kinase CK2 and that opposing kinase and phosphatase activities modulate the apparent Ca^{2+} sensitivity of the channels.

Figure 13 Legend.

PP2A is co-assembled with SK2 channels.

a, Amino acid sequence comparison of PP2A binding sites on SV40 small T-antigen, CK2α, and SK2 (467–476). Mutated residues are underlined, and the position of the truncation, R471, is indicated. **b,** Top, Anti-His Western blot of proteins eluted from GST pull-down experiments with His-tagged PP2A PR65 as prey with the following baits: GST, SK2 396-end containing the mutation EQRK to AQAA, and SK2 396-end. Bottom, Coomassie blue-stained gel showing the input GST-fusion bait proteins. **c,** Average deactivation time constants for control SK2, SK2 co-expressed with the dominant negative PP2A (PR65 K416E), the SK2 EQRK to AQAA triple mutant, SK2 co-expressed with CaM T80D, and the SK2 truncation at position 471.

Figure 13.

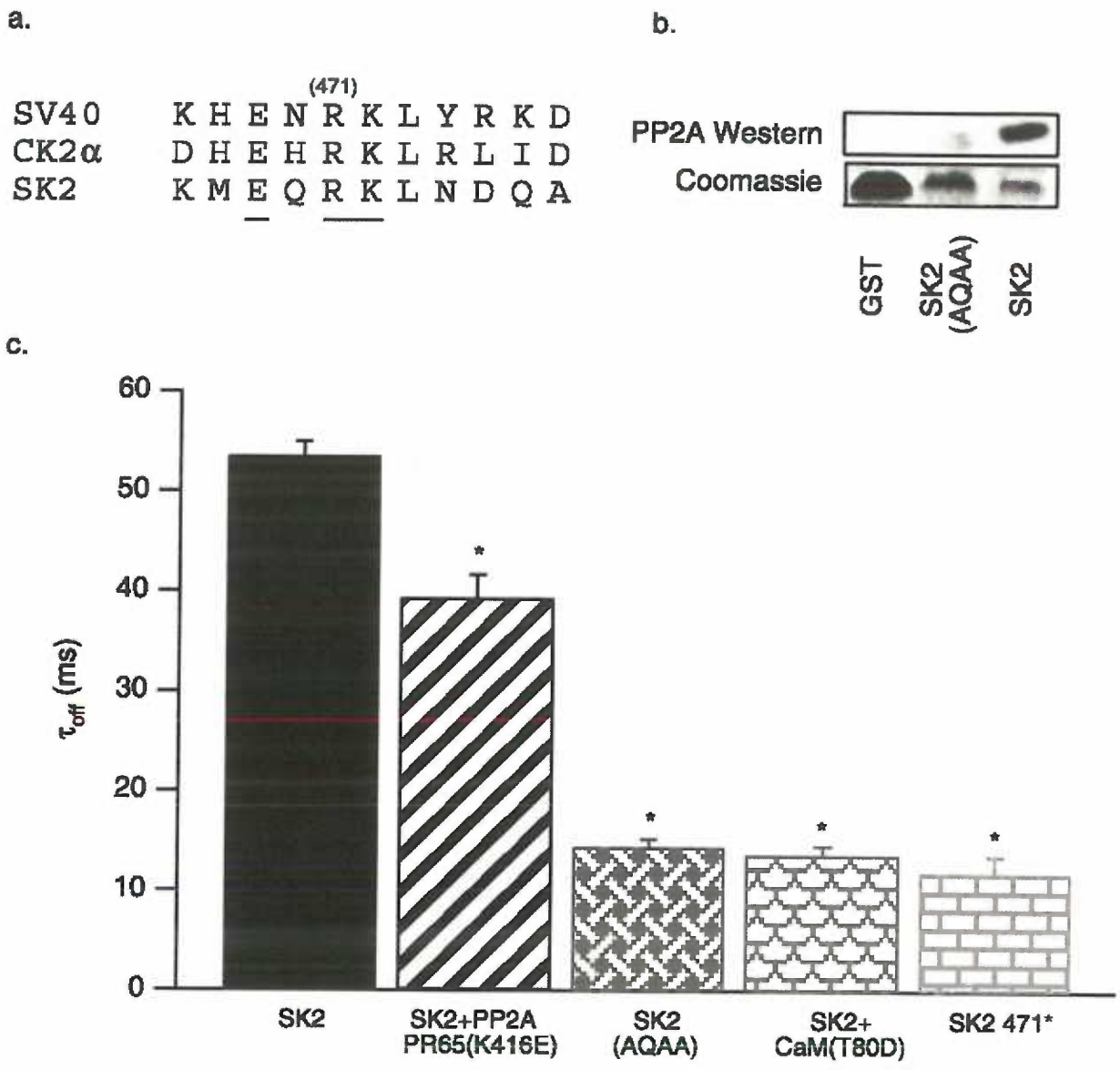
a.
(471)
SV40 K H E N R K L Y R K D
CK2α D H E H R K L R L I D
SK2 K M E Q R K L N D Q A
b.
PP2A Western
Coomassie
GST
SK2 (AQAA)
SK2
c.
τ_{off} (ms)
60
50
40
30
20
10
0
SK2
SK2+PP2A PR65(K416E)
SK2 (AQAA)
SK2+ CaM(T80D)
SK2 471*

Truncation of SK2 at amino acid 471 leads to rapid rundown that is not rescued by Ca^{2+}/CaM application.

During the course of the experiments with SK2 channel mutant 471* it was observed that, unlike the PP2A-free E_RK to ala mutant, 471* resulted in rapid run-down of the channel. To test the speed of this run-down and whether it could be rescued by application of Ca^{2+}/CaM complex, the following time course was performed: background current amplitude determined in 0 Ca^{2+} bath solution, maximum current amplitude determined in 100μM Ca^{2+} bath solution, current amplitude after waiting 1 minute in 100μM Ca^{2+} bath solution, current amplitude after waiting 5 minutes in 100μM Ca^{2+} bath solution, current amplitude after an 8 minute wait in 100μM Ca^{2+} bath solution^{+} 10μM Ca^{2+}/CaM complex. Results indicate that rundown is rapid and is not rescued by Ca^{2+}/CaM.

Figure 14 Legend.

The truncation of SK2 at amino acid 471 leads to rapid rundown, which is not rescued by Ca/CaM application (10μM)

a, Background currents immediately observed from inside-out patches from CHO cells transfected with SK2 471* and held in 0 Ca^{2+}; this is followed by absolute current amplitudes observed from SK2 471* in 100μM Ca^{2+} containing bath solution immediately after the background currents are determined. Currents are then determined for patches held for one minute in 100μM Ca^{2+} containing bath solution, after five minute in 100μM Ca^{2+} containing bath solution, and after an 8 minute wait in 100μM Ca^{2+} bath solution containing 10μM Ca^{2+}/CaM. **b**. Relative currents, normalized to maximal current amplitude in 100μM Ca^{2+} condition, under the same conditions as in panel **a**.

Interactions between SK2 and CK2

CK2 was isolated as an SK2 binding protein based on its ability to refold onto the isolated intracellular C-terminal domain of the channel. In control experiments, CK2 was also shown to bind to the intracellular N-terminal domain of SK2, suggesting a complex interaction between CK2 and noncontiguous segments of the SK channel subunit [163]. This also implied that the N- and C-terminal domains of the SK2 channel might themselves interact. Therefore, the sites of interaction between CK2 α and β subunits and the SK2 N- and C-terminal domains, and interactions between the intracellular domains themselves, were investigated with GST pull-down experiments. GST was fused with a series of overlapping bacterially expressed proteins that span the N-terminal domain of SK2, and these were immobilized on glutathione-agarose beads. A 6xHis tag was fused to the CK2α and β subunits and to the SK2 N terminus. These prey were exposed to the GST-fusion protein baits. After washes, the proteins were separated by PAGE and probed as Western blots with an anti-6xHis horseradish peroxidase-coupled monoclonal antibody. The results (Fig. 15a) showed that the CK2 α and β subunits bound to a fragment encompassing most of the N-terminal domain (2–140). For CK2β this could not be defined further. CK2α additionally bound to fragment 107–129 but did not bind to fragment 107–124, suggesting that 125–129 (RRALF) comprise the N-terminal binding site for CK2α. A similar strategy was used to examine C-terminal interactions. In this case, a segment of the N-terminal domain of the channel

(72–129) also served as prey (Fig. 15b). Together, the results showed that the N-terminal domain (72–129) interacts with the CaMBD (433–460) and with a segment close to the C terminus of the channel (558–568). CK2 α and β showed similar patterns of interaction with the C-terminal domain, binding to the CaMBD (433–446) and a segment close to the C terminus (558–568).

Figure 15 Legend.

Interactions between domains of SK2 and CK2.

a, GST pull-down experiments used the indicated fragments of the N-terminal domain of SK2 as baits to detect interactions with N-terminally His-tagged CK2α or CK2β. Specifically bound prey proteins were detected by Western blotting with an anti-His antibody. **b**, Same as in **a** but with GST-fusion proteins of the C-terminal domain of SK2 as baits and additional testing for interactions with the membrane proximal portion of the SK2 N-terminal domain. Subunit schematics represent the interactions detected by the pull-down results.

Figure 15.

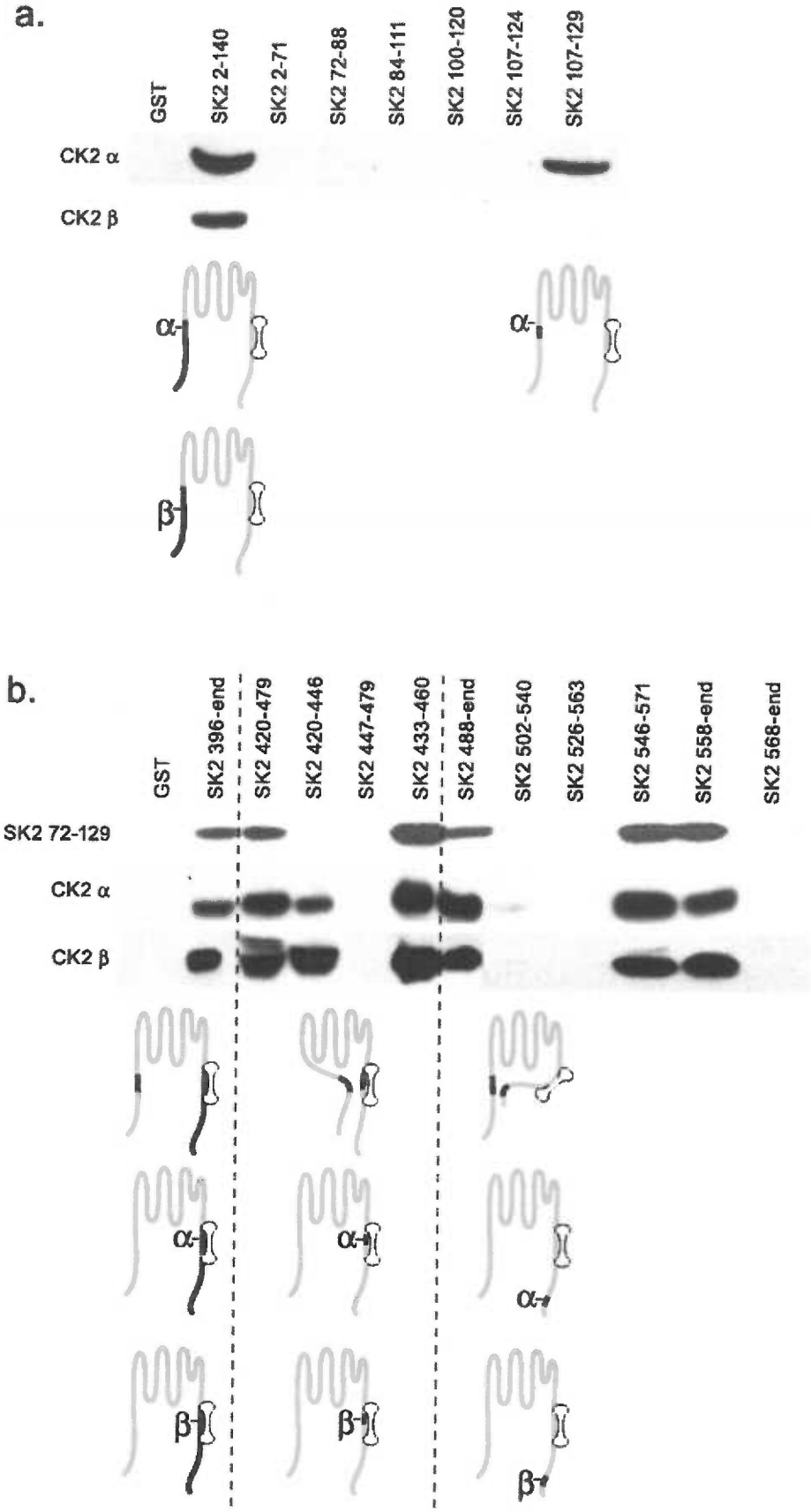
a.
GST
SK2 2-140
SK2 2-71
SK2 72-88
SK2 84-111
SK2 100-120
SK2 107-124
SK2 107-129
CK2 α
CK2 β
α
β
b.
GST
SK2 396-end
SK2 420-479
SK2 420-446
SK2 447-479
SK2 433-460
SK2 488-end
SK2 502-540
SK2 526-563
SK2 546-571
SK2 558-end
SK2 568-end
SK2 72-129
CK2 α
CK2 β

The binding sites for CK2 and PP2A can be mapped onto the crystal structure of the CaM/CaMBD complex.

To better visualize the regions of interaction between the components of the SK2 channel multiprotein complex, the binding sites of CK2 and PP2A were mapped onto the published crystal structure of the CaM/CaMBD complex [94]. The results indicate that both map to regions that could conceivably accommodate a large protein-binding partner, yet they are close to one another and to CaM (fig.16). This makes sense, since all these proteins must work together to phosphorylate and dephosphorylate CaM on T80.

Figure 16 Legend.

The binding sites of CK2 and PP2A both map to regions that could accommodate a large protein-binding partner.

The previously determined regions of interaction between CK2 and SK2 (green) and between PP2A and SK2 (blue) were mapped onto the crystal structure of the CaM/CaMBD complex. Both proteins are in close proximity to residue T80 of CaM (red).

Figure 16.

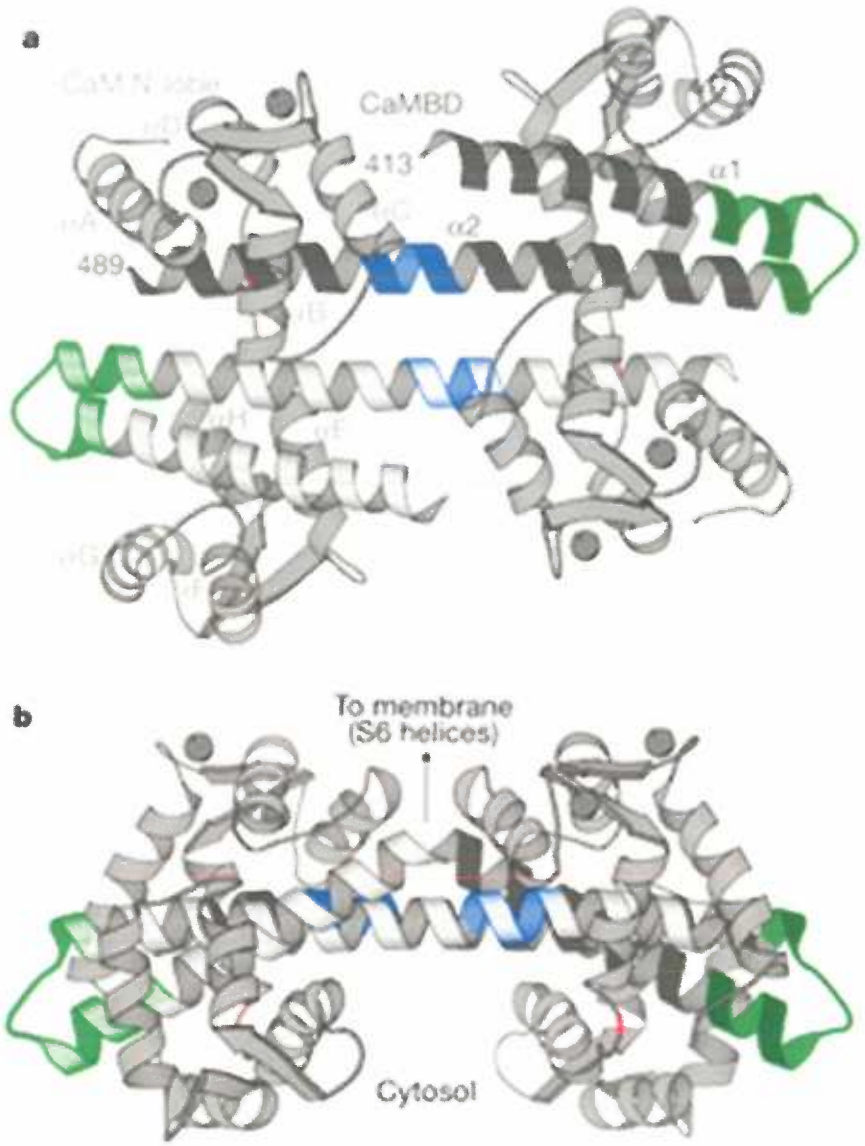

Green = CK2 Interaction Sites
Blue = PP2A Interaction Sites
Red = T80 Residues

Crystal Structure from Schumacher, et al., Nature (2001) 410 (6832) page 1120-4

A comparison of the regions of homology between SK channel family members suggest CK2 is associated with SK1, SK2, &SK3, but not IK1, while PP2A is associated with SK2 and SK3, but neither SK1 nor IK1.

Using the GST-pulldown data and alignments of the SK channel family the conservation of the CK2 and PP2A binding sites among the SK channel family members was investigated. What was observed was that that the N-terminal binding site of CK2α was clearly retained among SK1, SK2, and SK3, but was totally absent in IK1. The residues responsible for binding to CK2 in the CaMBD were completely maintained among the SK2 isoforms, differed by 2 amino acids (out of 14) in SK3 and 3 amino acids in human and rat SK1. In contrast, only 4 amino acids were identical in IK1. The C-terminal CK2 binding site, in contrast, was completely maintained among all the SK2 channel family members, but appeared to be absent from the rest of the SK channel family. These data suggest that CK2 is bound to SK1, SK2, and SK3, but not to IK1.

The binding site for PP2A in the CaMBD of SK2 is completely maintained among SK2 isoforms and SK3, but appears disrupted in SK1 and IK1. In SK1 the positively charged arginine of the E_RKL motif is mutated to glycine and in IK1 the negatively charged E is reversed to a positively charged K residue. Both of these mutations would be predicted to destabilize PP2A binding. These data suggest that PP2A is contained within the macromolecular complex for both SK2 and SK3, but not for SK1 or IK1.

Figure 17 Legend.

CK2 (green underlining) and PP2A (blue underlining) binding site conservation among SK channel family members.

a, Alignment of the CK2 interacting segment in the N-terminus of SK2 with the homologous sequences in the SK channel family. **b**, Alignment of the CK2 interacting segment in the CaMBD of SK2 with the homologous sequences in the SK channel family, and alignment of the PP2A interacting segment in the CaMBD of SK2 with the homologous sequences in the SK channel family. **c**, Alignment of the CK2 interacting segment in the C-terminus of SK2 with the homologous sequences in the SK channel family.

Figure 17.

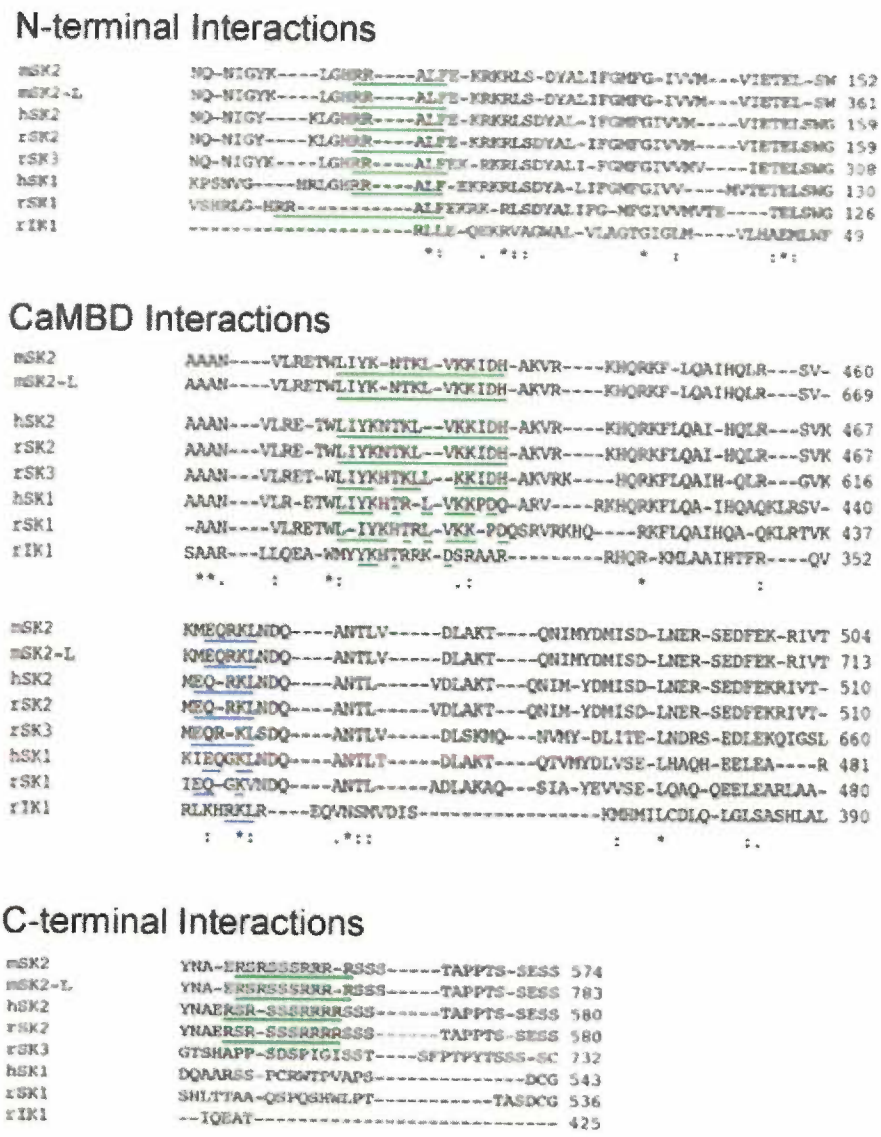
N-terminal Interactions
CaMBD Interactions
C-terminal Interactions

SK2 K121 activates SK2-associated CK2

CK2 requires positively charged compounds such as poly-L-lysine or spermine to phosphorylate CaM [151], yet in excised patch experiments, CK2 activity required only MgATP to phosphorylate SK2-associated CaM. The N-terminal domain of SK2 contains a cluster of positively charged residues close to the site of interaction with CK2α. Therefore, the N-terminal domain of SK2, residues 2–140, was expressed in bacteria as a GST-fusion, and the isolated protein was used in CK2 activation assays, in the absence of poly-L-lysine. As shown in Figure 18a, the N-terminal domain of SK2 significantly enhanced CK2 activity to phosphorylate a prototype CK2 phosphorylation substrate peptide. The N-terminal domain of SK2 was also used to stimulate CK2 activity to phosphorylate CaM, either alone or in complex with the CaMBD, without or with Ca^{2+} present in the reaction. Similar to the results with poly-L-lysine to stimulate CK2 activity (Fig. 9c), CaM was efficiently phosphorylated by SK2 N-terminal domain-stimulated CK2 in the absence of Ca^{2+}, whether or not CaM was bound to the CaMBD. The presence of Ca^{2+} did not reduce the efficiency of CaM phosphorylation in the absence of the CaMBD, but when CaM was bound to the CaMBD, Ca^{2+} reduced the efficiency of CK2 phosphorylation by 42 ± 9% in 10 μM and 50 ± 9% in 100 μM (Fig. 18b). To further define the residues responsible for influencing CK2 activity, site-directed mutations were introduced into the SK2 N-terminal domain, replacing positively charged residues with alanine (Fig. 19a). The channels were expressed in CHO

cells, and the effects of MgATP were evaluated. Only substitution at a single position showed an effect: the point mutation K121A increased the deactivation time constant from 48 ± 2 to 93 ± 4 ms (n = 10) and eliminated the effect of MgATP (80 ± 5 ms; n = 10) (Fig. 19b,c). The apparent Ca^{2+} sensitivity of K121A channels was appropriately left-shifted to 0.29 ± 0.3 μM (n = 6; data not shown). Although not significant (p = 0.09), there was a trend to reduced deactivation time constants with MgATP, suggesting that in the absence of K121, other nearby positive charges may influence the activity of SK2-associated CK2. Therefore, all five proximal lysine residues were simultaneously changed to alanine (SK2 5K to A). In this case, the trend with MgATP application was eliminated (100 ± 2 ms before MgATP; 98 ± 3 ms after MgATP; n = 6; p = 0.58) (Fig. 19b,c).

Figure 18 Legend.

The SK2 N-terminal domain activates CK2.

a, Average CK2 phosphorylation of a prototypic CK2 substrate peptide stimulated by control GST, the SK2 N-terminal domain, or spermine. **b**, In vitro CK2 phosphorylation of CaM, either bound to the CaMBD (left) or alone (right), stimulated by the SK2 N-terminal domain. Autoradiograph of phosphorylated CaM shows representative results for the conditions indicated, and the bar graph shows the average relative phosphorylation of CaM.

Figure 18.

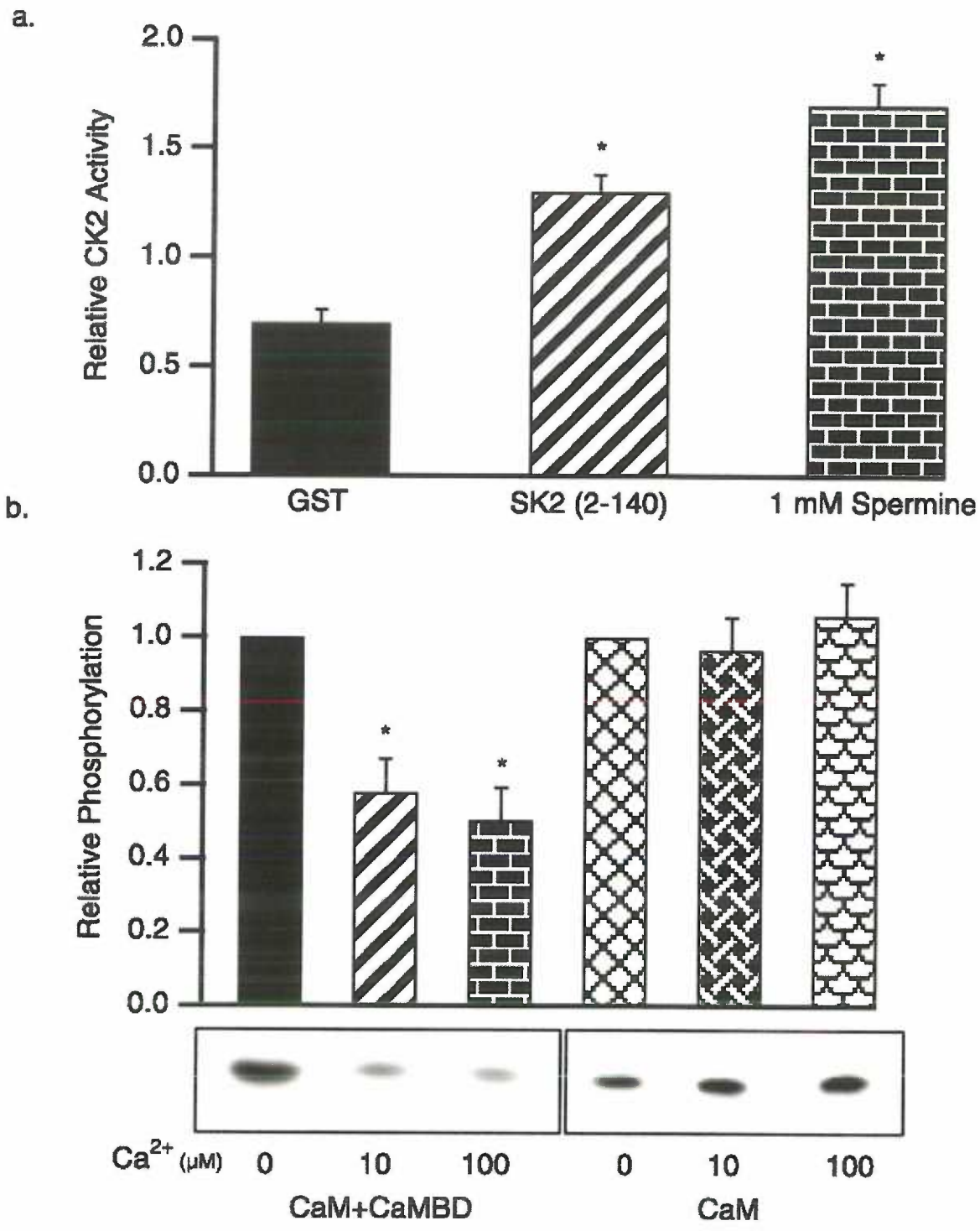
a.
Relative CK2 Activity
2.0
1.5
1.0
0.5
0.0
*
*
GST
SK2 (2-140)
1 mM Spermine
b.
Relative Phosphorylation
1.2
1.0
0.8
0.6
0.4
0.2
0.0
*
*
Ca2+ (μM)
0
10
100
0
10
100
CaM+CaMBD
CaM

Figure 19 Legend.

K121 regulates CK2 co-assembled with SK2 channels.

a, Amino acid sequence (109–134) of the positively charged cluster in the SK2 N-terminal domain that includes the identified CK2α binding site (RRALF; underlined). Asterisk indicates K121; the mutated lysine residues are in bold type. **b**, Examples of SK2 current deactivation for control SK2 (black traces) and after application of 5 mM MgATP (gray traces) for WT, SK2 K121A, and SK2 5KtoA channels. Calibration, 50 msec. **c,** Average τ_{offs} for SK2, SK2 K121A, and SK2 5KtoA before and after 5 mM ATP application.

Figure 19.

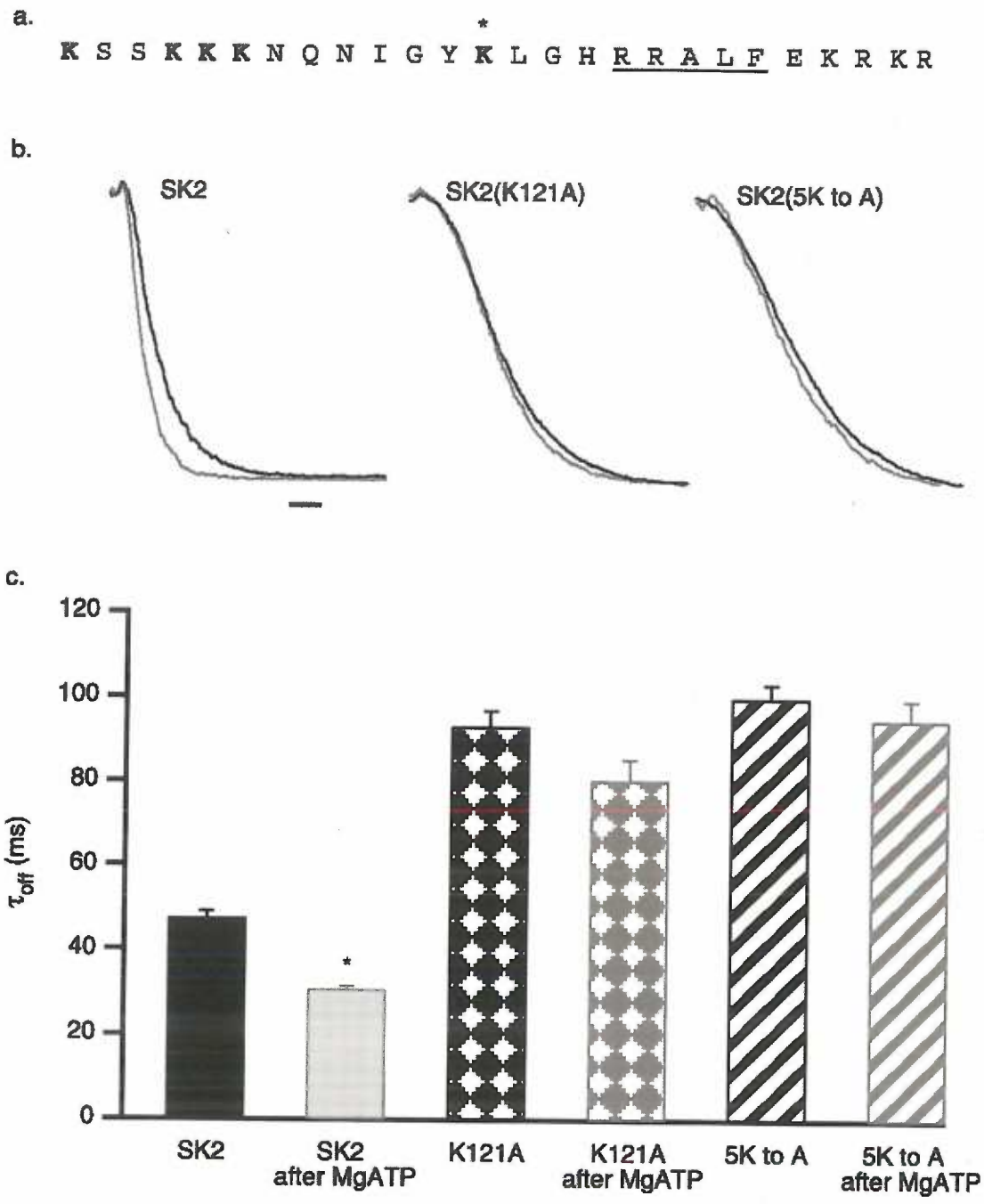
a.
K S S K K K N Q N I G Y K L G H R R A L F E K R K R
*
b.
SK2
SK2(K121A)
SK2(5K to A)
c.
τ_{off} (ms)
120
100
80
60
40
20
0
*
SK2
SK2 after MgATP
K121A
K121A after MgATP
5K to A
5K to A after MgATP

Generation of a model for the SK2 channel multiprotein complex

Using the data we obtained through the previously described experiments a working model of the SK2 channel multiprotein complex was created. In this model the C-terminus of SK2 is bound to CaM, a feature that is both well established and reproduced (data not shown) in parallel with the work presented in this thesis [92-94]. A second feature of our model is that the N and C-termini of adjacent subunits are bound together. This is supported by our GST-pulldown experiments where we observe an interaction between these two regions of the channel and by the observation that functional concatamers of SK2 channel subunits have been difficult [84], if not impossible to obtain. The remaining interactions in out model, those between CK2 and the N- and C-terminus of the channel and PP2A and the C-terminus of the channel, are supported by the GST-pulldown experiments. The CK2 activating residue K121 is located adjacent to CK2 in the model (fig.20).

Figure 20 Legend.

Model for co-assembled SK2, CaM, CK2, and PP2A.

The model, consistent with pull-down results and other data, represents two of the four SK2 subunits and invokes an inter-subunit interaction. CK2 and PP2A are drawn approximately to scale. In this configuration, the N-terminal domain of SK2 that includes K121 is positioned close to CK2 that binds to the adjacent sequence, RRALF.

Figure 20.

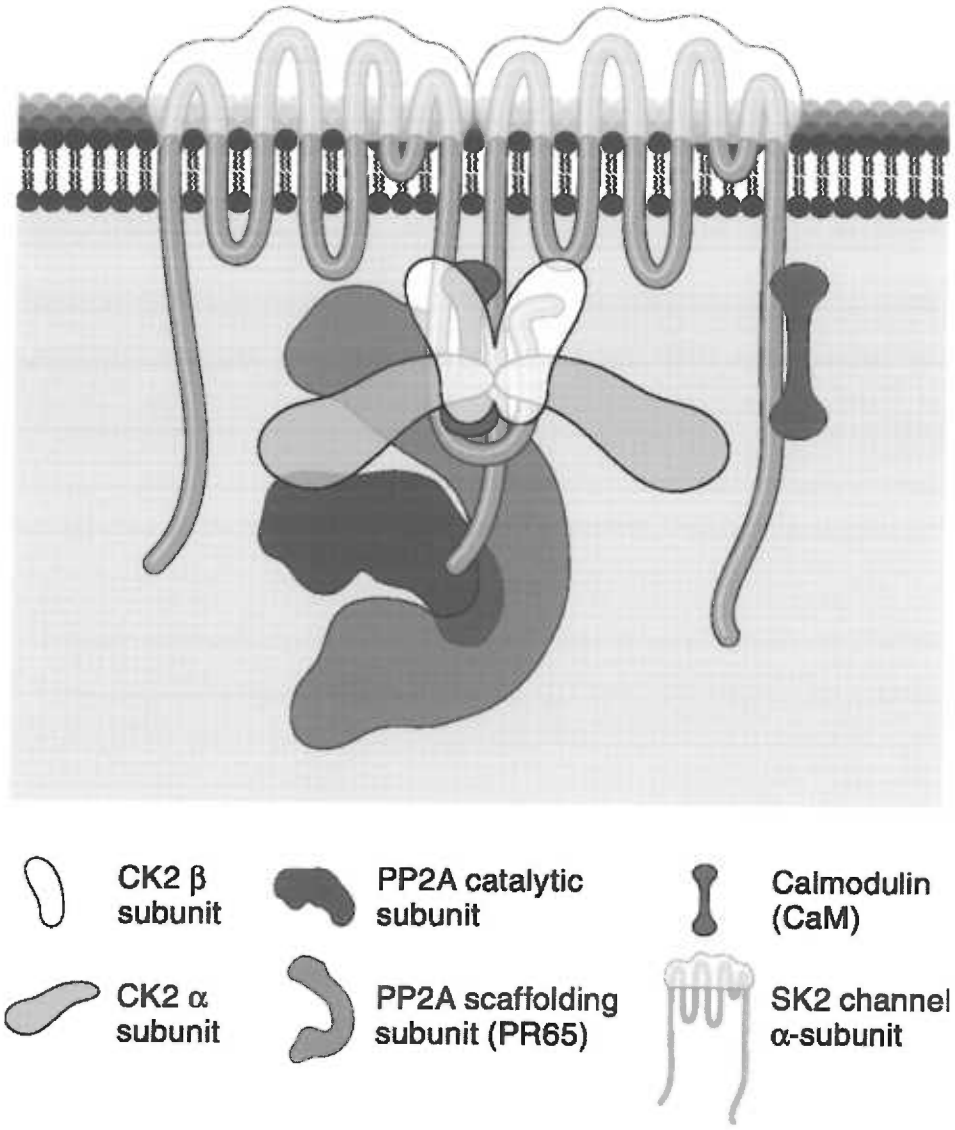
CK2 β subunit
CK2 α subunit
PP2A catalytic subunit
PP2A scaffolding subunit (PR65)
Calmodulin (CaM)
SK2 channel α-subunit

Summary of the extensive mutagenesis performed in order to test the proposed SK2 channel multiprotein complex model

During the course of this thesis a number of mutations were made that tested our model of the SK2 channel multiprotein complex. These mutations are grouped into three sections 1) N-terminal mutations, 2) C-terminal mutations, and 3) miscellaneous mutations. In all conditions, results of the mutation are compared to two sets of WT control data (baseline and $^{+}$MgATP) that were produced with different batches of DNA and bath solutions (old and new). P-values are quoted for comparison with the 'new' condition and are not qualitatively different from the 'old' condition, unless otherwise stated. The details and relevance of each mutation is discussed below.

To investigation the potential activation of CK2 by positive charges within the N-terminus of the channel, amino acids 11-129 were looped out, thus eliminating the majority of the positive charges within the N-terminus. This massive deletion prevented the detection of Ca^{2+}-activated currents on the surface of transfected CHO cells, clearly demonstrating that the N-terminus is essential for normal channel function. To further investigate this question specific basic residues were mutated to alanines. The obvious residues to begin with were those involved in binding of CK2α RR125,126. Unfortunately, channels containing alanines at these positions are normal both at baseline (p=1) and in their response to MgATP (p=1). This indicates that CK2 has not been dislodged by this mutation, and RR125,126 are not

the positive charges involved in CK2 activation. Mutations RKR132,133,134AAA and KRKR 131,132,133,134AAAA were analyzed next. Although RKR132,133,134AAA was phenotypically normal both at baseline (p=0.99) and after MgATP application (p-0.67), KRKR 131,132,133,134AAAA failed to produce detectable Ca^{2+}-activated currents. Remarkably, when the same mutation was made in an SK2 channel background that contains a triple-myc (myc3) tag in the S3-S4 loop Ca^{2+} sensitive currents were again observed. These currents, however, were not significantly different from WT either at baseline (p=0.98) or in response to MgATP application (p=1). The combination of the KRKR 131,132,133,134AAAA and the RR125,126AA mutations ($KRKR^{+}RR$ to $AAAA^{+}AA$) in the myc3 background returned the Ca^{2+} sensitive currents to background levels (n=10, fig.21). Notably, this is the third difference discovered between the WT channels and the myc3-tagged version of SK2, with the other two differences being loss of apamin sensitivity (Adelman lab, unpublished data) and decrease in base-line τ_{off} (WT= 49^{+}/-3 msec,n=6; SK2myc3= 35^{+}/-2 msec, n=7, $p<0.01$; data not shown). This suggests that significant structural changes have occurred in this channel with the introduction of the myc3 tags.

The most important N-terminal mutation was K121A. As was previously mentioned this mutation both increases the τ_{off} to a level indistinguishable from that observed when the CK2 inhibitor TBB is applied to the WT channel, and furthermore, it eliminates the MgATP effect. K121A

is significantly different from the WT condition at baseline ($p<0.0001$) and eliminates the MgATP effect ($p=0.06$, fig. 21). This basic residue is clearly the most essential for activating CK2, yet a trend towards CK2 activation still clearly exists. Consequently, the remaining four lysines in the region were mutated to alanines in two groups KKK112,113,114AAA and K109A. Results demonstrated a significant baseline shift in τ_{off} for the group of three ($p<0.0001$), but not for the K109A mutation ($p=0.26$), although a trend towards larger values was possibly present. However, in both cases a robust MgATP effect was observed ($p<0.01$ for KKK112,113,114AAA and $p<0.0001$ for K109A). Collectively these data suggest that these four lysine residues, especially the three adjacent lysines, have some minimal contribution to CK2 activation, at least in mutant channels. To control for this, all five lysine residues were mutated to alanines (5KA). Results indicated that baseline τ_{off} was significantly slowed ($p<0.0001$) and the MgATP effect was completely eliminated ($p=1$). Collectively, these data identify the primarily residue responsible for CK2 activation as K121 and demonstrate a minimal, but measurable, role for the four adjacent lysines K109, K112, K113, and K114 (fig. 21).

Mutations in the C-terminus of SK2 were done primarily to investigate three questions: first, can a mutation be made that prevents PP2A from binding to the channel; second, are the C-terminal serine and threonine residues contributing to baseline channel function or the MgATP

response; third, does elimination of the C-terminal CK2 binding site alter baseline channel function or the MgATP response.

Prior to the investigation of the first question, a literature search had revealed that a conserved PP2A binding motif (E_RK) existed in both SV40 small-T antigen and CK2α [137] (see fig. 13a) and it had been observed that a similar motif existed in the C-terminus of SK2 (E469, R471, K472). In light of this, four mutations were made: the first truncated the channel after the motif, 477*, the second in the middle of the motif, 471*; the third replicating the alanine mutation used in Heriche et al. (E_RK to ala), and the fourth expanding upon this mutation slightly by mutating Q470 and L473 to alanines as well (E_RK $^{+}$QL to ala). What was observed is that all four mutations significantly decreased the baseline τ_{off} of the SK2 channel, consistent with destabilization of PP2A binding (WT versus 477* n= 10,6 $p<0.0001$; WT versus 471* n= 10,6 $p<0.0001$; WT versus E_RK to ala n= 10,5 $p<0.0001$; WT versus E_RK $^{+}$QL to ala n= 10,6 $p<0.0001$, fig 22). However, two major differences did exist among these constructs: first, 471* resulted in rapid rundown of the channel (see Fig. 14), while the other channels were comparatively stable; second, 477* speeded τ_{off} by approximately half as much as the other constructs (471*, 1^{2+}/-2; 477*, 24^{+}/-2; E_RK to ala 14.4 $^{+}$/- 0.8; E_RK $^{+}$QL to ala, 16^{+}/-2), and comparisons revealed that this difference was significant (471* vs. 477* $p<0.01$, E_RK ala vs. 477* $p<0.05$, E_RK^{+}QL ala vs. 477* $p<0.05$, fig.22). This suggests that the truncation 477* only partially destabilizes the binding of PP2A.

Notably both the 471* and 477* truncations impact the other two questions about the C-terminus, since they both eliminate the C-terminal serine and threonine residues and the C-terminal binding site of CK2. Although the rapid rundown of 471* prevented an accurate assessment of the MgATP effect in this construct, 477* displays a highly significant response to a 2.5 minute application of 5mM MgATP (477*, n=6, $p<0.0001$, fig.22). This supports a model in which deletion of the C-terminal CK2 binding site does not prevent CK2 from interacting with the channel and one where the presence or absence of the C-terminal serine and threonine residues do not significantly alter baseline τ_{off} or the MgATP effect.

Large truncations in the channel, however, do not directly address either of the second two questions about the C-terminus, since compensatory changes could be occurring. Consequently, additional mutations were made to more directly investigate these questions. To begin, an additional truncation was made that removed only the C-terminal CK2 binding site and the C-terminal threonine and serine residues. Again, the channel was essentially normal at baseline (557* vs. WT old, n=10,6 p=0..99) and continued to display a robust MgATP effect ($p<0.0001$, fig. 22). In fact, whether the four arginine residues contained within the C-terminal CK2 binding site were mutated to alanines (RRRR 564,565,566,567 AAAA), the three serines immediately preceding these arginines were mutated to aspartates (SSS561,562,563 DDD), or the five terminal threonine and serine residues were mutated to alanines (T574, S575, S576, S578, S579

AAAAA) the effect was qualitatively identical; no significant difference between WT and the mutant, either at baseline or in response to MgATP (RRRR 564,565,566,567 AAAA vs. WT, n=5,10, p=1; SSS561,562,563 DDD vs. WT, n=4,10, p=0.15; T574, S575, S576, S578, S579 AAAAA vs. WT, n=6,10, p=1, fig. 22).

One additional mutation that was examined was the combined mutation of the N-terminal CK2 (RR125,126AA) binding site and the C-terminal CK2 binding site (RRRR 564,565,566,567 AAAA). This double mutation (RR125, 126AA $^{+}$RRRR 564,565,566,567 AAAA) prevented Ca^{2+}-activated currents from being detected on the surface of the CHO cells (n=10, data not shown).

Collectively, these data support a model in which the C-terminal CK2 binding site and the terminal serine and threonine residues serve merely as structural components of the complex and have no role in modulating the channel τ_{off} and MgATP sensitivity. Nevertheless, a previous paper from Anne Anderson's laboratory [122], and recent *in vivo* work from our laboratory [119], has demonstrated that three serine residues in the C-terminus of SK2 (S568, S569, S570) regulate surface expression of the channel. Consequently, it is possible that the phosphorylation state of surrounding serines and threonines may modulate this process.

Three additional mechanisms of regulating channel kinetics and MgATP sensitivity of the SK2 channel multiprotein complex were examined during the testing of our model. They are the following: 1) CK2

phosphorylation of a low or medium stringency CK2 consensus sequence on the channel, 2) the auto-phosphorylation sites on CK2-β, 3) potential CK2 phosphorylation sites on the catalytic subunit of PP2A. However, none of the experimental conditions proved significantly different than WT with respect to either baseline kinetics or response to MgATP (fig.23). The results are summarized as follows: The medium stringency (by http://scansite.mit.edu/) CK2 phosphorylation site phosphorylation surrogate, SK2 S495D, was similar to SK2 WT at baseline (n=4,10; p=0.90), and maintained a significant MgATP effect (n=4, p<.05, paired-t-test). The low stringency CK2 phosphorylation site phosphorylation surrogate, SK2 S501D, was similar to SK2 WT at baseline (n=3,10; p=0.99), and maintained a significant MgATP effect (n=3, p<.05, paired-t-test). Coexpression with the WT SK2 channel of a CK2β subunit lacking the autophosphorylation residues (S2,S3,S4) resulted in a baseline τ_{off} that was similar to SK2 WT (n=4,10; p=0.81), and maintained a significant MgATP effect (n=4, p<.05, paired-t-test). Coexpression with the WT SK2 channel of a PP2A catalytic subunit CK2 phosphorylation surrogate (S201D) resulted in a baseline τ_{off} that was similar to SK2 WT (n=4,10; p=0.1), and maintained a significant MgATP effect (n=4, p<.05, paired-t-test). The dephosphorylation surrogate at this position (S201A) was likewise similar to WT SK2 (n=3,10; p=1), and application of MgATP produced an effect that was nearly significant, and unremarkable considering a sample-size of three (n=3, p=0.051). Coexpression with the WT SK2 channel of a PP2A catalytic

subunit CK2 phosphorylation surrogate (Y307D) resulted in a baseline τ_{off} of (48.3 msec) that was similar to SK2 WT (τoff = 47^{+}/-1 msec) and appeared to respond to $^{+}$MgATP τoff = 32.5. Likewise, the dephosphorylation surrogate at this position (Y307A) appeared similar to WT both baseline (τ_{off} =39 msec) and after MgATP application (τ_{off} = 27 msec). However, in both cases the sample size was one, so statistics could not be performed. The data are summarized in figure 23.

Figure 21 Legend.

Summary of τ_{off} obtained from SK2 channel N-terminal mutants before and after 2.5 minute application of 5mM MgATP.

a, WT old, 53^{+}/-1 (n=6); WT old $^{+}$ MgATP, 28.1^{+}/-0.4 (n=6); WT, 47^{+}/-1 (n=10); WT $^{+}$MgATP, 30.3 $^{+}$/- 0.8 (n=10); 11-129 loop-out, 0 (n=20); RR125,126AA, $47.^{2+}$/-0.8 (n=7); RR125,126AA $^{+}$MgATP, 33^{+}/-1 (n=7); RKR132,133,134AAA, 4^{2+}/-3 (n=13); RKR132,133,134AAA $^{+}$MgATP, 23.0^{+}/-0.7 (n=13); KRKR 131,132,133,134AAAA, 0 (n=9); KRKR to AAAA (myc3 background), 41^{+}/-3 (n=9); KRKR to AAAA (myc3 background) $^{+}$MgATP, 3^{2+}/-2 (n=9); KRKR^{+}RR to AAAA^{+}AA (myc3 background), 0 (n=10); K121A, 93^{+}/-4 (n=10); K121A $^{+}$MgATP, 80^{+}/-5 (n=10); KKK112,113,114AAA, 7^{2+}/-3 (n=4); KKK112,113,114AAA $^{+}$MgATP, 50^{+}/-3 (n=4); K109A, 59^{+}/-5 (n=5); K109A $^{+}$MgATP, 3^{2+}/-1 (n=5); K109,112,113,114,121A^{+}AAA^{+}A(5K to A), 100^{+}/-2 (n=6); K109,112,113,114,121A^{+}AAA^{+}A(5K to A) $^{+}$MgATP, 98^{+}/-3 (n=6).

Figure 21.

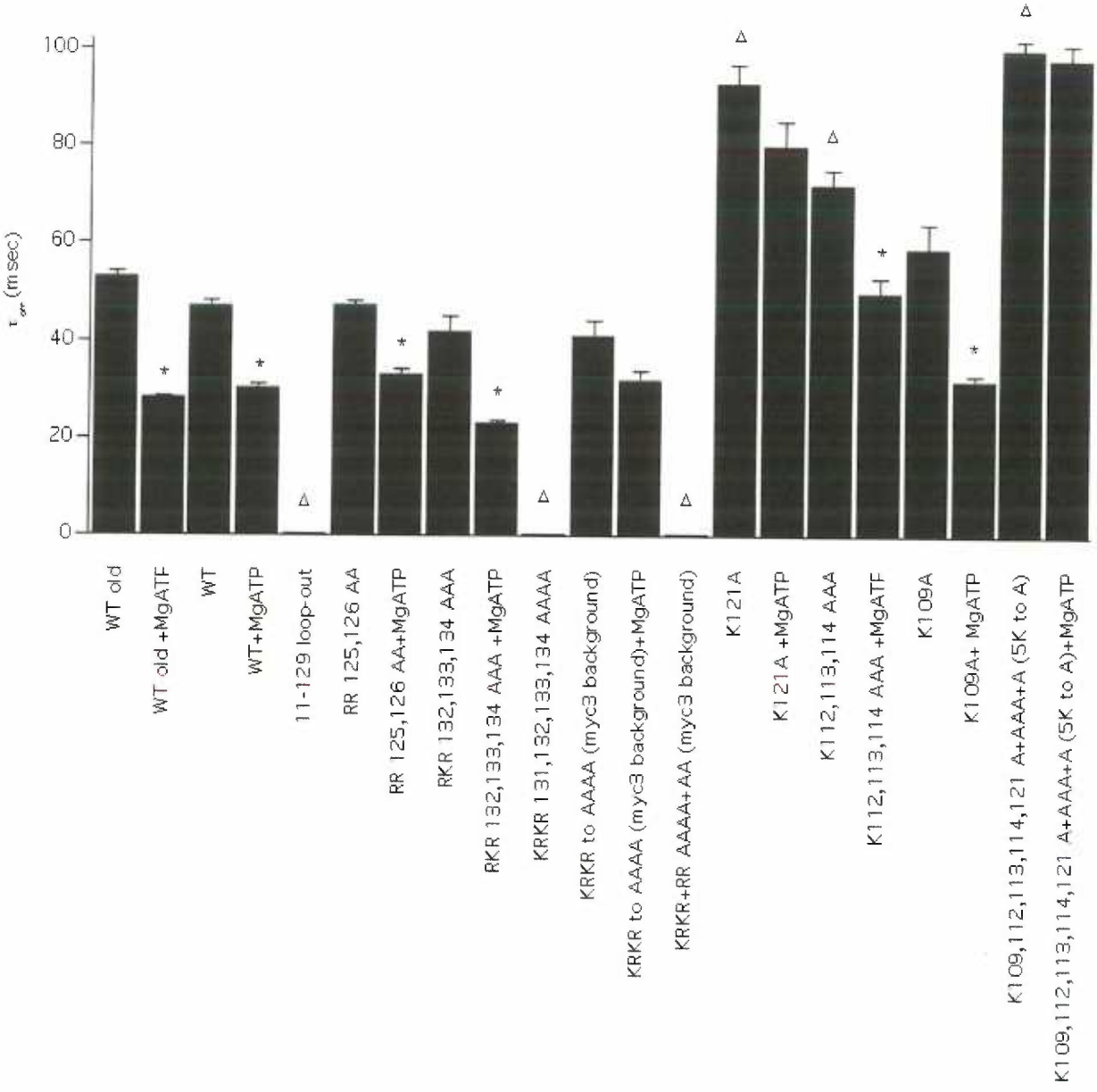
100
80
60
40
20
0
τ_{off} (msec)
WT old
WT old +MgATF
WT
WT+MgATP
11-129 loop-out
RR 125,126 AA
RR 125,126 AA+MgATP
RKR 132,133,134 AAA
RKR 132,133,134 AAA +MgATP
KRKR 131,132,133,134 AAAA
KRKR to AAAA (myc3 background)
KRKR to AAAA (myc3 background)+MgATP
KRKR+RR AAAA+AA (myc3 background)
K121A
K121A +MgATP
K112,113,114 AAA
K112,113,114 AAA +MgATF
K109A
K109A+ MgATP
K109,112,113,114,121 A+AAA+A (5K to A)
K109,112,113,114,121 A+AAA+A (5K to A)+MgATP

Figure 22 Legend.

Summary of τ_{off} obtained from SK2 channel C-terminal mutants before and after 2.5 minute application of 5mM MgATP.

a, Alignment of SK2 C-terminus showing R464/K467 (blue underlined residues), the PP2A binding site E_RK (red underlined residues), sites of truncation (bold numbers), known PKA phosphorylation sites (bold residues), potential phosphorylation sites mutated (tan underlined residues). **b**, , WT old, 53^{+}/-1 (n=6); WT old $^{+}$ MgATP, 28.1^{+}/-0.4 (n=6); WT, 47^{+}/-1 (n=10); WT $^{+}$MgATP, 30.3 $^{+}$/- 0.8 (n=10); 471*, 1^{2+}/-2 (n=6); 471* $^{+}$MgATP, 7^{+}/-2 (n=2); E_RK to ala, 14.4 $^{+}$/- 0.8 (n=6); E_RK to ala (old), 15 $^{+}$/- 2 (n=5); E_RK to ala (old) $^{+}$MgATP, 13 $^{+}$/- 1 (n=5); 477*, 24^{+}/-2 (n=6); 477*, 11.1^{+}/-0.8 (n=6); 557*, 57^{+}/-3 (n=10); 557*$^{+}$MgATP, 31^{+}/-1 (n=10); S561,562,563DDD, 37^{+}/-3 (n=4); S561,562,563DDD $^{+}$MgATP, 20^{+}/-2 (n=4); RRRR 564,565,566,567 AAAA, 46^{+}/-2 (n=5); RRRR 564,565,566,567 AAAA $^{+}$MgATP, 31^{+}/-2 (n=5); T574,S575,S576,S578,S579 AAA^{+}AA, 47^{+}/-2 (n=6); T574,S575,S576,S578,S579 AAA^{+}AA $^{+}$MgATP, 27^{+}/-2 (n=6).

Figure 22.

a.

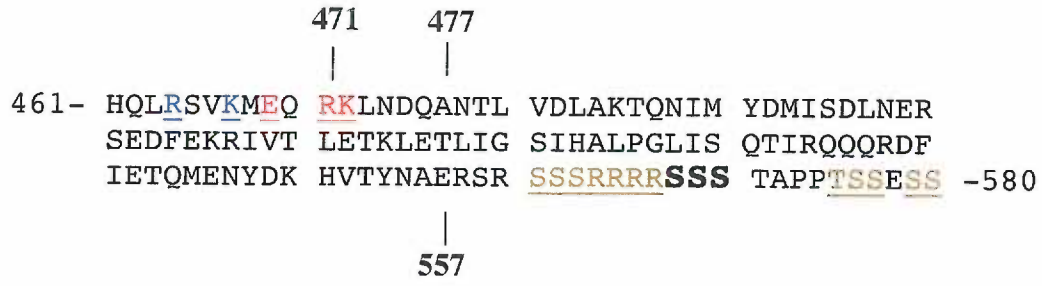

b

Summary of mutations in the C-terminus of rat SK2 on the deactivation time constant and the response to 5mM MgATP applicaiton.

- Δ Significantly different from WT
- * Significantly different after MgATP application
- α Channel has rundown before τ_{off} determination in most cases.

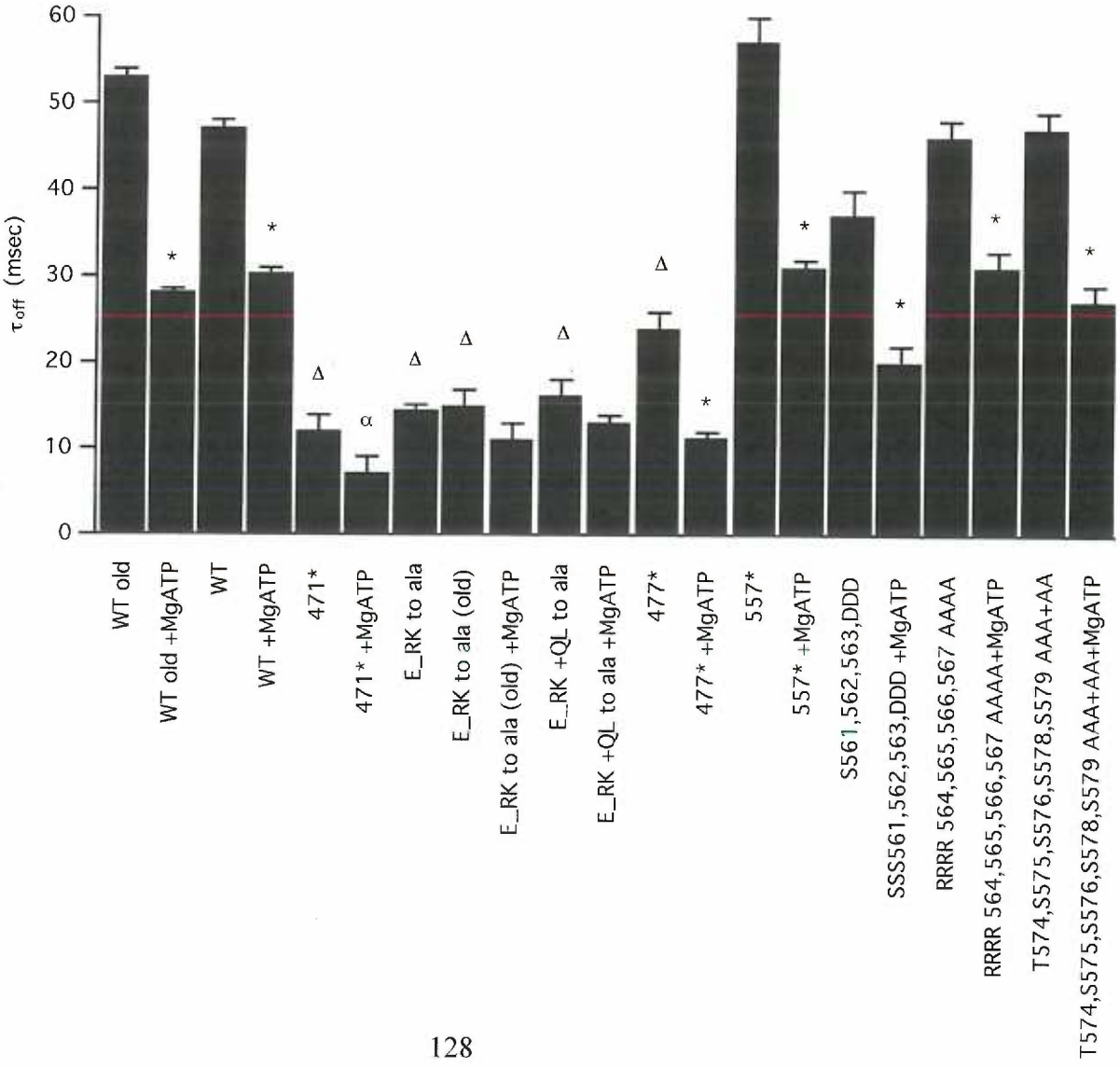

Figure 23 legend.

Other possible mechanisms of τ_{off} modulation do not appear important for our model of the SK2 channel multiprotein complex.

Comparison of deactivation time constants between WT SK2 channels and 1) those containing possible CK2 phosphorylation sites on the SK2α subunit (red line, S495D vs. WT, baseline n=4,10; p=0.90, after MgATP n=4, p<.05, paired-t-test; S501D vs. WT, baseline n=3,10; p=0.99, after MgATP n=3, p<.05, paired-t-test), 2) known CK2 β autophosphorylation sites (yellow line, CK2$\beta\Delta$ S2,S3,S4 coexpression vs. WT, baseline n=4,10; p=0.81, after MgATP n=4, p<.05, paired-t-test), and 3) possible CK2 phosphorylation sites on the PP2A catalytic subunit (purple line, $PP2A_{cat}$ S201D coexpression vs. WT, baseline n=4,10; p=0.1, after MgATP, n=4, p<.05, paired-t-test; $PP2A_{cat}$ S201A coexpression, baseline n=3,10; p=1, after MgATP, n=3, p=0.051; $PP2A_{cat}$ Y307A coexpression, baseline τ_{off} =39 msec., after MgATP τ_{off} = 27 msec.; $PP2A_{cat}$ Y307D coexpression, baseline τ_{off} = 48.3 msec., after MgATP τ_{off} = 32.5 msec.

Figure 23.

* Significantly different after MgATP application by ANOVA

\# Significantly different after MgATP application by paired t-test

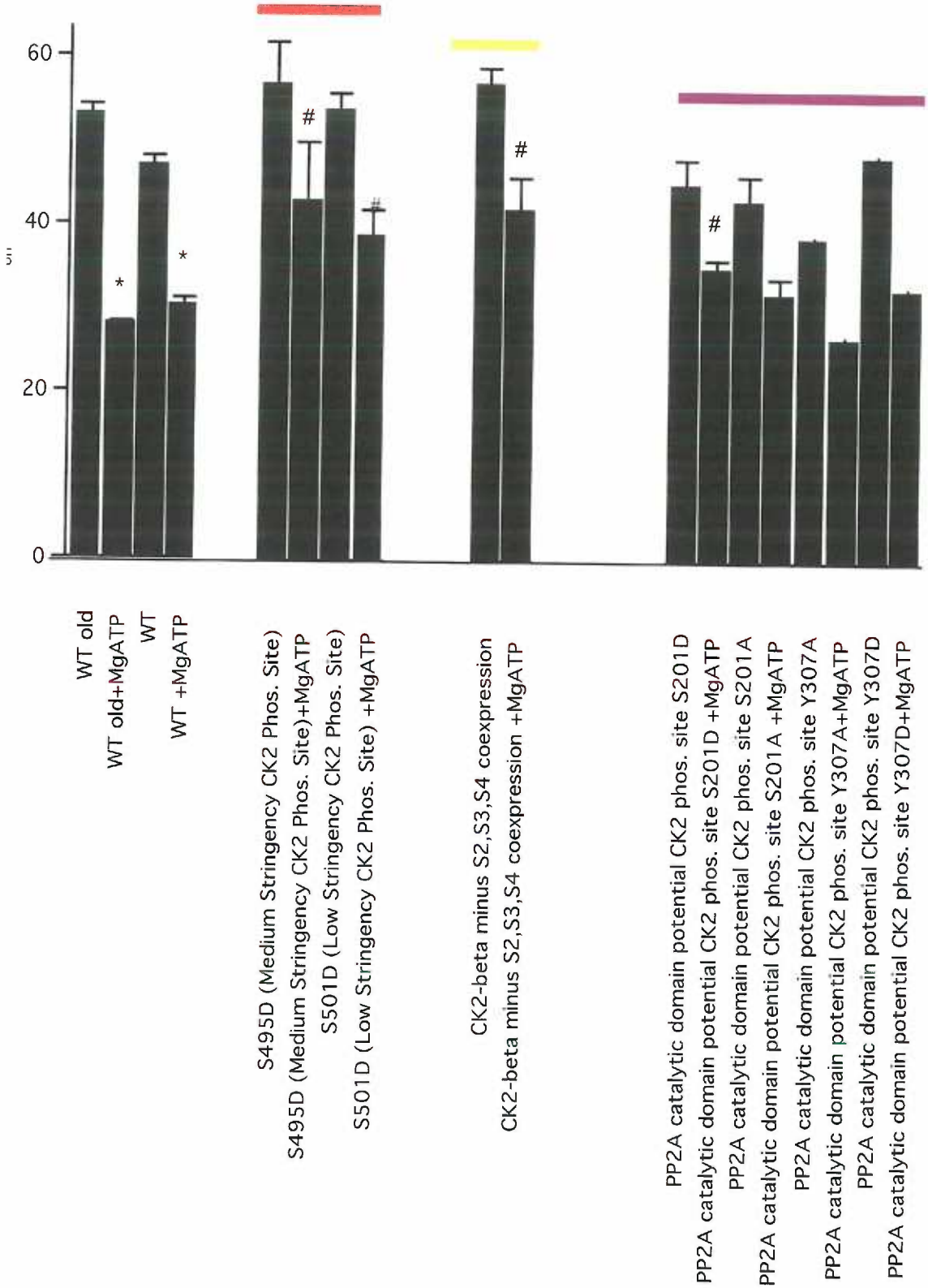

Discussion

In the paper Bildl et al. (2004)[163] evidence was presented that SK2 channels are part of a multiprotein complex that contains, at a minimum, the proteins SK2, CaM, $PP2A_{A\ (PR65)}$, $PP2A_C$, CK2α, and CK2β. Furthermore, it was suggested that the CaM surrogates T80A and T80D, when co-expressed with the WT SK2 channel, recapitulate the two extremes of SK2 channel Ca^{2+} sensitivity. However, while the CaM surrogate T80D clearly altered the τ_{off} of the WT channel, the only clear effect of co-expressing CaM T80A with WT SK2 channels was an increase in how well the concentration response data were fit by a Hill equation with a single component. In contrast, the CHO cell concentration response data presented in this thesis was always well fit by a Hill equation with a single component, regardless of whether the channel was co-expressed with CaM WT, CaM T80A, or CaM T80D. To investigate this issue further we performed rtPCR on CHO cells expressing CaM WT, CaM T80A, or CaM T80D alone, and our results indicated that the mRNA for T80A is destabilized (fig. 5b). Although there may be differences in RNA processing and degradation between CHO cells and Xenopus oocytes, we hypothesize that T80A does not accurately reflect the upper limit of SK2 channel τ_{off}. Additional data presented in this thesis agrees with this hypothesis.

Additional experiments with CHO cells expressing SK2 channels relied on their ability to co-assemble with native CaM, CK2 and PP2A. To demonstrate that a kinase was indeed associated with the SK2 channel

multiprotein complex 5mM MgATP was applied for 2.5 minutes. Results confirmed that MgATP application significantly speeded the τ_{off} from ~50 msec. to ~30 msec., consistent with activation of an associated kinase (fig.6a,b). Notably, this effect reached a steady-state level (τ_{MgATP} effect 0.5msec., fig. 6d) that was significantly different than that observed when CaM T80D is co-expressed with the WT SK2 channel, a τ_{off} of ~15msec (fig. 5a). To demonstrate that this kinase activity was CK2, the specific inhibitor of CK2 TBB (10μM) was applied along with the MgATP. Consistent with the inhibition of protein kinase CK2, τ_{off} shifted to ~100 msec. in TBB (fig.6a,b). Furthermore, both the MgATP and $MgATP^{+}TBB$ data were qualitatively consistent with shifts in SK2 channel Ca^{2+} sensitivity (fig.6c). Collectively, these data indicate that 1) CK2 is responsible for T80 phosphorylation *in vivo*, and 2) the upper limit of SK2 τ_{off} resulting from completely dephosphorylated CaM is ~100msec., which results in a dynamic range of ~7 fold. These data also suggest that a steady-state is formed between CK2 phosphorylation of SK2-associated CaM on T80, on one hand, and dephosphorylation of SK2-associated CaM on T80 by an associated phosphatase (latter shown to be PP2A), on the other. In a previous study that examined single-channel recordings from SK2 channels both a low and a high Po were obtained [167]. This duel Po may represent the two phosphorylation states of SK2-associated, CaM T80. However, future single-channel recording experiments are needed to confirm this.

TBB is structurally very similar to the SK channel family activator 1-EBIO [97], both being benzimidazolinones. To test whether TBB and 1-EBIO are working through similar mechanisms to enhance SK2 channel τ_{off}, a time course was performed in which a 20 second exposure of TBB, given prior to application of MgATP, completely blocked the MgATP effect. In contrast, a robust MgATP effect still occurred when channels were pre-exposed to 1-EBIO (fig. 7). It can be concluded from this that 1-EBIO does not inhibit CK2 (confirmed by Lorenzo Pinna's laboratory, private communication), and, consequently, it can be surmised that 1-EBIO increases the τ_{off} of SK2 channels through a non-specific allosteric mechanism, whereas TBB exerts its effects through the specific inhibition of the associated kinase, CK2.

A strong association between CK2 and SK2 has been suggested from both proteomic experiments and *in vitro* binding data. The stable association was again confirmed by holding inside-out patches in CK2-free bath solution for 10 minutes prior to assaying for the MgATP response. The fact that a robust MgATP response still occurs indicates that CK2 is stably associated with the SK2 channel multiprotein complex (fig.8). The small, but significant, 'run-down' in magnitude of the MgATP response may represent a fraction of CK2 washing off the complex, loss of some additional cofactor, or non-specific rearrangements of the complex that leave it unable to respond to MgATP.

phosphatase inhibitor cocktail 2 (PIC2) contains sodium vanadate, sodium molybdate, sodium tartrate and imidazole at proprietary concentrations (Sigma Pharmaceuticals) and inhibits acid, alkaline, and tyrosine phosphatases. A significant effect was observed with the PIC1, but not the PIC2, cocktail of inhibitors (fig.10). This supports the hypothesis that PP2A is the associated phosphatase in the SK2 channel multiprotein complex.

Like the CK2 dependent MgATP effect, the PIC1 effect is maintained even after the patch is held in bath solution for 5 minutes prior to PIC1 exposure. It can be concluded from this that PP2A is stably associated with the SK2 channel multiprotein complex (fig.11).

The activity of PP2A was neither state-dependent nor was it speeded by SAP, even though the concentration used (10U/mL) was twice that used in Gerlach et al (2000) [168] to decrease the phosphatase activity in single-channel experiments on the SK channel family member IK1 (fig.12). One possible explanation for this is that CaM T80 might be shielded from the bath solution by CaM and the other components of the macromolecular complex.

Previous work on CK2 identified a PP2A binding motif that is shared with another PP2A binding protein SV40 small-T antigen (fig.13a). When a triple alanine mutation was made in this motif binding of PP2A was eliminated [137]. Mutation of a similar motif in the SK2 C-terminus results in the loss of binding of the PP2A scaffolding subunit to the C-terminus of the channel (fig.13b) Furthermore, the τ_{off} is shifted to a level identical to that

observed when CaM T80D is co-expressed with the WT SK2 channel. Also a dominant negative PP2A scaffolding subunit speeds τ_{off} when co-expressed with the WT SK2 channel (fig.13c). Collectively, these data indicate that PP2A is bound to a consensus sequence in the C-terminus of the channel.

The presence of PP2A is especially interesting in the context of two other sets of data. The first is from Lee et al (2003) [99] and the second is from Gerlach et al (2001) [169]. In the first paper, Ca^{2+} dose-response experiments were performed on SK2 R464E/R467E^{+}WT CaM, WT SK^{2+}CaM E84R/E87K, and SK2 R464E/R467E $^{+}$ CaM E84R/E87K. When the Ca^{2+} sensitivity of these conditions are compared to WT SK2 the first two conditions result in a moderate decrease in the Ca^{2+} sensitivity. This, perhaps, should be expected since each contains a mutation that destabilizes the binding of CaM to the SK2 channel. However, when the mutants are expressed together the Ca^{2+} sensitivity decreases even further, to a level equivalent to that observed when the E_RK to ala mutation is made in the WT channel. This is, perhaps, surprising, since the salt-bridge should be reconstituted by this double mutation. Interestingly enough, R467 is only two amino acids away from the E in the E_RK mutant. Consequently, it is possible that the shift in Ca^{2+} sensitivity observed in Lee et al (2003) was due to a dislodging of PP2A from its binding site. Furthermore, the fact that SK2 R464E/R467E $^{+}$ CaM E84R/E87K coexpression made the Ca^{2+} sensitivity worse, suggests that PP2A is also stabilized by residues within

CaM. The second paper, Gerlach et al (2001) [169] tracks the PKA mediated activation of hIK1 to a specific region of the channel. This region, RL**K**H**RK**LREQVNSM, contains the amino acids that are homologous to E_RK in SK2. Furthermore, when the single PKA consensus site in IK1, S334, is mutated to alanine the PKA effect remains. Consequently, the PKA must be acting through an indirect mechanism [168]. These data, combined with the fact that the C-terminus of IK1 can physically bind the scaffolding subunit of PP2A (data not shown), suggests that the PKA mediated activation of hIK1 proceeds through PP2A.

An interesting feature of the PP2A interacting domain in CK2α is that it can also bind to casein kinase interacting protein 1 (CKIP-1), and possibly other protein targets. CKIP-1 is an actin-capping protein that causes cytoskeletal and morphological modifications [170]. This association could link SK2 channel activity with dendrite morphology and synapse remodeling.

Of the many C-terminal mutations and truncations that have been made in SK2 only 471* has robust current amplitudes immediately after excision of an inside-out patch, yet a significantly decreased τ_{off} and rapid rundown. This combination of phenotypes is odd, because it suggests that some cofactor that is present in the cell is being lost as the inside-out patch sits in the bath solution. Since this rundown could not be rescued by 10μM Ca^{2+}/CaM application, as the R464E/R467E mutant was in Lee et al[99], loss of CaM can be ruled out. Another possibility is that PP2A is required for

functional SK2 channels and the truncation 471* binds PP2A even less well than the E_RK to alanine mutant. This combination of factors would result in slow rundown of the E_RK to alanine mutant and a fast rundown of 471*, after loss of the pool of free PP2A available inside the cell. Now with absolutely no phosphatase to oppose the kinase, phosphorylation of CaM T80 by CK2 will approach 100% of SK2-bound CaM. This hypothesis requires that an SK2 channel that has all four associated CaMs phosphorylated on T80 is nonconductive. More experiments will be required to determine the validity of this conjecture.

Bildl et al (2004)[163] previously demonstrated that CK2α and CK2β could both bind to the C-terminus of SK2 through their initial proteomics approach and, furthermore, demonstrated that the purified proteins could bind both the N- and C-termini of SK2 [163]. The experiments presented in this thesis both repeated all of the previously reported interactions and greatly expand on those results in order to identify the precise regions of interaction between CK2α and the SK2 N- and C-termini, CK2β and the SK2 N- and C-termini, and the SK2 N- terminus and the SK2 C-terminus (fig.15). The interaction between CK2α and the SK2 N-terminus could be narrowed down to a precise region of interaction, RRALF, that turns out to be immediately adjacent to the CK2 activating residue K121. Although this binding site likely serves to stabilize CK2α and enhance the efficiency of K121 mediated activation, it is not essential, in the sense that the two arginines (R125 and R126) can be mutated to alanines without loss of channel function or

MgATP response, see (fig.21). Notably, this was not true once four arginines in the SK2-channel specific (fig.17), C-terminal CK2 binding site (R564, R565, R566, R567) were mutated to alanines in parallel with R125 and R126 (data not shown), an effect which prevented Ca^{2+} activated currents from being detected on the surface of transfected CHO cells. In addition to the N-terminal and C-terminal CK2α binding sites, CK2α also binds to a region in the CaMBD. Although one mutation was made in this region in an attempt to dislodge CK2α (R450A, K451A), the results were similar to WT SK2 both at baseline and with respect to MgATP response (n=4, p=1, p=1). Further mutagenesis was not performed since CaM also binds to this region and, consequently, mutations may also dislodge CaM. Consequently, results from mutagenesis in this region are difficult to interpret. Furthermore, the primary goal of our mutagenesis was to create a channel that could no longer bind CK2 and, consequently, no longer phosphorylate SK2-associated CaM. Once it was discovered that K121A eliminates CK2 activation, attempts to dislodge CK2α binding were abandoned.

Binding of CK2β, on the other hand, could not be narrowed down to a specific region of interaction with the N-terminus of SK2. Hence, it is unclear whether CK2β binds to the N-terminus of the channel *in vivo* and the tertiary structure is not maintained in the smaller N-terminal fragments, or whether binding is merely an artifact of *in vitro* pull-down experiments. Nonetheless, CK2β could bind robustly to both a region within the CaMBD

and the same C-terminal, serine and arginine rich motif that CK2α, and the N-terminus of the channel, bind.

Some evidence that the N- and C-termini of SK1 are bound together as a functional unit comes from a paper from Martin Stocker's laboratory that suggests that an ER-retention signal for rSK1 is encoded within a complex of the N- and C-termini [171]. Also, evidence for an interaction between the N- and C-termini of SK3 was recently reported by Heike Jager's laboratory [172], as demonstrated by a yeast-2-hybrid assay. In contrast to that paper, we did see a robust interaction between the N- and C-termini of SK2, one that could be observed even after 4 washes with PWB containing 300mM salt. Interestingly enough, this interaction occurred between amino acids 72-129 of the SK2 N-terminus and the same two regions of the SK2 C-terminus observed to interact with CK2α and CK2β (fig.15). The fact that we see more than one protein binding to the same region in the SK2 channel can be explained by several different models, a few of which are the following: 1) one protein out of the three (CK2α, CK2β, SK2 N-terminus) dominates binding to both these regions *in vivo*, 2) one protein binds with greater affinity to one region and a second protein binds with greater affinity to another, 3) one protein binds at an earlier point in time during the life cycle of the channel, but is later replaced by a second protein, 4) one protein binds during one conformation of the channel complex, but is displaced by a second protein during another conformation of the complex, 5) there is less than 4-fold symmetry of the intracellular

domains of the channel, as suggested by the crystal structure of the CaM/CaMBD [94], 6) binding of two proteins to one site can occur simultaneously, with the site sandwiched between the two protein binding partners.

One interesting feature of our *in vitro* binding data is that it identifies the CaM binding domain as a very busy region of the SK2 channel. Not only does CaM bind there, but so does CK2 and PP2A. So how is there enough room for all these proteins? Well, if the binding domains of CK2 and PP2A are mapped onto the crystal structure of the CaM/CaMBD complex it is obvious that both regions could accommodate a large protein-binding partner (fig.16). Yet, these regions are close to one another and close to CaM. This makes sense, because all these proteins must work together in a highly coordinated fashion to phosphorylate and dephosphorylate CaM T80.

An alignment of the protein sequences of the SK channel family allows for a comparison of the PP2A and CK2 binding sites among the SK channel family (fig.17). A visual inspection of this comparison suggests that CK2 is associated with SK1, SK2, &SK3, but not IK1, while PP2A is associated with SK2 and SK3, but neither SK1 nor IK1. One testable hypothesis that comes from this data is that SK1 is associated exclusively with CK2α, which can itself bind PP2A, but not with CK2α'. This feature would result in the absence of selective pressure on SK1 to evolve, or maintain, a PP2A binding site. However, homology comparisons like these require functional confirmation. IK1, for instance, can bind the scaffolding

subunit of PP2A quite tightly in a GST-pulldown assay (data not shown), despite a charge reversal in the PP2A-binding motif (fig.17). It remains to be seen whether this interaction is important for IK1 physiology *in vivo*, as suggested in Gerlach et al (2001) [169].

Mutagenesis on the N-terminus of the channel (fig.21) revealed that a single lysine residue, K121, controls the activation of SK2-associated CK2. This is surprising since activation of CK2 is usually ascribed to polybasic compounds like poly-K or spermine. On the other hand, this is the first example of this type of *in vivo*, CK2 activator; consequently, strategic location of single, positive charges may be a general theme in CK2 activation by associated protein binding partners. Nevertheless, the mechanism by which K121 works is likely the same as that for the polybasic compounds. The current model for this is the following: an acidic-loop exists on CK2β that usually repels negative charges in the CaM C-terminus; however, when polybasic compounds (or K121A) are present they shield the acidic-loop so that CaM can enter the active site of CK2 [153].

During the course of this thesis many mutations were made in the SK2 channel in order to test various hypotheses about structure and function, and ultimately, to test our model of the SK2 channel multiprotein complex. These are discussed below: First, looping out the N-terminus of the channel, residues 11-129, results in no Ca^{2+} sensitive current being detected on the surface of the cell. However, like the other "dead" channels discovered over the course of this project, it is not clear whether this

channel reaches the surface and is non-functional or remains trapped in the ER. Unfortunately, our tool for assessing this question, SK2 myc3, is itself a problem, since an SK2 mutation that contains the tags (KRKR 131,132,133,134, AAAA) results in a functional channel, whereas an SK2 channel lacking the myc tags, but containing the mutation, does not result in Ca^{2+} sensitive currents on the surface of CHO cells. Interestingly, the KRKR motif is similar to the ER-retention signal RKR in Kir6.2 and SUR1 subunits of the K(ATP) channel [173]. However, expected results would be in the opposite direction as observed with this sequence in SK2, so this motif is serving some alternative function.

Four mutations were made of lysine residues adjacent to the CK2α binding site (RRALF) that were hypothesized to be responsible for CK2 activation. Mutation to alanine of the lysine furthest away from the CK2α binding site K109A, had a non-significant effect on the baseline τoff of the channel or MgATP. Mutation of the triplet of lysine residues slightly closer to the CK2α binding K112,113,114 to alanine, had a significant effect on the baseline τoff of the channel, but didn't significantly alter the response to MgATP. Only mutation of K121 to alanine significantly increased both the baseline τoff of the channel and eliminated the MgATP effect. However, because a trend towards MgATP activation still exists in the K121A mutant, a mutation was made where all 5 lysines were mutated to alanine residues (5KA). In this mutation all traces of the MgATP effect were eliminated. These data support a model in which K121 is the primary in vivo activator of

CK2, but a small contribution is made from the adjacent lysine triplet K112, 113, 114. Support for a small contribution from the lysine triple is provided by the fact that baseline τ_{off} is significantly altered by mutation to alanine ($p<0.001$), but the central role of K121 in our model as the primary activator of CK2 is supported first by the fact that its τ_{off} is significantly increased not merely over WT SK2, but over that of the triplet mutant K112, 113, 114AAA ($p<0.01$), and second, by absence in K121A of a significant change in τoff after a 2.5 minute application of 5mM MgATP.

Mutations in the C-terminus of SK2 were focused around truncations, PP2A binding site mutations, and mutations of C-terminal serine and threonine residues. The most extreme C-terminal mutation 471*, eliminates all the potential C-terminal phosphorylation sites, the PP2A binding site, and either destabilizes CaM or alters the structure of the channel enough so that rapid rundown is observed with this mutation. Nevertheless, it is important to note that a large amount of current is observed immediately after pulling an inside-out patch. Thus some feature of the intracellular solution, perhaps a readily available supply of PP2A, perhaps an unidentified cofactor, is not replicated by out artificial bath solution. Another interpretation is that the opening of the channels somehow dislodges CaM when it is not held in place by PP2A. However, evidence against this hypothesis is the fact that 471* is not rescued by Ca/CaM application. In contrast, 477*, a truncation beginning only 6 amino acids away, eliminates all the potential C-terminal phosphorylation sites, but does

not experience rapid rundown. It does, however have a decreased baseline τoff, suggesting that binding of PP2A is partially destabilized by this mutant. Truncation 557*, on the other hand, has a τoff that is equivalent to WT SK2, despite the elimination of all phosphorylatable serines and threonine residues at the very C-terminus of the channel. This fact combined with additional mutations that change these residues to alanines or aspartates (S561, 562, 563DDD and T574, S575, S576, S578, S579AAAAA) suggest that the phosphorylation status at these residues has minimal effects on SK channel Ca^{2+} sensitivity and gating kinetics.

The specific PP2A binding site mutants E_RK to ala and EQRKL to ala, were based on the reported PP2A binding site motif shared between CK2α and SV40 small-t antigen. As expected, these mutations prevent the majority of PP2A from binding to the channel (fig.22) and shift τoff to a level indistinguishable from that observed when CaM T80D is co-expressed with the WT channel. These mutations were not statistically different from one another (p=1), so the triple alanine mutation that was used in Heriche et al (1997) [137] to dislodge PP2A was used for further experiments in this thesis.

Another interesting mutant is the combination of the K121A mutation and the E_RK ala mutation. As might be expected, this channel has a large variability in its baseline τ_{off}, with a range from 59 to 92 msec., and this variability was significantly larger than the variability observed in a sample of WT channels (F-test, $p<0.001$). This result suggests that the

K121A mutation is more effective at preventing CK2 activation than E_RK to alanine is at dislodging PP2A.

Three additional hypotheses were tested in the course of testing our model for the SK channel multiprotein complex. All were negative results. First, it is well established *in vitro* that the CK2β subunit can be auto-phosphorylated by CK2 on three N-terminal serine residues [141]. Could this contribute to baseline SK channel τoff or the response to MgATP? A CK2β that lacks these residues was co-expressed with CK2α and the SK2 channel in CHO cells, inside-out patches were pulled and gating kinetics were assessed. The results were not significantly different from WT.

The second hypothesis was that, although the Fakler laboratory had shown that CK2 could not phosphorylate a residue within the CaMBD of SK2 (a fact that is not surprising since not even a low-stringency CK2 phosphorylation site exists there...), one medium (S495) and one low-stringency (S501) site exist in the D-helix of the SK2 channel. Could CK2 be phosphorylating these residues and altering baseline SK channel τoff or the response to MgATP? Mutations were made to aspartate to mimic CK2 phosphorylation in intact channels, the mutants were expressed in CHO cells an gating kinetics were assessed. Neither position had a significant effect baseline SK channel τoff or the response to MgATP.

The third hypothesis was that CK2 could be phosphorylating the catalytic subunit of PP2A on one of the two potential CK2 phosphorylation site (S201 and Y307) and this could be altering baseline SK channel τoff

and the response of the channel complex to MgATP. Mutations were made in the catalytic subunit of PP2A both to alanine and to aspartate residues, mutant PP2A catalytic subunits were co-expressed with WT SK2 channels in CHO cells, inside-out patches were pulled and gating kinetics were assessed. None of the four mutations resulted in SK2 channels with altered τoffs or MgATP effects.

Collectively, these data support the model of the SK2 channel multiprotein complex presented in figure 20, and they reject a contribution from CK2β autophosphorylation, phosphorylation of the channel itself by CK2, and phosphorylation of associated PP2A catalytic subunits by CK2, as components of that model.

Chapter III.

The *in vivo* function of SK2 channel Ca^{2+}-sensitivity modulation

Introduction and Background

Although some evidence available at the beginning of this project suggested that SK2 channel, Ca^{2+} sensitivity modulation was important in the auditory outer hair cells of the cochlea [163], our laboratory is primarily interested in the role of SK2 channels in learning and memory. Consequently, we set out to find a physiological role of SK2 channel, CK2 and PP2A mediated, Ca^{2+} sensitivity modulation in hippocampal CA1 neurons.

The experiments described in chapter II identified two SK2 channel mutations that shift the Ca^{2+} sensitivity and gating kinetics in opposite directions. SK2 K121A prevents SK2-bound CK2 from being efficiently activated; hence, it shifts SK2-bound CaM toward the dephosphorylated state. SK2 E_RK to ala, on the other hand, destabilizes the binding of SK2-associated PP2A, and it shifts the phosphorylation state of SK2-bound CaM towards phosphorylation. The range of Ca^{2+}-sensitivity between these two mutants is ~7-fold. Importantly, these mutants can serve as a set of tools to investigate the *in vivo* function of SK2 channel Ca^{2+} sensitivity modulation. To utilize these mutants, we needed to introduce the mutant channel back into the neurons of a living mouse so that hippocampal slices can be made and slice-physiology experiments can be performed.

The quickest and most efficient way to introduce a gene back into a living animal is viral-mediated gene transfer [174], and this is the method we chose to pursue for our subsequent experimentation with the SK2 channel

mutants K121A and E_RK ala. More specifically we used adeno-associated viral (AAV) vectors for this project.

AAV is a single-stranded DNA parvovirus that has been widely studied for its promise as a gene therapy vector and experimental tool. It has been widely reported that AAV infection is non-pathogenic and this feature, along with high viral titers and the potential for site-specific integration into the host cell's genome, has been the driving force behind its development. Furthermore, AAV has two distinct advantages over lentivirus as a gene therapy vector. First, it is a small virus, ~25 nm in diameter, and this small size facilitates its spread in the brain tissue following injection. Lentiviruses in comparison are over 100 nm in diameter. Second, AAV constructs exist that incorporate bidirectional promoters. The advantage to this is that use of internal-ribosomal-entry-sites (IRES) can be avoided. This is very helpful when fluorescent markers, like GFP, need to be produced in a target cell along with a gene of interest, because the approximately 10-fold decrease in expression of the gene following an IRES can be avoided [174].

The best characterized AAV serotype is 2 (AAV2) which binds to heparin sulfate proteoglycan, a component of the extracellular matrix. This feature allows for easy, efficient purification of high-titer virus using heparin columns (see additional methods). After binding to the exterior of the cell, endocytosis occurs, followed by transport to the nucleus of the infected cell by an early and late endosomal route. Once in the nucleus, the virus is

uncoated and the single-stranded DNA genome is converted into double-stranded DNA by host DNA polymerases. Although some percentage of AAV integrates stably into the long-arm of chromosome 19, the majority remains episomal where it forms stable, head to tail concatamers.

AAV only replicates in the presence of a helper-virus, typically adenovirus or herpes-simplex virus (HSV), although a minimal set of helper proteins, E4 and E2A, and a helper RNA, VA [175] , can replace the requirement for an intact virus. This feature has allowed the development of AAV-helper-virus-free vectors that avoid contamination of AAV preparations with a helper-virus and their associated proteins [176].

The function of these essential AAV helper genes is the following: VA RNAs increase mRNA translation by inhibiting the interferon-inducible, RNA-dependent e1F-2 alpha protein kinase. The E4orf6 (34-Mr) protein is the only essential product of the E4 gene and assists AAV replication by inactivating p53. However, it has also been shown to form a hetero-dimer with the E1B (55-Mr) that facilitates the export of viral mRNA from the nucleus and inhibits the translocation of host mRNA. The E2A protein (72-Mr) is a DNA-binding protein that can bind both single and double-stranded DNA. Although a clear understanding of all its functions remains elusive it is known to increase intracellular levels of the cap proteins, spliced forms of the rep proteins, and both single- and double-stranded forms of the AAV genome. E2A is the most important of the genes for AAV production [176].

The core components of AAV are two inverted-terminal-repeat (ITR) motifs at either end of the virus, a rep gene, a cap gene and three promoters. These have been named p5, p19 and p40. After duplication of the single-stranded AAV genome by host DNA polymerases, host RNA-polymerases produce mRNAs from the p5, p19 and p40 promoters. Transcription of all AAV mRNAs end at a single poly-adenylation site. The first proteins to be produced are Rep78 and Rep68. The primary function of these two proteins is to resolve the covalently closed end of the ITR element. They do this by binding to a 16bp element in the A-stem of the ITR. This mediates a local denaturation of the ITR and cleavage of one DNA strand in the terminal resolution site (*trs*) of the ITR. Rep78 then becomes covalently attached to a thymidine residue in the *trs* where it mediates the unwinding of the ITR through its helicase activity and allows it to serve as a replication template. Rep 78 and Rep 68 also mediate the site-specific integration into Chromosome 19. After replication Rep52 and Rep 40 mediate the insertion of single-stranded DNA into the preformed virons.

Our AAV vector system uses two independent plasmids to produced AAV in transfected cells. The first, pDP1 (or pDP2), contains all the AAV genes necessary for replication and packaging, all the helper adenovirus genes, and a fluorescent marker (tdTomato) to monitor transfection efficiency. The second plasmid (A17) has AAV ITRs that surround a multicloning site. This set of plasmids creates a replication

incompetent AAV that transports the gene cloned into the multicloning site into a living cell.

Two separate viruses are needed to obtain the neuronal specificity for our SK2 channel expression. The first created by plasmids pDP1^{+}A17/tTA, produces the tet-transactivator (tTA) under the neuron-specific, human synapsin promoter. The second plasmid combination, pDP1^{+}A41/SK2 (or A41/cre), contains the bidirectional tTA-sensitive promoter driving a fluorescent marker in one direction (Venus) and our gene of interest (an SK2 channel mutant or cre-recombinase) in the other direction.

There are two strategies we considered for our experiments. The first, illustrated in figure 24, is simpler, but has a potential problem. In this strategy SK2 WT, or a mutant SK2 channel, is expressed in SK2-null mice using AAV mediated gene delivery. The potential problem is that SK2-null mice have overgrown dendritic branches (unpublished data) and so this developmental effect may confound physiological experiments. The second strategy, illustrated in figure 25, is more complicated, but avoids this caveat. In this strategy SK2-floxed mice are injected with three distinct viruses. The first two are the same as those used in the null-mouse strategy, but the third expresses cre-recombinase (and tdTomato) from the A41/Cre plasmid. Floxed SK2 is around throughout development and the mice develop normally. When the three viruses infect a cell the WT floxed SK2 is eliminated and, simultaneously, a new SK2 gene (WT, K121A, or E_RK ala)

replaces it. This swapping strategy should avoid the developmental problems of the SK2-null mouse strategy. Because of this advantage, viral mediated gene transfer in SK2 floxed mice is the one we initially chose to pursue.

Figure 24 Legend

Strategy for in vivo mutagenesis using SK2-null mice.

Plasmids encoding AAV will be transfected into HEK293T cells, where they will produce infectious, but replication incompetent AAV. Two separate viruses will be produced: the first drives the production of the tTA protein from the neuron-specific synapsin promoter, and the second contains a bi-directional tTA responsive promoter that drives a fluorescent marker in one direction and either WT, K121A, or E_RK to ala mutant SK2 channels in the other direction.

Figure 24.

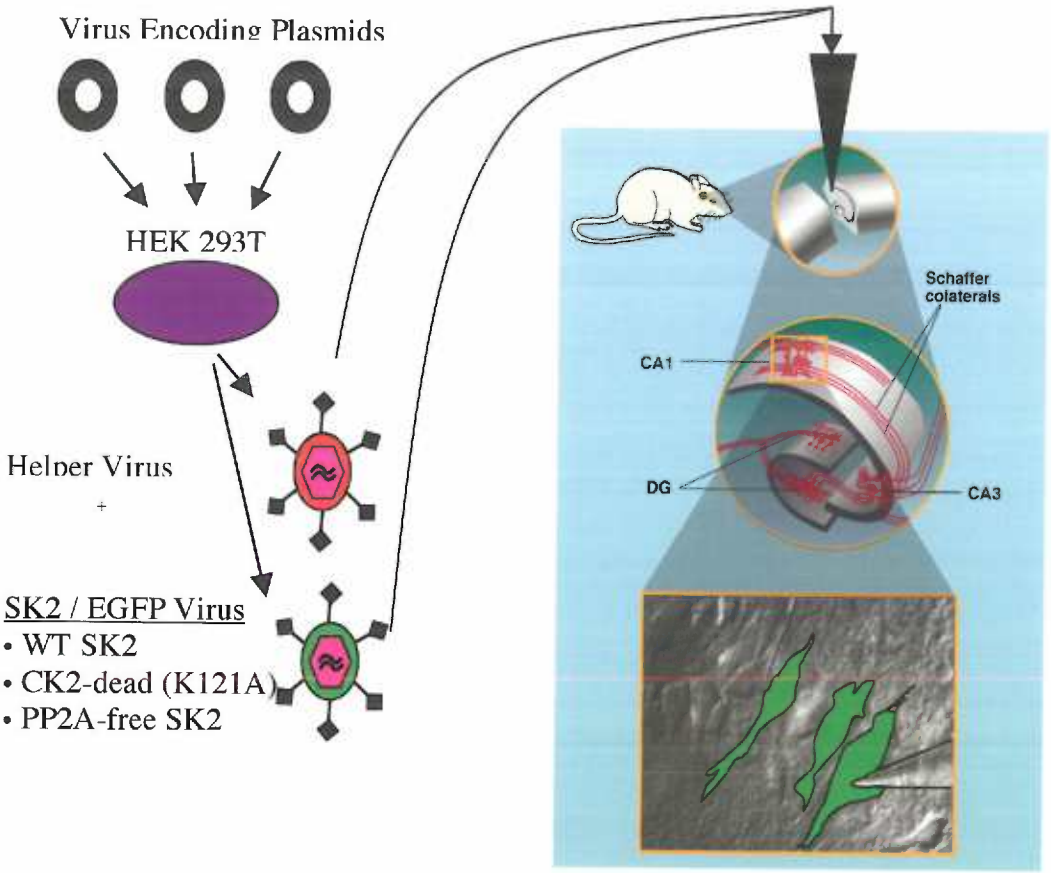

Adapted from a figure created by JPA and LV.

Figure 25 Legend.

Our strategy for in vivo mutagenesis in SK2-floxed mice.

Plasmids encoding AAV will be transfected into HEK293T cells, where they will produce infectious, but replication incompetent AAV. Three separate viruses will be produced: the first drives the production of the tTA protein from the neuron-specific synapsin promoter, the second contains a bi-directional tTA responsive promoter that drives a fluorescent marker (dsRed) in one direction and CRE-recombinase in the other direction, the third contains a bi-directional tTA responsive promoter that drives a fluorescent marker (eGFP) in one direction and either WT, K121A, or E_RK to ala mutant SK2 channels in the other direction.

Figure 25

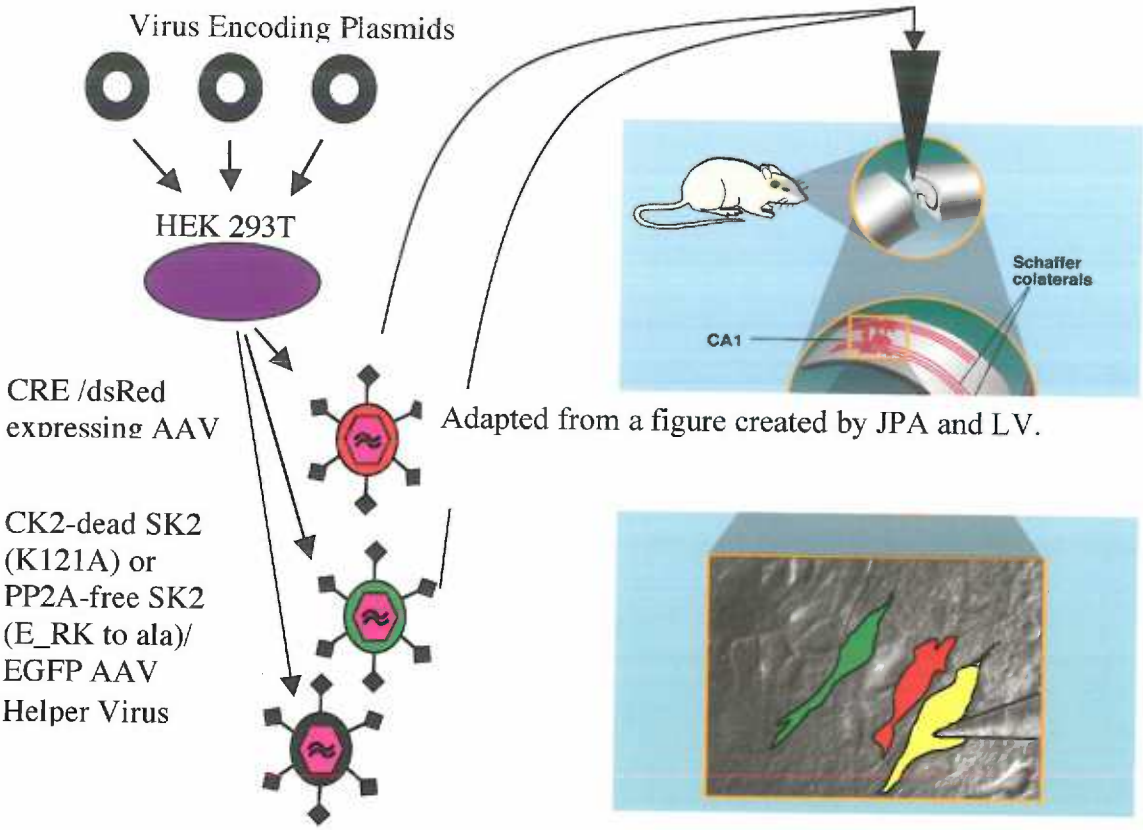
Virus Encoding Plasmids
HEK 293T
CRE /dsRed expressing AAV
CK2-dead SK2 (K121A) or PP2A-free SK2 (E_RK to ala)/ EGFP AAV
Helper Virus
Schaffer colaterals
CA1
Adapted from a figure created by JPA and LV.

Additional Methods for Slice Physiology Experiments

Cell Culture

Human 293T obtained from ATCC were grown in Isocove's modified Dulbeco's media (IMDM) + 10% fetal calf serum, 100units/ml penicillin, 100units/ml streptomycin, 2mM L-glutamine, and 1% non-essential amino acids (NEAA) in 5% CO2 at 37 ° C.

Transfection

293T cells were grown on 15cm cell culture plates (Nunc #157150) coated with 0.2% gelatine. Once cells were 50% confluent they were transfected by the following Ca_2PO_4 method (per 15cm plate): 7μg helper plasmid pDP1, 7μg helper plasmid pDP2, 7μg construct containing plasmid A41, 125μL 2M $CaCl_2$, add sterile H_20 to 1mL, then rapidly add 1mL 2xBBS [(in mM) 50 BES, 280 NaCl, 1.5 $Na_2HPO_4x7H_2O$, pH 7.0, 2.0μm sterile filtered]. Add solution drop-wise to cells. Transfections were performed at 3% CO_2 and transfection reagent was allowed to sit on cells for between 4-6 hours before media was replaced and cells were returned to 5% CO_2.

AAV isolation and purification

Cell culture media was aspirated, cells were scraped, and pelleted at 800g for 5 minutes at 10° C. Remaining supernatant was aspirated, cells were washed in PBS, and pelleted at 800g for 5 minutes at 10° C. Supernatant was aspirated and cells were resuspended, 1mL per 15cm

cut with a vibratome (Leica VT 1000S; Leica, Nussloch, Germany) in ice-cold ACSF. Slices were subsequently incubated at 35°C for 30 min in ACSF and allowed to recover at room temperature for 30 min before recording. All recordings were performed at room temperature. The ACSF solution contained (in mM): 119 NaCl, 26 $NaHCO_3$, 2.5 KCl, 1 NaH_2PO_4, 1.3 $MgCl_2$, 2.0 $CaCl_2$, and 25 dextrose, saturated with 95% O_2/5% CO_2, pH 7.35.

Hippocampal slice physiology recordings

CA1 neurons were visualized with a microscope equipped with infrared-differential interference contrast optics (Leica). Pipettes were made from thin-wall borosilicate glass, had a resistance of 1.5-3 MΩ, and were filled with an intracellular solution containing (in mM): 130 $KMeSO_4$, 10 KCl, 10 HEPES, 2 MgATP, 0.4 NaGTP, and 10 phosphocreatine, with pH adjusted to 7.3 with KOH (290 mOsm). Slices were continuously superfused with ACSF saturated with 95% O_2/5% CO_2. Whole-cell patch-clamp currents were recorded with a Axopatch-1B amplifier (Axon Instruments, Foster City, CA), digitized using an ITC-16 analog-to-digital converter (InstruTech, Greatneck, NY), and acquired onto a computer using Pulse software (Heka Elektronik, Lambrecht, Germany). To measure the IAHP, CA1 neurons were held at -50 mV for 300 msec., depolarized to 20 mV for 200 msec., and then returned to -50 mV for 2000 msec. All cells had a resting Vm more hyperpolarized than -55 mV. Access resistance was <20

MΩ and was 80% compensated. IAHP recordings were filtered at 1 kHz and digitized at a sampling frequency of 1 kHz.

Pharmacology

Apamin was obtained from Tocris and used at a concentration of 100nM.

Data Analysis

Data were analyzed in Igor Pro (Wavemetrics, Lake Oswego, OR). Data are presented as mean ± SEM and ANOVA was used to judge statistical significance. A p-value of < 0.05 was considered significant.

Results

SK2-floxed mouse recordings

Whole-cell recordings performed in voltage clamp elicited robust apamin-sensitive currents in hippocampal slices from WT mice. In contrast, similar recordings from SK2-floxed mice generated apamin-sensitive currents that were an order of magnitude smaller (fig.26). Recordings were made in the presence of XE991 to block any contaminating M-current and 1mM TEA to block any contaminating current from non-inactivated BK channels.

Although fluorescent CA1 neurons in AAV injected SK2-floxed mice were observed, they were not abundant. However, one recording was eventually obtained from an infected SK2-floxed mouse CA1 neuron. The apamin-sensitive current obtained in this instance was nearly zero. However, there is not enough data to conclude whether this was a random event or whether the cre-recombinase had successfully deleted the floxed SK2 channel genes in this neuron.

Figure 26 Legend.

Minimal apamin-sensitive currents are detected in SK2 floxed mice.

Although the floxed mouse strategy appears technically feasible, whole-cell recordings from SK2 floxed mice produce approximately 10-fold less apamin-sensitive current than recordings from WT control mice. Whole-cell currents detected (in picoamps) are the following: 131^{+}/-28 SK2 WT, 20^{+}/-6 SK2 Floxed, 1^{+}/-0 SK2 Floxed^{+}CRE.

Figure 26

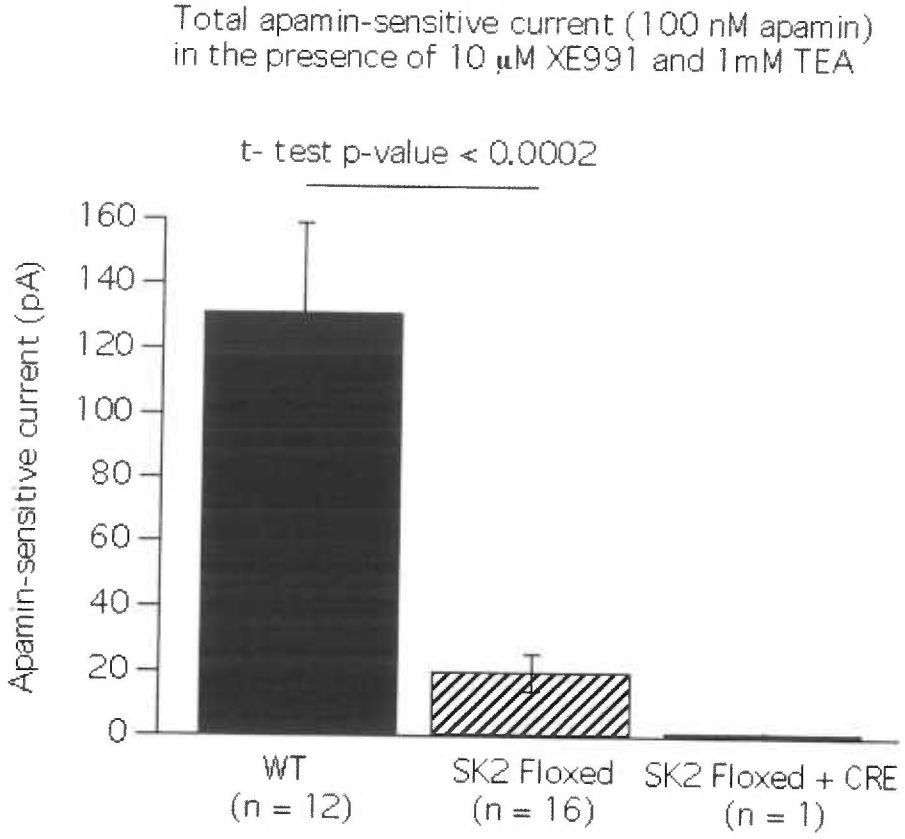
Total apamin-sensitive current (100 nM apamin)
in the presence of 10 μM XE991 and 1mM TEA
t- test p-value < 0.0002
Apamin-sensitive current (pA)
160
140
120
100
80
60
40
20
0
WT
(n = 12)
SK2 Floxed
(n = 16)
SK2 Floxed + CRE
(n = 1)

Discussion

The *in vivo* function of SK2 channel Ca^{2+} sensitivity modulation was investigated through viral mediated gene transfer in SK2-floxed mice. Whole-cell, slice physiology recordings obtained during the course of this thesis project compared apamin-sensitive currents from WT mice with those obtained from SK2-floxed mice and to one example of an apamin sensitive current recorded from an AVV infected, cre-recombinase expressing, SK2-floxed mouse, CA1 neuron. Results suggest that the apamin-sensitive currents detected in SK2 floxed mice at baseline are nearly an order of magnitude less than those obtained in WT mice (fig.26). This will make results from experiments where SK2 channels are reintroduced difficult to interpret because it will never be clear whether the cre-recombinase mediated excision of the floxed SK2 gene is partial or whether the reintroduced SK2 channel is poorly expressed or mistargeted. Furthermore, triple infection of a tTA expressing virus, a cre-recombinase expressing virus, and a SK2 mutant expressing virus would be a rare event and would make the length of time needed to obtain statistically meaningful results prohibitively lengthy.

So why do SK2 floxed mice have less apamin-sensitive current? A western blot probed with an antibody that recognizes the C-terminus of SK2 and compares relative levels of SK2 from WT, SK2 floxed, and SK2 null mouse brains revealed that both the level of SK2-S was decreased in the SK2 floxed animals and that SK2-L was absent (fig.28).

Collectively, these results suggest that we need to resort to our alternative method of investigating the function of SK2 channel Ca^{2+} sensitivity modulation in hippocampal physiology, which is viral mediated gene transfer in SK2-null mice (fig.24).

Figure 27 Legend

Floxed mice do not express SK2-L and have decreased expression of SK2-S.

Western blots prepared from whole mouse brain from SK2 WT, SK2 floxed mice (f/f), and SK2-null mice (Δ/Δ). The blot was probed with a C-terminal SK2 antibody that recognizes both the long and short form of SK2 (unpublished data, courtesy of Chris Bond).

Figure 27.

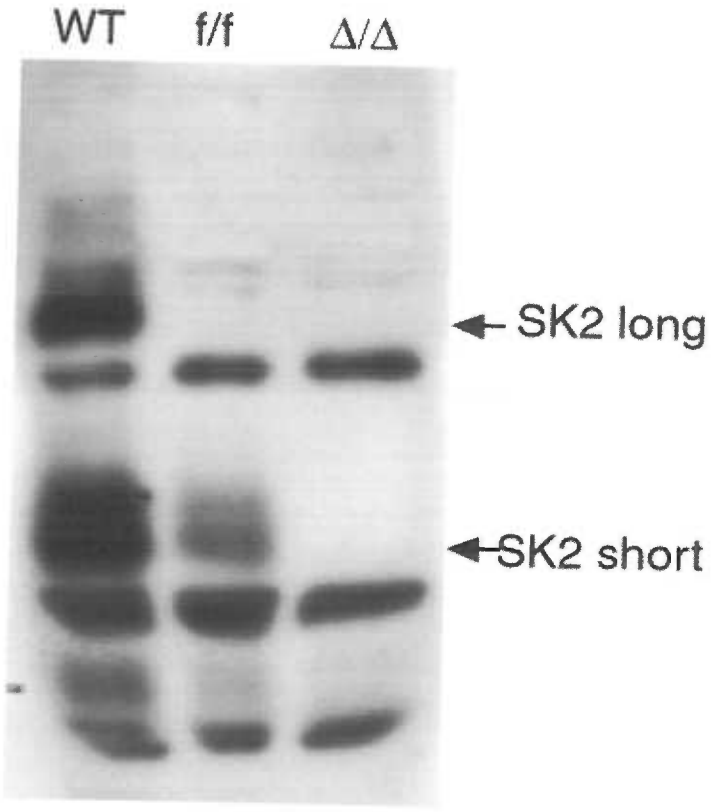

Chris Bond, unpublished data.

Chapter IV

Thesis Discussion

Thesis Discussion

The results presented in this thesis demonstrate that CK2 and PP2A are components of native SK2 channel multiprotein complexes, show that they serve opposing roles in regulating Ca^{2+} gating, and demonstrate that this mechanism serves an important *in vivo* role in neuronal physiology. Using our results we have generated a model of the SK2 channel multiprotein complex, and all the major features of this model have been confirmed by both an independent laboratory and our own. The SK2 channel multiprotein complex in a low Ca^{2+} environment is depicted in figure 28, and the SK2 channel multiprotein complex in a high Ca^{2+} environment is depicted in figure 29. Evidence for the features detailed in these two figures is discussed below.

Evidence for CK2 as a component of the SK2 channel macromolecular complex comes from at least four sources: 1) MgATP decreases the Ca^{2+} sensitivity and τ_{off} of SK2 channels when applied to inside-out patches, consistent with activation of an associated kinase; 2) a specific inhibitor of CK2 (TBB) both eliminates this MgATP effect and increases the τ_{off} of the channels, 3) CK2 can physically bind to the channel at three locations, a 5-amino-acid motif in the membrane-proximal region of the intracellular N terminus, the predicted hinge in the extended "BC" helix of the CaMBD [93,94], and a 10-amino-acid domain close to the C-terminus of the channel; 4) inhibitors of CK2, a kinase-dead CK2, elimination of the hypothesized CK2 phosphorylation site (via CaM T80A coexpression), and

elimination of the hypothesized mechanism of CK2 activation (K121A) all prevent the effects of NE application in primary cultures of SCG neurons.

The relevant target of CK2 phosphorylation in the SK2 channel multiprotein complex is T80 of SK2-bound CaM. This is demonstrated through the use of CaM surrogate T80D, which decreases τ_{off}. Other possible targets of CK2 phosphorylation exist, in CaM, SK2 itself, and the catalytic subunit of the associated phosphatase, PP2A. However, when these additional sites were examined, no other site appeared to significantly contribute to the CK2 mediated regulation of SK2 channel gating kinetics.

CK2 requires polybasic compounds to be present in order to phosphorylate the protein substrate CaM *in vitro*. In the SK2 channel multiprotein complex a single lysine charge, K121, serves as the activator of CK2. Polybasic compounds stimulate CK2 activity by shielding an acidic cluster on the CK2β subunit that normally repels the negatively charged CaM and prevents it from entering the active site of the kinase [139]. The residue K121 likely functions in an identical manner and is perfectly positioned in the closed state of the channel to activate CK2. Although single and combinatorial mutagenesis was performed on many positive charges in both the N- and C-terminus of the channel the only residue that both increased the τ_{off} to the same level observed in WT channels following TBB application and eliminated the MgATP effect was K121. Further evidence to support this residue as the sole activating charge is the following: expression of the mutant SK2 channel K121A both recapitulates

the baseline Ca^{2+} sensitivity in primary SCG cultures and prevents any alteration of the Ca^{2+} sensitivity following NE application.

Perhaps the most important piece of information about the SK2 channel multiprotein complex obtained during the course of my thesis work is that CK2 can only phosphorylate SK2-bound CaM when the channel is closed. This feature of CK2 activation allows the channel to become more active during depolarization and subsequent Ca^{2+} influx. The consequence of this is that the hyperpolarizing K currents of SK2 channels are dialed down in the low Ca^{2+} environment of the cell, and it is only during an increase in intracellular Ca^{2+} that the channels become fully active, thus generating negative feedback on the depolarization and the Ca^{2+} influx. This is the first example of absolutely state-dependent regulation of an ion channel by a kinase.

Several lines of evidence suggest that the SK2 channel multiprotein complex exists in a steady-state between CK2 phosphorylation and dephosphorylation by a phosphatase. The evidence that PP2A is the phosphatase in the complex is the following: 1) PP2A scaffolding subunit was specifically identified as an SK2 channel, C-terminus, protein binding partner in the initial proteomics experiments performed in the Fakler laboratory, 2) MgATP application can not shift the τ_{off} to the level observed when CaM T80D is coexpressed with the WT SK2 channel, 3) TBB not only eliminates the MgATP effect, but doubles the τ_{off} of the WT channel, 4) a phosphatase inhibitor cocktail containing PP2A inhibitors decreases SK2

channel τ_{off}, 5) coexpression of a dominant-negative PP2A scaffolding subunit with the WT SK2 channel decreases τ_{off}, 6) mutation, or truncation, of a known PP2A binding motif in the C-terminus of the channel decreases τ_{off}, 7) physical binding can be demonstrated *in vitro* between the scaffolding subunit of PP2A and the C-terminus of the SK2 channel, and this binding is eliminated by a mutation (E_RK to ala) that disrupts the previously described PP2A binding motif; 8) expression in primary cultures of SCG neurons of an SK2 mutant channel that contains the mutation E_RK to ala recapitulates the NE effect, and is itself only minimally altered by subsequent NE application.

Collectively, these data support a model in which PP2A is bound to the C-terminus of the channel, approximately ¾ of the way along the C-helix at a specific binding motif that is similar to the PP2A binding site on CK2α [137]. Creating a triple alanine mutation in SK2, analogous to the mutation in CK2α that eliminates PP2A binding, generates an SK2 mutant channel with gating kinetics and Ca^{2+} sensitivity that is consistent with decreased binding of an associated phosphatase. Furthermore, because it has been demonstrated that CK2α is bound to SK2 channels *in vivo* [163], the possibility exists for a second population of PP2A to exist in the SK2 channel multiprotein complex.

The results detailed within this thesis redefine the native SK2 channel as a multiprotein complex of 4 channel α-subunits, 4 CaM proteins, up to as many as 16 CK2 subunits (4 x $\alpha 2\beta 2$), and 8 PP2A subunits (4 x

PP2A/C and PR65/A). Furthermore, this structure may include B regulatory subunits of PP2A and G-protein coupled receptors responsible for neurotransmitter-mediated activation of CK2, via SK2 K121A. The NMDA receptor has also been shown to reside extremely close to the SK2 channels in dendritic spines [118]. Whether this channel is physically touching the SK2 channel, or is bridged by another protein (possibly CK2) remains to be determined.

An additional feature of the model presented for the SK2 channel multiprotein complex is the physical association between the N- and C-termini of adjacent channel subunits. This suggests that the termini are constrained *in vivo*, and has been hinted at by two previous studies [171,172]. Evidence that supports this model is the following: 1) a region in the membrane-proximal half of the SK2 N-terminus interact with the same 10-amino-acid motif near the C terminus that interacts with CK2α and CK2β, 2) attaching tags to the N- or C-termini decreases current amplitudes observed in transfected CHO cells, and having large molecules (CFP and YFP) on either terminus eliminates the majority of the Ca^{2+} sensitive current observed in CHO cells (data not shown), 3) efforts to create functional concatamers of SK2 channels have not been successful, with one exception [84].

The N-terminus of the channel was also observed to bind to the CaMBD. How can we reconcile this with binding to the C-terminus? Our model is a static picture of a dynamic complex of proteins. Consequently,

the location the N-terminus is bound to, intersubunit versus intrasubunit or CaMBD versus C-terminus, may be state-dependent, under control of phosphorylation, or determined by the presence or absence of a protein-binding partner. Future experiments will need to be performed in order to determine the dynamic details of the SK2 channel multiprotein complex.

Evidence exists for an *in vivo* role of SK2 channel Ca^{2+} sensitivity modulation in three different systems, all in different states of description. These are the following: 1) the outer hair cells of the cochlear, 2) NE induced modulation of excitability, via CK2 activation, in the neurons of the superior ganglion and, possibly, the SLM of hippocampal CA1 neurons 3) modulation of Ca^{2+} influx through the NMDA receptors and synaptic plasticity in the spines of hippocampal CA1 neurons. The current state of description of each system is reviewed below:

The auditory outer hair cells have a unique mechanism of producing inhibitory post-synaptic current (IPSCs). Here nicotinic acetylcholine receptors (nAChRs) that contain a subunit (α9) that makes them permeable to Ca^{2+} are tightly coupled to SK channels. Opening of these nAChR provides the Ca^{2+} that, in turn, opens the K permeable SK channels, which generate the IPSC. The kinetics of the SK channel response is similar to what is observed *in vitro* from heterologously expressed SK channels [111], although the specific value for the decay kinetics of the IPSC vary considerably between OHCs [163]. CK2 is also colocalized to the OHCs, by immunofluorescence. Interestingly, the removal

possible scenarios where this might occur are the following: 1) after a rapid series of depolarizations at the synapse, perhaps following burst-firing of the presynaptic neuron, 2) after removal of the Mg^{2+} block of the NMDA receptor and activation of the receptor by glutamate, 3) after insertion of Ca^{2+} permeable GluR1 homomeric channels following LTP.

The third *in vivo* role for SK2 channel Ca^{2+} sensitivity modulation is in the neurons of the SCG, a region that provides sympathetic input to the head and neck. Here a link between the application of NE and activation of SK2-associated CK2 has been clearly established, as discussed previously. Furthermore, the results were generalized to the neurotransmitter somatostatin, and to DRG neurons. However, all the experiments were performed in dissociated neuronal cultures, and the majority of the recordings included the expression of non-native SK2 and Cav2.3. In summary, although an *in vivo* role for SK2 channel Ca^{2+} sensitivity modulation by NE, via CK2 activation, has been well established in dissociated neuronal cultures, this role has not yet been extended to neurons in slices or to whole animal experiments. Nevertheless, the available evidence suggests that this system is an important downstream effect of NE, and, furthermore, that it will generalize to different brain regions and to other neurotransmitters, such as somatostatin. One area of the brain that is especially promising as a target for further investigation is the SLM portion of the hippocampal CA1 neurons dendrites.

Figure 28 Legend.

Summary of the SK2 channel multiprotein complex in a low Ca^{2+} environment

The known components of the SK2 channel multiprotein complex are depicted in an environment where intracellular Ca^{2+} is low. Hence, the SK2 channel is closed, SK2 K121 is in a position to activate CK2, T80 is phosphorylated, and Ca^{2+} sensitivity of the channel is dialed down.

Figure 28.

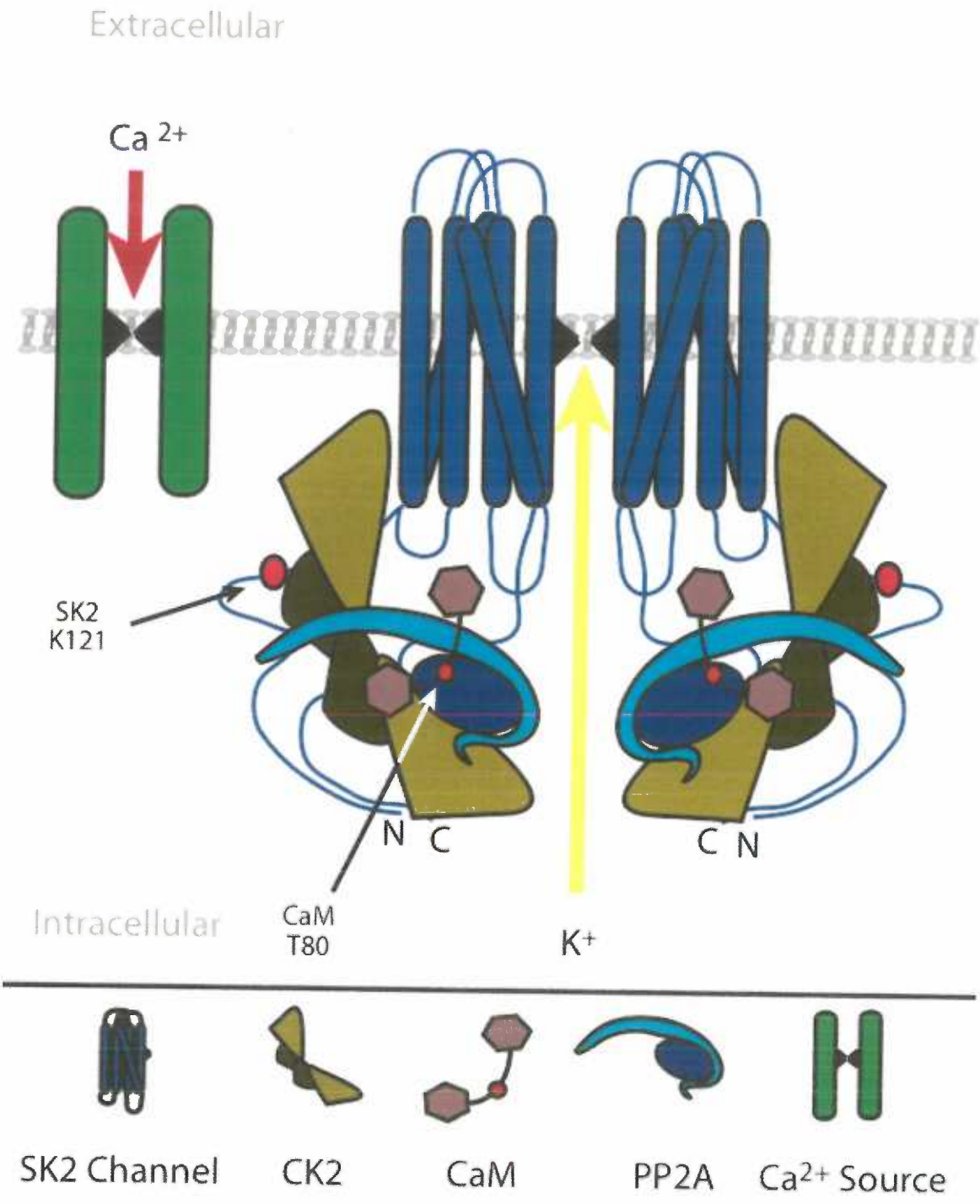
Extracellular
Ca 2+
SK2
K121
N C
C N
Intracellular
CaM
T80
K+
SK2 Channel
CK2
CaM
PP2A
Ca2+ Source

Figure 29 Legend.

Summary of the SK2 channel multiprotein complex in a high Ca^{2+} environment

The known components of the SK2 channel multiprotein complex are depicted in an environment where intracellular Ca^{2+} is high. Hence, the SK2 channel is open, SK2 K121 is not in a position to activate CK2, T80 is dephosphorylated, and Ca^{2+} sensitivity of the channel has increased due to PP2A activity.

Figure 29.

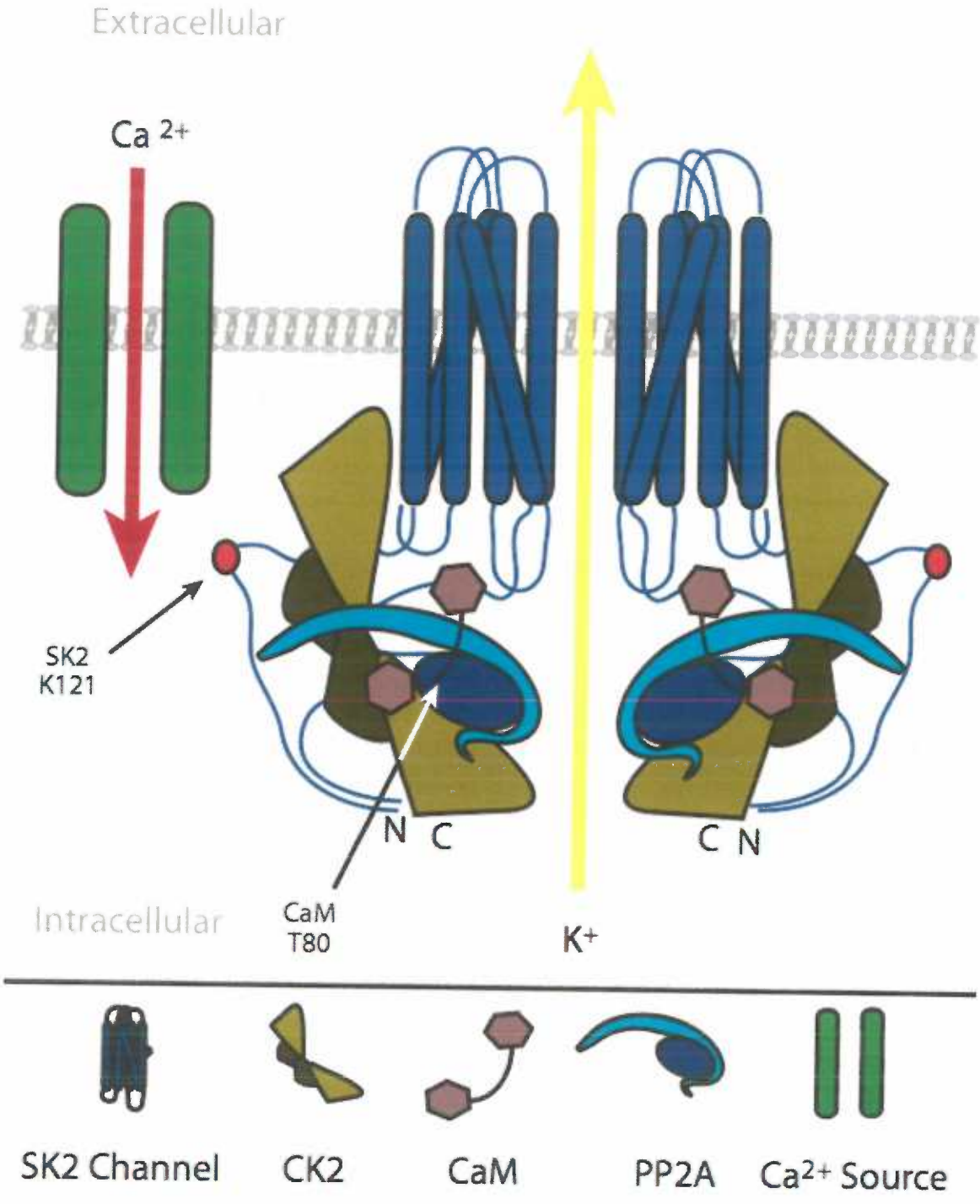
Extracellular
Ca 2+
SK2
K121
N C
C N
Intracellular
CaM
T80
K+
SK2 Channel
CK2
CaM
PP2A
Ca2+ Source

Chapter V.

Summary and Conclusions

Summary and Conclusions

The data contained within this thesis detail a novel mechanism for the modulation of SK channel Ca^{2+} sensitivity. Although the binding of SK2 to CK2 and PP2A had been previously described, and it had been previously proposed that CK2 phosphorylation of CaMT80 decreases the Ca^{2+} sensitivity of SK channels, the work detailed within this thesis greatly expands upon the previous results and details the mechanics of how the Ca^{2+} sensitivity of SK2 channel multiprotein complexes are regulated. Furthermore, this thesis project identified two mutant SK2 channels that shift the Ca^{2+} sensitivity to one extreme or the other, and these mutant channels have already proved to be valuable tools for investigating the *in vivo* role of CK2 and PP2A mediated regulation of SK2 channel Ca^{2+} sensitivity.

During the course of this thesis, a model was proposed for the SK2 channel multiprotein complex, and this model was rigorously tested. Perhaps the most important feature of this model is that the activity of CK2 towards SK2-associated CaM is state dependence and only occurs when the channel is closed. This is the first report of absolutely state-dependent regulation of an ion channel by a kinase. The significance of this is that phosphorylation of SK2 associated CaM on residue T80 can only occur when the channel is in a low Ca^{2+} environment, which is the baseline state of a hippocampal CA1 neuron. Consequently, the Ca^{2+} sensitivity of the SK2 channel multiprotein complex is normally in its dialed down, phosphorylated state. Now importantly, CK2 exists in a steady-state with an associated

phosphatase, PP2A. Consequently, during an influx of Ca^{2+}, when activation of CK2 is prevented, PP2A takes control of the steady-state, decreases the level of phosphorylation, and increases the Ca^{2+} sensitivity of the channel. The net result is that a negative feedback loop is created with the Ca^{2+} source. At least three possible scenarios exist where persistent elevation in Ca^{2+} should occur in CA1 neurons and SK2 channel Ca^{2+} sensitivity modulation should play an important role: 1) after a rapid series of depolarizations at the synapse following burst-firing of the presynaptic neuron, 2) after removal of the Mg^{2+} block of the NMDA receptor, and 3) after insertion of Ca^{2+} permeable GluR1 homomeric channels following LTP.

The relationship between SK2 channels and NMDA receptors is particularly relevant to hippocampal dependent learning and memory, and both are directly influenced by CaM and CK2, but in opposite directions. For SK channels, CaM mediates Ca^{2+} gating, increasing activity, whereas CK2 phosphorylation of SK2-associated CaM reduces channel activity. For NMDA receptors, CaM mediates Ca^{2+}-induced inactivation [178] whereas CK2 phosphorylation enhances activity [145]. Therefore, the activation of CK2 may additively increase the NMDA component of EPSPs, by directly increasing NMDA receptor activity and decreasing the SK-mediated repolarization that favors reblock of NMDA receptors by external Mg^{2+} ions. A key question to be addressed in future studies is whether SK2 channels and NMDA receptors share a population of CK2, and, if this is true, is CK2 active towards both substrates simultaneously, does it alternate from one

substrate to another, or is activity towards one substrate regulated while the other is not.

At the beginning of this thesis the following question was proposed: how do SK2 channels fit into the milieu of proteins that create, maintain and modulate synaptic plasticity? Two ways are currently described in the literature. First, SK2 channels form a negative feedback loop with the NMDA receptor, where their hyperpolarizing K currents promote external $Mg^{+}2$ block and limit Ca^{2+} influx. Second, SK2 channels actively contribute to synaptic plasticity itself, and this value has been calculated to be ~13% of the total. This thesis has researched and described a third method by which SK2 channels can modulate hippocampal dependent learning and memory, the regulation of SK2 channel Ca^{2+} sensitivity via the associated kinase CK2 and the associated phosphatase PP2A. Although a precise role for this mechanism in hippocampal physiology remains to be fully described, a large amount of evidence has accumulated that suggests a role does indeed exist there. Furthermore, work resulting from the experiments detailed within this thesis has demonstrated the relevance of this mechanism to neurophysiology outside of the hippocampus by establishing an *in vivo* role for SK2 channel Ca^{2+} sensitivity modulation by CK2 and PP2A in a different system, SCG neurons. Here NE application decreases SK2 channel Ca^{2+} sensitivity by activating CK2. Importantly, this finding has already been extended to other types of neurons (DRG neurons) and other neurotransmitters (somatostatin), and more are likely to follow. Because

regulation by NE is also important for hippocampal physiology, two distinct roles for SK2 channel multiprotein complex Ca^{2+} sensitivity modulation may have been discovered from work presented in this thesis.

So in conclusion, the data contained within this thesis have expanded our understanding of SK2 channel multiprotein complexes and how they participate in hippocampal dependent learning and memory.

References

References:

1 D. E. Goldman, *J. Gen. Physiol.* **27**, 37 (1934).

2 A.L. and Huxley Hodgkin, A.F., *Nature* **144** (1939).

3 A. L. Hodgkin and B. Katz, *J. Physiol.* **117**, 500 (1952).

4 K.S. and Curtis Cole, H.J., *Journal of General Physiology* **22**, 649 (1939).

5 B. Hille, *Ionic Channels of Excitable Membranes*. (Sinauer Associates Inc., Sunderland, 1992).

6 E. Neher and B. Sakmann, *Nature* **260** (5554), 799 (1976).

7 M. Noda, S. Shimizu, T. Tanabe et al., *Nature* **312**, 121 (1984).

8 D. M. Papzian, T. L. Schwarz, B. L. Tempel et al., *Science* **237**, 749 (1987).

9 D. A. Doyle, J. Morais Cabral, R. A. Pfuetzner et al., *Science* **280** (5360), 69 (1998).

10 W. B. Scoville and B. Milner, *Journal of Neurology, Neurosurgery & Psychiatry* **20** (1), 11 (1957).

11 Richard Morris Per Anderson, David Amaral, Tim Bliss, John O'Keefe, *The Hippocampus Book*. (Oxford University Press, Inc., 2007).

12 C. A. Sailer, W. A. Kaufmann, J. Marksteiner et al., *Mol Cell Neurosci* **26** (3), 458 (2004).

13 C. T. Bond, P. S. Herson, T. Strassmaier et al., *Journal of Neuroscience* **24** (23), 5301 (2004).

14 T. V. Bliss and T. Lomo, *Journal of Physiology* **232** (2), 331 (1973).

15 J. Lisman, J. W. Lichtman, and J. R. Sanes, *Nature Reviews Neuroscience* **4** (11), 926 (2003); R. C. Malenka, *Nature Reviews Neuroscience* **4** (11), 923 (2003); R. C. Malenka and M. F. Bear, *Neuron* **44** (1), 5 (2004); R. C. Malenka and R. A. Nicoll, *Science* **285** (5435), 1870 (1999); J. R. Sanes and J. W. Lichtman, *Nature Neuroscience* **2** (7), 597 (1999).

16 G. Neves, S. F. Cooke, and T. V. Bliss, *Nature Reviews Neuroscience* **9** (1), 65 (2008).

17 J. R. Whitlock, A. J. Heynen, M. G. Shuler et al., *Science* **313** (5790), 1093 (2006).

18 G. Buzsaki, *Neuron* **33** (3), 325 (2002).

19 J. C. Magee and D. Johnson, *Science* **275**, 209 (1997).

20 D. O. Hebb, *The Organization of Behaviour*. (John Wiley & Sons, New York, 1949).

21 A. Losonczy and J. C. Magee, *Neuron* **50** (2), 291 (2006).

22 S. Gasparini and J. C. Magee, *Journal of Neuroscience* **26** (7), 2088 (2006).

23 W. B. Levy and O. Steward, *Neuroscience* **8** (4), 791 (1983).

24 Y. Dan and M. M. Poo, *Neuron* **44** (1), 23 (2004).

25 Y. W. Lin, M. Y. Min, T. H. Chiu et al., *Journal of Neuroscience* **23** (10), 4173 (2003).

26 D. Chin and A. R. Means, *Trends in Cell Biology* **10** (8), 322 (2000).

27 B. L. Sabatini, T. G. Oertner, and K. Svoboda, *Neuron* **33** (3), 439 (2002).

[28] B. L. Bloodgood and B. L. Sabatini, *Current Opinion in Neurobiology* **17** (3), 345 (2007).
[29] D. Neveu and R. S. Zucker, *Journal of Neurophysiology* **75** (5), 2157 (1996).
[30] R. A. J. Lester, J. D. Clements, G. L. Westbrook et al., *Nature* **346**, 565 (1990).
[31] V. Scheuss, R. Yasuda, A. Sobczyk et al., *Journal of Neuroscience* **26** (31), 8183 (2006).
[32] R. Yasuda, B. L. Sabatini, and K. Svoboda, *Nat Neurosci* **6** (9), 948 (2003).
[33] J. Lisman, H. Schulman, and H. Cline, *Nature Reviews Neuroscience* **3** (3), 175 (2002).
[34] T. Meyer, P. I. Hanson, L. Stryer et al., *Science* **256** (5060), 1199 (1992).
[35] J. D. Petersen, X. Chen, L. Vinade et al., *Journal of Neuroscience* **23** (35), 11270 (2003).
[36] K. Shen, M. N. Teruel, J. H. Connor et al., *Nature Neuroscience* **3** (9), 881 (2000).
[37] M. C. Oh and V. A. Derkach, *Nature Neuroscience* **8** (7), 853 (2005).
[38] Y. Hayashi, S. H. Shi, J. A. Esteban et al., *Science* **287** (5461), 2262 (2000).
[39] K. U. Bayer, P. De Koninck, A. S. Leonard et al., *Nature* **411** (6839), 801 (2001).
[40] R.J. Colbran, Y.L. Fong, C.M. Schworer et al., *J. Biol. Chem.* **263**, 18145 (1988).
[41] J. M. Bradshaw, Y. Kubota, T. Meyer et al., *Proceedings of the National Academy of Sciences of the United States of America* **100** (18), 10512 (2003).
[42] S. Schorge and D. Colquhoun, *Journal of Neuroscience* **23** (4), 1151 (2003).
[43] A. Barria and R. Malinow, *Neuron* **35** (2), 345 (2002).
[44] L. Liu, T. P. Wong, M. F. Pozza et al., *Science* **304** (5673), 1021 (2004).
[45] S. Berberich, P. Punnakkal, V. Jensen et al., *Journal of Neuroscience* **25** (29), 6907 (2005).
[46] J. W. Johnson and P. Ascher, *Biophysical Journal* **57** (5), 1085 (1990); L. Nowak, P. Bregestovski, P. Ascher et al., *Nature* **307** (5950), 462 (1984).
[47] D. N. Lieberman and I. Mody, *Nature* **369** (6477), 235 (1994).
[48] N. Sans, K. Prybylowski, R. S. Petralia et al., *Nature Cell Biology* **5** (6), 520 (2003).
[49] K. Plant, K. A. Pelkey, Z. A. Bortolotto et al., *Nature Neuroscience* **9** (5), 602 (2006).
[50] P. H. Seeburg and J. Hartner, *Current Opinion in Neurobiology* **13** (3), 279 (2003).
[51] V. A. Derkach, M. C. Oh, E. S. Guire et al., *Nature Reviews Neuroscience* **8** (2), 101 (2007).
[52] J. A. Esteban, S. H. Shi, C. Wilson et al., *Nature Neuroscience* **6** (2), 136 (2003).
[53] M. C. Oh, V. A. Derkach, E. S. Guire et al., *Journal of Biological Chemistry* **281** (2), 752 (2006).
[54] R. Malinow, Z. F. Mainen, and Y. Hayashi, *Current Opinion in Neurobiology* **10** (3), 352 (2000); M. F. Barry and E. B. Ziff, *Current Opinion in Neurobiology* **12** (3), 279 (2002).
[55] Eleonore Real Charles D. Kopec, Helmut W. Kessels, and Roberto Malinow, *J. Neurosci.* **27** (2007).
[56] H. K. Lee, K. Takamiya, J. S. Han et al., *Cell* **112** (5), 631 (2003).
[57] Y. Meng, Y. Zhang, and Z. Jia, *Neuron* **39** (1), 163 (2003).

58 Leon Reijmers Matsuo, Mark Mayford, *Science* **319**, 1104 (2008).
59 U. Frey and R. G. Morris, *Nature* **385** (6616), 533 (1997).
60 M. L. Dell'Acqua, K. E. Smith, J. A. Gorski et al., *European Journal of Cell Biology* **85** (7), 627 (2006).
61 K. E. Smith, E. S. Gibson, and M. L. Dell'Acqua, *Journal of Neuroscience* **26** (9), 2391 (2006).
62 C. C. Garner, J. Nash, and R. L. Huganir, *Trends in Cell Biology* **10** (7), 274 (2000).
63 G. M. Elias and R. A. Nicoll, *Trends in Cell Biology* **17** (7), 343 (2007).
64 T. Nakagawa, K. Futai, H. A. Lashuel et al., *Neuron* **44** (3), 453 (2004).
65 G. M. Elias, L. Funke, V. Stein et al., *Neuron* **52** (2), 307 (2006).
66 S. Tomita, L. Chen, Y. Kawasaki et al., *Journal of Cell Biology* **161** (4), 805 (2003).
67 Whitesell JD Bedoukian MA, Peterson EJ, Clay CM, Partin KM., *J Biol Chem* (in press).
68 L. Chen, D. M. Chetkovich, R. S. Petralia et al., *Nature* **408** (6815), 936 (2000).
69 S. Tomita, V. Stein, T. J. Stocker et al., *Neuron* **45** (2), 269 (2005).
70 E. Schnell, M. Sizemore, S. Karimzadegan et al., *Proceedings of the National Academy of Sciences of the United States of America* **99** (21), 13902 (2002).
71 S. H. Shi, Y. Hayashi, R. S. Petralia et al., *Science* **284** (5421), 1811 (1999).
72 D. Johnston, B. R. Christie, A. Frick et al., *Philos Trans R Soc Lond B Biol Sci* **358** (1432), 667 (2003).
73 J. C. Magee and E. P. Cook, *Nature Neuroscience* **3** (9), 895 (2000).
74 S. Gasparini and J. C. Magee, *Journal of Physiology* **541** (Pt 3), 665 (2002).
75 B. L. Sabatini and K. Svoboda, *Nature* **408** (6812), 589 (2000); J. C. Magee and D. Johnston, *J. Physiol.* **487**, 67 (1995).
76 M. F. Nolan, G. Malleret, J. T. Dudman et al., *Cell* **119** (5), 719 (2004).
77 J. C. Magee, *Journal of Neuroscience* **18** (19), 7613 (1998).
78 D. A. Hoffman, J. C. Magee, C. M. Colbert et al., *Nature* **387** (6636), 869 (1997).
79 D. Oliver, C. C. Lien, M. Soom et al., *Science* **304** (5668), 265 (2004).
80 H. Ceulemans and M. Bollen, *Physiological Reviews* **84** (1), 1 (2004).
81 G. Benaim and A. Villalobo, *European Journal of Biochemistry* **269** (15), 3619 (2002).
82 G. Gárdos, *Biochimica Biophysica Acta* **30**, 653 (1958).
83 R. W. Meech, *Comparative Biochemistry & Physiology A-Comparative Physiology* **42** (2), 493 (1972).
84 T. M. Ishii, J. Maylie, and J.P. Adelman, *J. Biol. Chem.* **272**, 23195 (1997).
85 M. Köhler, B. Hirschberg, C. T. Bond et al., *Science* **273** (5282), 1709 (1996).
86 T.M. Ishii, C. Silvia, B. Hirschberg et al., *Proc.Natl. Acad. Sci. USA* **94**, 11651 (1997).
87 M. Stocker and P. Pedarzani, *Mol Cell Neurosci* **15** (5), 476 (2000).
88 R. Rimini, J. M. Rimland, and G. C. Terstappen, *Brain Research. Molecular Brain Research* **85** (1-2), 218 (2000).
89 B. E. Shmukler, C. T. Bond, S. Wilhelm et al., *Biochim Biophys Acta* **1518** (1-2), 36 (2001).

90 A. S. Monaghan, D. C. Benton, P. K. Bahia et al., *J Biol Chem* **279**, 1003 (2004); D. C. Benton, A. S. Monaghan, R. Hosseini et al., *J Physiol* **553** (Pt 1), 13 (2003).
91 T. Strassmaier, C. T. Bond, C. A. Sailer et al., *Journal of Biological Chemistry* **280** (22), 21231 (2005).
92 X-M. Xia, B. fakler, A. Rivard et al., *Nature* **395**, 503 (1998).
93 J. E. Keen, R. Khawaled, D. L. Farrens et al., *J Neurosci* **19** (20), 8830 (1999).
94 M. A. Schumacher, A. F. Rivard, H. P. Bachinger et al., *Nature* **410** (6832), 1120 (2001).
95 A. Bruening-Wright, M. A. Schumacher, J. P. Adelman et al., *J Neurosci* **22** (15), 6499 (2002).
96 A. Bruening-Wright, W. S. Lee, J. P. Adelman et al., *Journal of General Physiology* **130** (6), 601 (2007).
97 P. Pedarzani, J. Mosbacher, A. Rivard et al., *J Biol Chem* **276** (13), 9762 (2001).
98 C. Hougaard, B. L. Eriksen, S. Jorgensen et al., *British Journal of Pharmacology* **151** (5), 655 (2007).
99 W. S. Lee, T. J. Ngo-Anh, A. Bruening-Wright et al., *J Biol Chem* **278** (28), 25940 (2003).
100 C. T. Bond, R. Sprengel, J. M. Bissonnette et al., *Science* **289** (5486), 1942 (2000).
101 G. M. Herrera, M. J. Pozo, P. Zvara et al., *Journal of Physiology* **551** (Pt 3), 893 (2003); A. Brown, T. Cornwell, I. Korniyenko et al., *American Journal of Physiology - Cell Physiology* **292** (2), C832 (2007).
102 N. A. Tamarina, Y. Wang, L. Mariotto et al., *Diabetes* **52** (8), 2000 (2003).
103 M. S. Taylor, A. D. Bonev, T. P. Gross et al., *Circulation Research* **93** (2), 124 (2003).
104 D. Jacobson, P. S. Herson, T. R. Neelands et al., *Muscle Nerve* **26** (6), 817 (2002).
105 T. Kimura, M. P. Takahashi, Y. Okuda et al., *Neurosci Lett* **295** (3), 93 (2000).
106 M. J. Miller, H. Rauer, H. Tomita et al., *Journal of Biological Chemistry* **276** (30), 27753 (2001).
107 A. Tse and B. Hille, *Science* **255** (5043), 462 (1992).
108 C. Villalobos, V. G. Shakkottai, K. G. Chandy et al., *Journal of Neuroscience* **24** (14), 3537 (2004).
109 C. T. Bond, P. S. Herson, T. Strassmaier et al., *J Neurosci* **24** (23), 5301 (2004).
110 C. T. Bond, J. Maylie, and J. P. Adelman, *Current Opinion in Neurobiology* **15** (3), 305 (2005).
111 D. Oliver, N. Klocker, J. Schuck et al., *Neuron* **26** (3), 595 (2000).
112 R. W. Stackman, R. S. Hammond, E. Linardatos et al., *J Neurosci* **22** (23), 10163 (2002).
113 C. A. Sailer, H. Hu, W. A. Kaufmann et al., *J Neurosci* **22** (22), 9698 (2002).
114 M. Stocker, M. Krause, and P. Pedarzani, *Proc. Natl. Acad. Sci. USA* **96**, 4662 (1999).
115 H. Hu N. Gu, K. Vervaeke, J.F. Storm, *Soc. For Neurosci.* **Abstract, program no. 53.1** (2003).
116 G. J. Obermair, W. A. Kaufmann, H. G. Knaus et al., *Eur J Neurosci* **17** (4), 721 (2003).
117 R. Roncarati, M. Di Chio, A. Sava et al., *Neuroscience* **104** (1), 253 (2001).

118 T. J. Ngo-Anh, B. L. Bloodgood, M. Lin et al., *Nature Neuroscience* **8** (5), 642 (2005).
119 Luján R Lin MT, Watanabe M, Adelman JP, Maylie J, *Nat Neurosci* **11** (2), 170 (2008).
120 X. Cai, C. W. Liang, S. Muralidharan et al., *Neuron* **44** (2), 351 (2004).
121 E. S. Faber, A. J. Delaney, and P. Sah, *Nature Neuroscience* **8** (5), 635 (2005).
122 Y. Ren, L. F. Barnwell, J. C. Alexander et al., *Journal of Biological Chemistry* **281** (17), 11769 (2006).
123 N.V. Marrion and S.J. Tavalin, *Nature* **395**, 900 (1998).
124 B. L. Bloodgood and B. L. Sabatini, *Neuron* **53** (2), 249 (2007).
125 E. J. Wagner, O. K. Ronnekleiv, and M. J. Kelly, *Journal of Pharmacology & Experimental Therapeutics* **299** (1), 21 (2001).
126 E. Galarraga, C. Vilchis, T. Tkatch et al., *Neuroscience* **146** (2), 537 (2007).
127 M. Martina, M. E. Turcotte, S. Halman et al., *Journal of Physiology* **578** (Pt 1), 143 (2007).
128 L. A. Pinna, *J Cell Sci* **115** (Pt 20), 3873 (2002).
129 F. Meggio and L. A. Pinna, *Faseb J* **17** (3), 349 (2003); D. W. Litchfield, *Biochem J* **369** (Pt 1), 1 (2003).
130 R. Padmanabha, J. L. Chen-Wu, D. E. Hanna et al., *Mol Cell Biol* **10** (8), 4089 (1990).
131 A. Donella-Deana, L. Cesaro, S. Sarno et al., *Biochem J* **372** (Pt 3), 841 (2003); O. Marin, F. Meggio, S. Sarno et al., *J Biol Chem* **274** (41), 29260 (1999).
132 N. Rekha and N. Srinivasan, *BMC Struct Biol* **3** (1), 4 (2003).
133 J. E. Allende and C. C. Allende, *FASEB Journal* **9** (5), 313 (1995).
134 G. Maridor, W. Park, W. Krek et al., *Journal of Biological Chemistry* **266** (4), 2362 (1991).
135 X. Xu, P. A. Toselli, L. D. Russell et al., *Nat Genet* **23** (1), 118 (1999).
136 D. W. Litchfield, D. G. Bosc, D. A. Canton et al., *Mol Cell Biochem* **227** (1-2), 21 (2001).
137 J. K. Heriche, F. Lebrin, T. Rabilloud et al., *Science* **276** (5314), 952 (1997).
138 K. Cieslik, C. M. Lee, J. L. Tang et al., *Journal of Biological Chemistry* **274** (49), 34669 (1999).
139 K. Niefind, B. Guerra, I. Ermakowa et al., *Embo J* **20** (19), 5320 (2001).
140 E. Valero, S. De Bonis, O. Filhol et al., *Journal of Biological Chemistry* **270** (14), 8345 (1995).
141 B. Boldyreff, F. Meggio, L. A. Pinna et al., *Journal of Biological Chemistry* **269** (7), 4827 (1994); F. Meggio, A. M. Brunati, and L. A. Pinna, *FEBS Letters* **160** (1-2), 203 (1983).
142 L. Bodenbach, J. Fauss, A. Robitzki et al., *European Journal of Biochemistry* **220** (1), 263 (1994).
143 P. R. Blanquet, *Prog Neurobiol* **60** (3), 211 (2000).
144 C. Charriaut-Marlangue, S. Otani, C. Creuzet et al., *Proc Natl Acad Sci U S A* **88** (22), 10232 (1991).
145 D. N. Lieberman and I. Mody, *Nat Neurosci* **2** (2), 125 (1999).
146 H. J. Chung, Y. H. Huang, L. F. Lau et al., *J Neurosci* **24** (45), 10248 (2004).

147 C. C. Chao, Y. L. Ma, and E. H. Lee, *Journal of Neuroscience* **27** (23), 6243 (2007).
148 F. Romero-Oliva, G. Jacob, and J. E. Allende, *Journal of Cellular Biochemistry* **89** (2), 348 (2003).
149 D. Leroy, J. K. Heriche, O. Filhol et al., *Journal of Biological Chemistry* **272** (33), 20820 (1997).
150 K. Lawson, L. Larentowicz, S. Artim et al., *Biochemistry* **45** (5), 1499 (2006).
151 F. Meggio, B. Boldyreff, O. Marin et al., *European Journal of Biochemistry* **205** (3), 939 (1992).
152 O. Marin, F. Meggio, and L. A. Pinna, *Biochem Biophys Res Commun* **256** (2), 442 (1999).
153 G. Arrigoni, O. Marin, M. A. Pagano et al., *Biochemistry* **43** (40), 12788 (2004).
154 S. Sarno, H. Reddy, F. Meggio et al., *FEBS Lett* **496** (1), 44 (2001).
155 R. Battistutta, S. Sarno, E. De Moliner et al., *Eur J Biochem* **267** (16), 5184 (2000).
156 V. Janssens and J. Goris, *Biochemical Journal* **353** (Pt 3), 417 (2001); V. Janssens, J. Goris, and C. Van Hoof, *Current Opinion in Genetics & Development* **15** (1), 34 (2005).
157 H. A. Widmer, I. C. Rowe, and M. J. Shipston, *J Physiol* **552** (Pt 2), 379 (2003).
158 C. Kamibayashi, R. L. Lickteig, R. Estes et al., *Journal of Biological Chemistry* **267** (30), 21864 (1992).
159 E. Jacinto and M. N. Hall, *Nature Reviews Molecular Cell Biology* **4** (2), 117 (2003).
160 U. S. Cho and W. Xu, *Nature* **445** (7123), 53 (2007); Y. Xu, Y. Xing, Y. Chen et al., *Cell* **127** (6), 1239 (2006).
161 M. R. Groves, N. Hanlon, P. Turowski et al., *Cell* **96** (1), 99 (1999).
162 S. Longin, K. Zwaenepoel, J. V. Louis et al., *Journal of Biological Chemistry* **282** (37), 26971 (2007).
163 W. Bildl, T. Strassmaier, H. Thurm et al., *Neuron* **43** (6), 847 (2004).
164 H. J. Abel, J. C. Lee, J. C. Callaway et al., *J Neurophysiol* **91** (1), 324 (2004).
165 F. Meggio, A. M. Brunati, and L. A. Pinna, *FEBS Letters* **215** (2), 241 (1987).
166 P. Turowski, B. Favre, K. S. Campbell et al., *European Journal of Biochemistry* **248** (1), 200 (1997).
167 B. Hirschberg, J. Maylie, J.P. Adelman et al., *J. Gen. Physiol.* **111**, 565 (1998).
168 A. C. Gerlach, N. N. Gangopadhyay, and D. C. Devor, *Journal of Biological Chemistry* **275** (1), 585 (2000).
169 A. C. Gerlach, C. A. Syme, L. Giltinan et al., *Journal of Biological Chemistry* **276** (14), 10963 (2001).
170 D. A. Canton, M. E. Olsten, H. Niederstrasser et al., *Journal of Biological Chemistry* **281** (47), 36347 (2006).
171 D. D'Hoedt, K. Hirzel, P. Pedarzani et al., *J Biol Chem* **279** (13), 12088 (2004).
172 E. Frei, I. Spindler, S. Grissmer et al., *Cellular Physiology & Biochemistry* **18** (4-5), 165 (2006).
173 N. Zerangue, B. Schwappach, Y. N. Jan et al., *Neuron* **22** (3), 537 (1999).
174 P. Osten, V. Grinevich, and A. Cetin, *Handbook of Experimental Pharmacology* **178**, 177 (2007).

175 T. Matsushita, S. Elliger, C. Elliger et al., *Gene Therapy* **5** (7), 938 (1998).
176 J. Timpe, J. Bevington, J. Casper et al., *Current Gene Therapy* **5** (3), 273 (2005).
177 A. Cetin, S. Komai, M. Eliava et al., *Nature Protocols* **1** (6), 3166 (2006).
178 M.D. Ehlers, S. Zhang, J.P. Bernhardt et al., *Cell* **84**, 745 (1996).

Appendix A.

Manuscripts resulting from this thesis work

Appendix A

Listed are the publications that resulted from my studies of the SK2 channel multiprotein complex during my graduate student tenure.

1. **Allen** D, Fakler B, Maylie J, Adelman JP. Organization and regulation of small conductance Ca^{2+}-activated K^+ channel multiprotein complexes. J Neurosci. 2007 Feb 28;27(9):2369-76

2. François Maingret, Bertrand Coste, Jizhe Hao, **Duane Allen**, Marcel Crest, David W Litchfield, John P. Adelman & Patrick Delmas. Neurotransmitter modulation of SK channels by regulation of Ca^{2+} gating. **Neuron** (accepted) 2008.

1. Page numbers for each figure on list of figures.
2. Fix the visibility of figures, i.e. larger texts and figures where needed.
3. Take the collaborators' data out that you didn't explain well, i.e. SEG data out.
4. Raise + and 2+ to superscript throughout.
5. Change "exponential fit" in the explanation of the dose response curves.
6. Insert one overview figure of the whole mechanism of regulation of SK channels, i.e. like the one you drew on the white board.